NUREG/CR-6767
PNNL-13832

Evaluation of Hydrologic Uncertainty Assessments for Decommissioning Sites Using Complex and Simplified Models

Prepared by

P. D. Meyer
S. Orr

T. J. Nicholson, NRC Project Manager

Pacific Northwest National Laboratory
Richland, WA 99352

March 2002

Prepared for

Division of Systems Analysis and Regulatory Effectiveness
Office of Nuclear Regulatory Research
U. S. Nuclear Regulatory Commission
Washington, DC 20555-0001
NRC JCN W6933

Abstract

This report is the third (and final) report in a series that addresses issues related to hydrologic uncertainty assessment at decommissioning sites. Analyses in the first two reports in this series emphasized the application of relatively simplified models of subsurface flow and transport. Because of their relative computational speed, such simplified models are particularly attractive when the impact of uncertainty in flow and transport needs to be evaluated. These same simplifications, however, have the potential to provide unrepresentative estimates of dose and its uncertainty. Such misrepresentation may have important consequences for decisions based on the dose assessments. The significance of this concern was evaluated by comparing results from uncertainty assessments conducted on a test case using a simplified modeling approach and a more complex/realistic modeling approach.

The test case used a three-dimensional domain with a U-234 source in the near surface, a 5-m-thick aquifer 7 m below the surface, and a small well pumping directly downstream, on the boundary of the contaminated zone. Exposure was assumed to occur through the drinking water pathway only, with all drinking water originating from the pumped well. A series of Monte Carlo simulations of flow and transport were performed using STOMP as the complex model and RESRAD as the simplified model. Hydraulic conductivity and air entry were modeled as random fields in STOMP using geostatistics from the Las Cruces Trench site. Random distributions for hydraulic parameters in the RESRAD simulations were based on both site-specific data and generic distributions. Sensitivity analyses were conducted on both codes using a combination of Monte Carlo simulation and single parameter variation.

Peak doses predicted by the simplified model were several times higher than peak doses predicted by the complex model. This difference was attributed to the lack of dispersion in RESRAD and differences in aquifer mixing. The RESRAD concentration breakthrough curves exhibited a sharp peak with essentially no contaminant in the well until the time of the peak while STOMP predicted a much earlier arrival of contaminants in the well. Which code provided conservative results thus depended on whether the RESRAD peak occurred before the 1000-year regulatory criterion.

The random field characterization of the subsurface for the complex model used all available site data. Uncertainty in predicted dose was correspondingly small, with the peak dose coefficient of variation being 30%. When the variances of parameters in the simplified model were based on a generic dataset, the uncertainty in predicted peak dose was much larger; the coefficient of variation was 52% in this case. When the variances of parameters in the simplified model were based on the extensive site-specific data, the coefficient of variation for the peak dose was reduced to 22%. In this case, however, the mean peak dose was actually less similar to the STOMP results than the generic case.

For the RESRAD Monte Carlo simulations involving random soil hydraulic properties, the variability of peak dose was entirely attributed to variability in the aquifer hydraulic conductivity. Sensitivity to other parameters was examined by varying one parameter at a time. These results indicated that the recharge rate, the aquifer gradient, and the depth of penetration of the well were significant contributors to uncertainty in peak dose and the time of the peak dose. RESRAD predicted peak dose was more sensitive to the parameter values than was the STOMP predicted peak dose for the aquifer hydraulic conductivity, aquifer gradient, and depth of well penetration. Sensitivity to the recharge rate appeared to be comparable for the two codes.

Stochastic predictions of mean dose over time for the complex model were relatively insensitive to the geostatistical parameters. Ensemble mean peak dose predicted by the complex model was sensitive to the ensemble mean hydraulic conductivity. For a given ensemble mean hydraulic conductivity, however, the complex model showed no correlation between the spatial geometric mean aquifer conductivity of individual realizations and the resulting peak dose. This was in contrast to the simplified model in which the dose from individual realizations was strongly correlated with the aquifer conductivity. This result has implications for the value of hydraulic conductivity data. Adopting the homogeneous parameterization of RESRAD leads to a conclusion that reducing the uncertainty in the value of the aquifer hydraulic conductivity parameter will have a significant impact on the uncertainty in peak dose. Looking at the individual realization results from the STOMP model suggests that characterization of the average aquifer hydraulic conductivity is relatively unimportant in reducing uncertainty in peak dose. Characterizing the pattern of aquifer heterogeneity is likely to be more important than obtaining a value for the spatial mean hydraulic conductivity.

Contents

Figures

Tables

Executive Summary

Assessments of the dose from contaminated sites and waste disposal facilities may rely on the use of relatively simplified models of subsurface flow and transport. Common simplifications include steady state, one-dimensional flow; homogeneous and isotropic transport medium properties; and unit hydraulic gradient or piston-flow displacement in the unsaturated zone. Because of their relative computational speed, such simplified models are particularly attractive when the impact of uncertainty in flow and transport needs to be evaluated. Simplifications in the representation of flow and transport have the potential to provide unrepresentative estimates of dose and its uncertainty. "Unrepresentative" is used here to describe a dose or uncertainty estimate that significantly misrepresents the actual dose or the uncertainty associated with it. Such misrepresentation may have important consequences for decisions based on the dose assessments. The significance of this concern was evaluated here by comparing results from uncertainty assessments conducted on a test case using a simplified modeling approach and a more complex/realistic modeling approach. The test case followed the U.S. Nuclear Regulatory Commission's framework for site decommissioning analyses. Subsurface properties were derived from data obtained in the Las Cruces Trench experiments with source term data reflecting an actual decommissioning case. Comparisons between the two approaches included the probability distribution of peak dose, the relative importance of parameters, and the value of site-specific data in reducing uncertainty.

Characteristics of the test case were set to eliminate many differences between the codes and to highlight the differences due to the underlying conceptualization and parameterization of subsurface flow and transport. We considered a three-dimensional domain that resembled the subsurface at the Las Cruces Trench site – a site with abundant information on soil properties and information on their geostatistics. We assumed a decaying source of U-234 in the near surface, a 5-m-thick aquifer 7 m below the surface, and a small well pumping directly downstream on the boundary of the contaminated zone. Exposure was assumed to occur through the drinking water pathway only, with all drinking water originating from the pumped well. In order to evaluate doses at the pumping well over 1000 years, a series of Monte Carlo simulations of flow and transport were performed using the STOMP code for the complex model and RESRAD for the simplified model. The generated random fields for the STOMP model were based on the geostatistics of Las Cruces. Distributions of random parameters in the RESRAD simulations were based on both site-specific data and generic distributions.

Peak doses predicted by the simplified model (RESRAD) were several times higher than peak doses predicted by the complex model (STOMP). This difference was attributed to the lack of dispersion in the RESRAD model and differences in the mixing and dilution in the aquifer. For this test case, RESRAD provided conservative results in the sense that the peak dose was higher than that predicted by STOMP. The RESRAD concentration breakthrough curves exhibited a sharp peak, however, with essentially no contaminant in the well until the time of the peak. This could be interpreted as nonconservative behavior since the STOMP simulations predicted a much earlier arrival of contaminants and, prior to the arrival of the RESRAD peak, the well concentrations from the STOMP model were larger than those predicted by RESRAD. This point is particularly relevant because the regulatory criteria include a time limit: 1000 years from the time of decommissioning. Although the RESRAD predicted peak occurred prior to this limit, had the peak occurred after 1000 years, the RESRAD results would have been nonconservative in every sense of the word.

The complex model assumed the availability of an extensive dataset on which to base the random field characterization of the subsurface. Uncertainty in predicted dose was correspondingly small, with the peak dose coefficient of variation being 30%. When the variances of parameters in the simplified model were based on a generic dataset, the uncertainty in predicted peak dose was much larger; the coefficient of variation was 52% in this case. When the variances of parameters in the simplified model were based on the available site-specific data, the coefficient of variation for the peak dose was reduced to 22%. In this case, however, the mean peak dose was actually less similar to the STOMP results than the generic case. This unexpected result occurred because the site-specific mean aquifer hydraulic conductivity was significantly smaller than the generic value and because of the strong dependence of the RESRAD peak dose on aquifer hydraulic conductivity. The lognormal distribution of the hydraulic conductivity accentuated the effect.

Sensitivity analyses were conducted on both codes using a combination of Monte Carlo simulation and single parameter variation. The goals of the sensitivity studies were to determine the parameters critical to an understanding of the models' behavior. We also wanted to see whether the simplified and complex models were sensitive to the same parameters, thus indicating whether they represent the modeled flow and transport processes in a physically similar way.

For the RESRAD Monte Carlo simulations involving random soil hydraulic properties, the variability of peak dose was entirely attributed to variability in the aquifer hydraulic conductivity. Sensitivity to other parameters was examined by varying one parameter at a time. These results indicated that the recharge rate, the aquifer gradient, and the depth of penetration of the well were significant contributors to uncertainty in peak dose and the time of the peak dose.

Sensitivity analyses of the complex model showed that stochastic predictions of mean dose over time exhibited low

sensitivity to parameter variability (expressed by their variances), including to the variance of log hydraulic conductivity. This may have been due to the use of a relatively small simulation domain. Uncertainty in dose predictions, however, was directly (linearly) dependent on the variance of hydraulic conductivity. Ensemble mean dose was insensitive to the correlation scales of the hydraulic properties. Uncertainty in dose, however, increased somewhat with an increase in the correlation scale. Overall, the complex model showed robustness with respect to geostatistical parameters.

Ensemble mean peak dose predicted by the complex model was strongly sensitive to the ensemble mean hydraulic conductivity. Reducing the ensemble mean hydraulic conductivity by an order of magnitude resulted in more than a fivefold increase in the peak dose (due primarily to reduced mixing in the aquifer). Increasing the ensemble mean conductivity by an order of magnitude resulted in nearly a 90% reduction in peak dose. It was noted, however, that for a given ensemble mean hydraulic conductivity, the complex model showed no correlation between the spatial geometric mean aquifer conductivity of individual realizations and the resulting peak dose. This was in contrast to the simplified model in which the dose from individual realizations was strongly (negatively) correlated with the aquifer conductivity. This result has implications for the value of hydraulic conductivity data. Adopting the homogeneous parameterization of RESRAD leads to a conclusion that reducing the uncertainty in the value of the aquifer hydraulic conductivity parameter will have a significant impact on the uncertainty in peak dose. The individual realization results from the STOMP model suggest that characterization of the average aquifer hydraulic conductivity is relatively unimportant in reducing uncertainty in peak dose. Characterizing the pattern of aquifer heterogeneity is likely to be more important than obtaining a value for the spatial mean hydraulic conductivity.

RESRAD predicted peak dose was more sensitive to the parameter values than was the STOMP predicted peak dose for the aquifer hydraulic conductivity, aquifer gradient, and depth of well penetration. Sensitivity to the recharge rate appeared to be comparable for the two codes, perhaps a result of the boundary condition constraints imposed on the STOMP model. Differences in model sensitivities may lead to different conclusions about which parameters are critical to the analysis and about the importance of site-specific data.

Finally, we make some observations on computational issues. Flow and transport in single realizations of the complex model showed strong dependence on the spatial structure of generated hydraulic properties. These large variations in results, however, diminished sharply when averaged over the ensemble, as the number of realizations exceeded 200. A minimum of 200 realizations were thus conducted for each of the STOMP Monte Carlo simulations. STOMP model results showed some sensitivity to mesh resolution, particularly near the water table, where concentration gradients were extremely high. The relatively coarse mesh size (1 m) was a calculated compromise without which the Monte Carlo simulations could not be performed. The variety of numerical considerations required by the application of a complex, three-dimensional model was clearly illustrated. No such considerations were required to execute RESRAD as its internal conceptual-mathematical model is fixed. The complex model required many hours of computational time to execute a Monte Carlo simulation. RESRAD, on the other hand, required no more than a few minutes.

Foreword

This technical contractor report was prepared by Pacific Northwest National Laboratory[1] (PNNL) under their U. S. Department of Energy Interagency Work Order (JCN W6933) with the Radiation Protection, Environmental Risk and Waste Management Branch, Division of Systems Analysis and Regulatory Effectiveness, Office of Nuclear Regulatory Research. This final research report documents the testing and completion of PNNL's uncertainty assessment methodology. The testing utilized field datasets from complex ground-water flow and tracer experiments for comparison of alternative models and parameter representations. The field datasets were chosen in consultation with the NRC Project Manager and NRC licensing staff. Earlier application of the methodology involved a hypothetical test case provided by NRC licensing staff (i.e., NUREG/CR-6695). The PNNL methodology provides a strategy for identifying the critical hydrologic parameters and evaluating their contribution to uncertainty in dose calculations. Results from this work point to the importance of both parameter uncertainty and conceptual model uncertainty. The report's appendices provide a listing of the data distributions used in the testing. Further detailed information on the PNNL research study and a listing of PNNL's Simplified Transient Estimation of the Water Budget (STEWB) Model is available on the PNNL website: http://nrc-hydro-uncert.pnl.gov/.

The PNNL research study was undertaken in response to an Office of Nuclear Material Safety and Safeguards “user need” to support licensing needs for estimating and reviewing hydrologic parameter distributions and their attendant uncertainties for site-specific dose assessment modeling as outlined in NUREG-1549. As discussed in NUREG-1549, the NRC staff reviews the scenario, conceptual model, and input parameters. All three components may contribute to uncertainty. The PNNL research focuses on hydrologic parameter uncertainties in the context of dose assessments for decommissioning sites. The information provided in this and earlier reports (i.e., NUREG/CR's 6656 and 6695) supports the NRC staff's efforts in providing dose modeling guidance. Specifically, the report documents the methodology, its relationship to conceptual model uncertainty, and demonstrates its capabilities through the testing exercises which utilized site-specific data.

This final report is the third report in a series of three contractor reports documenting PNNL's uncertainty assessment methodology, its testing and applications to decommissioning sites. This report, as with the earlier ones, is not a substitute for NRC regulations, and compliance is not required. The approaches and/or methods described in this NUREG/CR are provided for information only. Publication of this report does not necessarily constitute NRC approval or agreement with the information contained herein. Use of product or trade names is for identification purposes only and does not constitute endorsement by the NRC or Pacific Northwest National Laboratory.

Cheryl A. Trottier, Chief
Radiation Protection, Environmental Risk and Waste Management Branch
Division of Systems Analysis and Regulatory Effectiveness
Office of Nuclear Regulatory Research

[1] Pacific Northwest National Laboratory is operated for the U.S. Department of Energy by Battelle Memorial Institute under Contract DE-AC06-76RLO 1830

Acknowledgments

The authors gratefully acknowledge the financial assistance of the Office of Nuclear Regulatory Research of the U.S. Nuclear Regulatory Commission (NRC) and the guidance of the NRC Project Manager, Tom Nicholson. The staff of the NRC have also contributed in reviewing and commenting on the activities described in this report.

Joel Malard and Mark White of PNNL provided significant help in performing the STOMP simulations. We also appreciate the comments of Dongxiao Zhang of Los Alamos National Laboratory who provided a review of this report.

1 Introduction

This report is the third report in a series that addresses issues related to hydrologic uncertainty assessment at decommissioning sites. The analyses described in these reports have been conducted under the general framework for license termination described in NUREG-1549 (NRC, 1998). This framework provides for an iterative approach to decommissioning analyses that moves from screening-type analyses using pre-defined models and generic screening parameters to site-specific analyses using more complex, realistic models and parameters based on site-specific data. A depiction of the framework taken from NUREG-1549 is shown in Figure 1-1.

A primary component of the decommissioning framework is a dose assessment (box 4 of Figure 1-1), used to provide future estimates of dose that can be compared to the regulatory criteria for license termination (10 CFR Part 20 Subpart E). The regulatory criteria are summarized in Table 1-1 and involve predictions of contaminant transport and exposure 1000 years from the time of decommissioning. This long time frame, coupled with complex contaminant exposure pathways and limitations on site-specific characterization data produce an inherent uncertainty in the results of a dose assessment.

Each of the reports in this series addresses a particular aspect of dose assessment uncertainty analysis. To provide a complete picture of the analyses completed, the first two reports are summarized here.

1.1 Summary of NUREG/CR-6656

The first report in this series, NUREG/CR-6656 (Meyer and Gee, 1999), described the basic conceptual models and mathematical implementations of three dose assessment codes (DandD, RESRAD, and MEPAS[1]). Uncertainty in the hydrologic parameters of these codes was discussed and

[1] DandD conceptual model and mathematical formulations are described in Kennedy and Strenge (1992)

RESRAD web page: http://web.ead.anl.gov/resrad/home2

MEPAS web page: http://mepas.pnl.gov:2080/earth/earth.htm

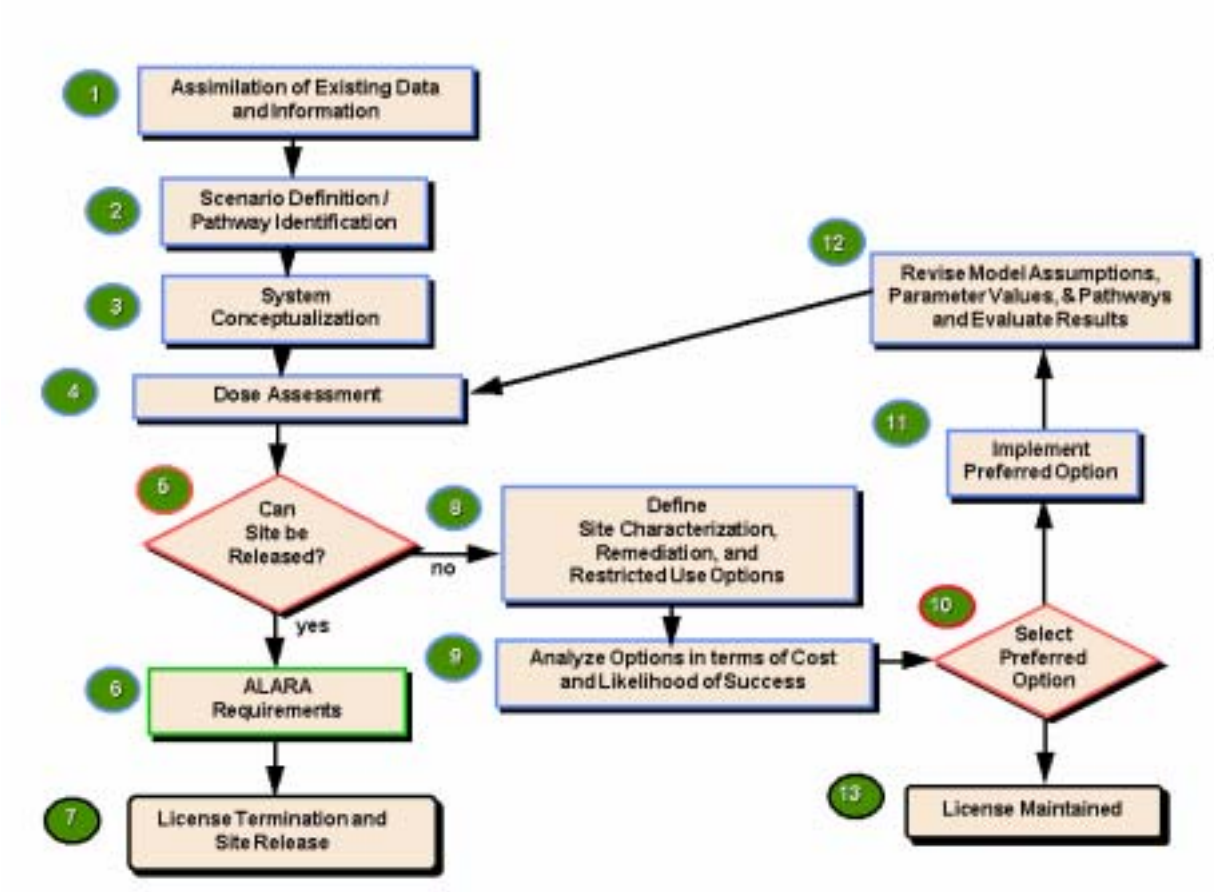

Figure 1-1. NRC decommissioning and license termination decision-making framework (from NRC, 1998)

Table 1-1. Summary of radiological criteria for license termination (10 CFR Part 20 Subpart E)

	Unrestricted Release[a]	Restricted Release	
Dose Criterion	25 mrem TEDE per year peak annual dose to the average member of the critical group	25 mrem TEDE per year peak annual dose to the average member of the critical group while controls are in place	100 or 500 mrem TEDE per year peak annual dose to the average member of the critical group upon failure of the controls
Time Frame	1000 years	1000 years	1000 years
Other Requirements	ALARA	ALARA, financial assurance, public participation	ALARA, financial assurance, public participation

a. TEDE: total effective dose equivalent; ALARA: as low as reasonably achievable

data sources for defining best-estimate parameter values and parameter uncertainty characterizations were identified. The three codes were selected because they were in use by NRC staff as part of their decommissioning analyses. The NRC does not require the use of these codes, however.

Each of the codes uses a fairly simplistic representation of flow and transport in the subsurface. The common simplifying conditions used in DandD, RESRAD, and MEPAS related to flow and transport in the subsurface were summarized as follows.

- Each code uses a relatively simple model for the near-surface water budget to determine the net infiltration rate, i.e., the flow of water through the system that drives the contaminant transport. In DandD the net infiltration is known, in RESRAD the water budget is based on average annual components (precipitation, evapotranspiration, and runoff), and for MEPAS the water budget is based on monthly average components.
- Steady-state flow throughout the system is imposed in each code. The net infiltration required by each code is a constant, average annual value.
- Flow throughout the system is one-dimensional. In addition, advective transport is also one-dimensional in all cases. (MEPAS includes the effect of dispersion, which can be three-dimensional in the saturated zone.)
- Only a small number of layers are allowed in the system and the physical, hydraulic, and chemical properties of each layer must be uniform. No other form of heterogeneity is allowed.
- A fairly simple model of mixing in the aquifer is used. In DandD mixing occurs instantaneously throughout the fixed aquifer volume. For RESRAD and MEPAS the aquifer has infinite lateral extent and a finite and constant thickness.

As a consequence of these simplifications, there are site-specific conditions under which the codes may provide inaccurate, potentially nonconservative results. These conditions include the following.

- The presence of significant preferential flow in the near surface could lead to greater net infiltration than might be anticipated when relying on the simple water budget calculations of the dose codes.
- The imposed condition of steady-state flow will be violated to some degree at all sites. Net infiltration and percolation to the saturated zone vary in time as a result of intermittent precipitation and seasonal changes in evapotranspiration and precipitation. The contaminant flux may be affected as a result of temporal variation in net infiltration and water content. In addition, transient flow conditions may affect transport in the unsaturated zone.
- Significant heterogeneity in physical, hydraulic, or chemical properties may result in two- or three-dimensional flow patterns. Contrasting properties that result in focused flow and fast transport paths may produce conditions under which the dose codes predict nonconservative results.
- Subsurface conditions under which flow and transport are significantly influenced by fractures or karst formations clearly contradict the simplified conceptual models of the dose assessment codes. Because of the potential for fast transport of contaminants under these conditions, the codes may produce nonconservative results.
- The presence of unmodeled processes such as colloidal transport, nonequilibrium adsorption, and vapor phase transport may render the model predictions nonconservative.

The hydrologic parameters of the three codes were listed and compared. The relative importance of the parameters to the analysis of uncertainty in predicted dose was summarized qualitatively as shown here in Table 1-2. The relative importance is composed of the sensitivity of the model to a parameter's value and the uncertainty in the parameter value. Sources of uncertainty were discussed and alternative measures of sensitivity were described.

Data sources for best-estimate parameter values and parameter uncertainty information were reviewed. The following sources of information were identified.

Table 1-2. Generalized relative importance of dose assessment code parameters in an uncertainty analysis from NUREG/CR-6656. Results for a specific application may vary.

		Uncertainty Due to Variability and/or Lack of Knowledge		
		Low	**Medium**	**High**
Model Sensitivity	**High**	UZ[a] Thickness		Distribution Coefficients Net Infiltration Rate
	Medium	Effective Porosity Bulk Density	Darcy Velocity Unsaturated Water Content	SZ[a] Exposure Parameters SZ Hydraulic Conductivity
	Low	Porosity	Soil-Type Exponent Field Capacity	UZ Sat. Hydraulic Conductivity Dispersivity

a. UZ = unsaturated zone, SZ = saturated zone

- UNSODA (Leij et al., 1996) is a database of soil physical and hydraulic property measurements compiled from a variety of international sources. UNSODA is available from the U. S. Department of Agriculture-Agricultural Resarch Service (USDA-ARS) Salinity Laboratory (http://www.ussl.ars.usda.gov/). UNSODA contains soil property measurements, but some analysis may be required to obtain soil parameters for use in dose assessments. Two related databases, compiled from U.S. sources, are summarized in Schaap and Leij (1998).
- In NUREG/CR-6565 (Meyer et al., 1997) generic probability distributions for soil parameters were presented for use directly in RESRAD and MEPAS. These parameter distributions were based on the work of Carsel and Parrish (1988) who used data from the National Soil Characterization Database. These distributions are included in this report as Appendices A and B. Soil bulk density distributions obtained using a similar analysis are included here as Appendix C.
- The National Soil Characterization Database is a large collection of soil properties available from the USDA Natural Resources Conservation Service (NRCS) (see http://www.nrcs.usda.gov/). This database consists of standard soil survey measurements on small-scale soil pedons generally obtained near the surface. Some analysis may be required to derive parameter values from the measured soil properties.
- SSURGO is a database of the original NRCS soil surveys digitized for use with Geographic Information System (GIS) software. These are the most detailed soil survey data available from the NRCS and are currently available for limited areas of the United States. SSURGO data are at a sufficiently small scale to be useful for parameter estimation in decommissioning analyses. Additional analyses may be required to derive parameter values from the soil property measurements in the database. More information and data are available at http://www.nrcs.usda.gov/.
- The STATSGO database is an NRCS product that generalizes the detailed soil survey data to a larger scale. This database is also intended for use with GIS software. The scale of STATSGO data is generally too large to be of significant use in estimating parameter values for decommissioning analyses, although it may be useful in characterizing uncertainty.
- The National Climatic Data Center (NCDC) provides meteorological data measured at locations throughout the United States. Many of these data are available at http://lwf.ncdc.noaa.gov/oa/ncdc.html, although it may require some analysis to derive the parameter values required for dose assessment analyses. The use of this data in evaluating uncertainty in net infiltration estimates was described by Meyer et al. (1997).
- The NWIS is a database of surface water, groundwater, and water quality information available from the U.S. Geological Survey (USGS) at http://water.usgs.gov/nwis/. The groundwater information is primarily limited to water table levels in selected wells.
- Extension Service agents; state, county, and municipal staff; and university or industry personnel with experience in local conditions may be excellent sources of information and data related to a site. Information related to specific soil types, land use patterns, and climatic data are often readily available from extension offices and other local sources. Water table depths and results of percolation tests (which give some indication of soil hydraulic properties) can be obtained in areas where septic tank systems are used. Local county or city files are often the source for such information.

Additional information on data sources for the RESRAD and MEPAS dose assessment codes can be found in Yu et al. (1993) and Buck et al. (1995), respectively.

Taken as a whole, NUREG/CR-6656 outlines a methodology for parameter uncertainty assessment that considers the potential data limitations and modeling needs of decommis-

sioning analyses. This methodology uses generic parameter distributions based on national or regional databases, sensitivity analysis, probabilistic modeling, and Bayesian updating to incorporate site-specific information. The uncertainty assessment methodology described in NUREG/CR-6656 is consistent with the technical basis for dose modeling evaluations prepared by NRC staff and presented in NUREG-1727 (NRC, 2000).

1.2 Summary of NUREG/CR-6695

The second report in the series, NUREG/CR-6695 (Meyer and Taira, 2001) used hypothetical decommissioning test cases to illustrate the application of the uncertainty assessment methodology presented in NUREG/CR-6656. The test cases were based on source term and scenario information provided by NRC staff and on the physical setting of a site in Arizona at which NRC-sponsored field studies have been carried out. Basic soil and climate information provided by University of Arizona staff were used in the application. The site consisted of a layered sand/loam soil with a water table 13 m below the ground surface. The climate was arid, but it was assumed that substantial irrigation occurred. Other regional information was obtained from electronic sources. For those aspects of the site without reliable data sources, national databases were used to estimate site characteristics.

A series of deterministic simulations were carried out using the codes DandD v. 1.0 and RESRAD v. 6.0. Simplifications to the conceptual model of the site were made to match the conceptual models embodied in the simulation codes. Following the framework described in NUREG-1549, a DandD screening simulation was executed with the test case source term and all default parameter values. The DandD code was subsequently run with parameter values more representative of the test case site. The RESRAD simulations used primarily site-specific parameter values for the subsurface physical, hydrologic, and chemical parameters. Two source scenarios were modeled with RESRAD. An in situ case left the waste in its original buried location and assumed that a cover was in place. An excavation case was also simulated in which the waste was assumed to have been excavated for construction of a house, mixed with clean soil from the excavation, and widely spread about in a surface layer. This case more closely resembled the DandD conceptual model. The resulting peak doses over a 1000-year period for these deterministic DandD and RESRAD simulations are shown in Table 1-3.

In all cases, the primary contributors to the peak dose were the uranium isotopes. For the RESRAD simulations, the uranium release occurred over a relatively short period of time producing a correspondingly sharp peak in dose. Because of this sharp peak, lengthening the travel time slightly (less than 10% in the excavation test case) would produce a result that satisfies the regulatory criterion by moving the peak dose pulse to a point beyond 1000 years. Such a result demonstrates the importance of considering the uncertainty in parameter values. This result also emphasizes the importance of considering uncertainty in the time at which the peak dose occurs, in addition to uncertainty in the magnitude of the peak.

Deterministic sensitivity analyses applied to the RESRAD in situ test case included use of a simplified model implemented in a spreadsheet and one-parameter sensitivity calculations applied to the base case parameter values and to a set of conservative parameter values. The various sensitivity measures were largely in agreement. For the in situ case, these analyses indicated that the evapotranspiration coefficient, the uranium distribution coefficients, and the well pumping rate were the most important parameters contributing to the uncertainty in peak dose. Soil hydraulic parameters were much less important for this case. Deterministic sensitivity analyses were not carried out for the excavation case.

Probabilistic analyses were carried out for the in situ and excavation cases using the Monte Carlo simulation capability of RESRAD. Histograms and cumulative distributions for the peak total dose and the time of the peak dose were derived. Figure 1-2(A) shows the empirical cumulative dis-

Table 1-3. Summary of test case deterministic base case simulation results from NUREG/CR-6695

Code	Description	Peak Dose (mrem/yr)	Peak Dose Time (yr)
DandD	Default Parameter Values	829	4
DandD	Site-Specific Physical & Hydrologic Parameters	285	17
DandD	Site-Specific Distribution Coefficients	198	10
DandD	All Site-Specific Parameters	70	98
RESRAD	In Situ Case	115	939
RESRAD	Excavation Case	16	973

tribution function for the RESRAD in situ test case. Statistics for the total dose as a function of time, used to obtain the peak of the mean dose, were also presented. A sample of these results is shown in Figure 1-2(B) for the RESRAD in situ test case. The probabilistic results can be used to compare the estimated site performance to the regulatory measures with consideration of parameter uncertainties.

Probabilistic measures of sensitivity presented were scatter plots of peak dose versus parameter values, statistical sensitivity measures calculated by RESRAD (such as the partial correlation coefficients), and single-parameter Monte Carlo simulations used to clarify the relationships between dose and critical parameter values. No single measure was a reliable indicator of the relative importance of the parameters. For the in situ case, the evapotranspiration coefficient, the well pumping rate, and the uranium distribution coefficients were of greatest importance. These results were consistent with the deterministic results. For the excavation case, the saturated zone hydraulic conductivity was the most important parameter followed by the uranium distribution coefficients. The applications illustrate the value of applying a variety of uncertainty analysis methods and understanding the behavior of the simulation code.

There are multiple measures of dose that could be used for comparison to the regulatory standard when probabilistic simulations are used in decommissioning analyses. One could use a statistic (such as the mean or the 50th percentile) of the distribution of peak dose. Peak dose as used here refers to the total (all pathways) dose occurring in the first 1000 years after decommissioning. This is the quantity used in Figure 1-2(A) (albeit without the 1000 year limit). An alternative measure of dose discussed in NRC (2000) is the peak of the mean dose, where the mean dose is calculated as a function of time by averaging over all Monte Carlo realizations for each year of the simulation as shown in Figure 1-2(B). The median and 90th percentile doses are shown in this figure as well as the deterministic base case dose. For the in situ test case, the mean dose at any time during the simulation was significantly less than the base case peak dose. This result occurred because of the sharp peak in the dose as a function of time for any given realization and the fact that the parameter variation resulted in the time of the peak varying significantly. At any particular time, in fact, the fraction of realizations that had a dose greater than the 25 mrem/yr limit was quite small. The differences in the statistical quantities that might be used to compare with the regulatory criteria require that these quantities be precisely defined.

A method to update parameter probability distributions (based on Meyer et al., 1997) was also applied to the excavation test case using the saturated zone hydraulic conductivity. Because site-specific measurements were not available for this parameter, data were generated using four measurements of physical properties from the deepest samples available at the test case site. Updating the saturated zone hydraulic conductivity distribution with this generated data had its greatest effect on the standard deviation of the peak dose, which was significantly reduced. The empirical cumulative distribution functions for the prior and updated peak dose (for the excavation case) are shown in Figure 1-3. The percentage of realizations exceeding 25 mrem/yr was reduced from 13% to 2% for this test case.

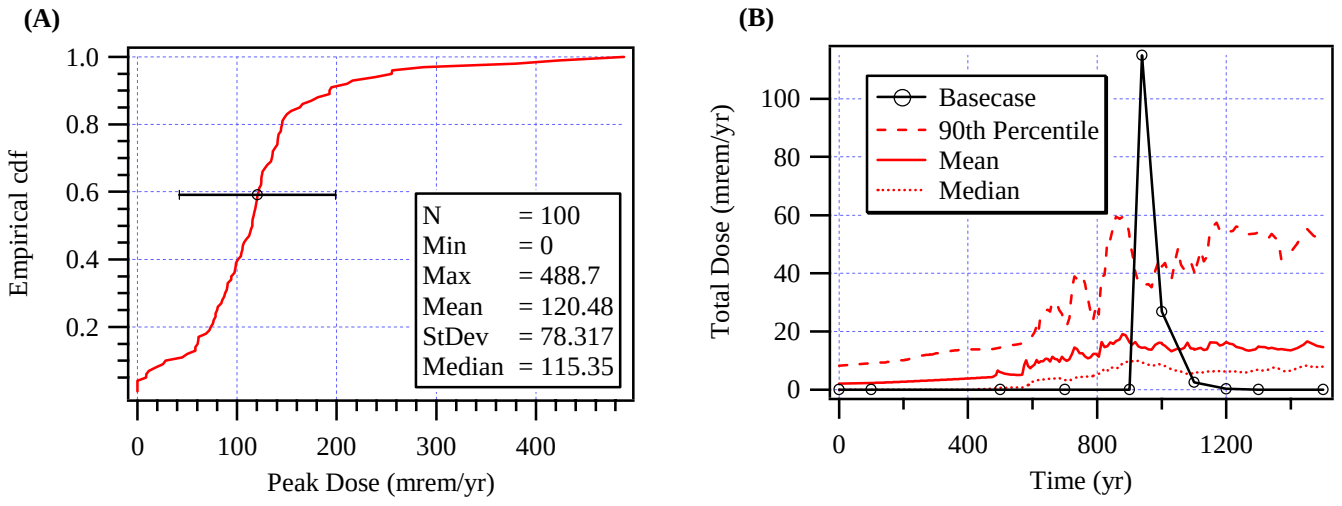

Figure 1-2. Probabilistic results from the RESRAD in situ test case simulations of NUREG/CR-6695

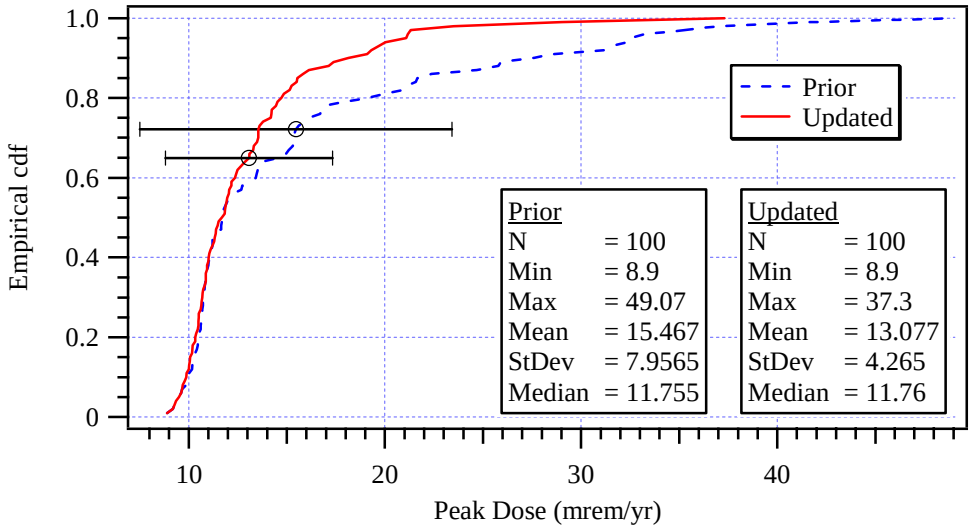

Figure 1-3. Prior and updated probabilistic results from the RESRAD excavation test case simulations of NUREG/CR-6695

1.3 Objectives and Methodology of the Current Report

Analyses in the first two reports in this series emphasized the application of relatively simplified models of subsurface flow and transport. Common simplifications of the codes examined in the reports include steady-state, one-dimensional flow, homogeneous and isotropic transport medium properties, and unit hydraulic gradient in the unsaturated zone. While recognizing the potential impact of these simplifications, the simplified codes are nonetheless attractive because of their relative computational speed. This speed is particularly important when the impact of uncertainty in flow and transport needs to be evaluated.

Simplifications in the representation of flow and transport have the potential to result in not only unrepresentative estimates of dose, but also unrepresentative estimates of uncertainty. “Unrepresentative” is used here to describe an estimate of expected values (or mean values) and their uncertainty that significantly misrepresent the “actual” mean and uncertainty. Such misrepresentation may have important consequences for decisions based on the dose assessment, including conclusions drawn about the relative importance of parameters and the value of site-specific data in reducing uncertainty. The significance of this concern is evaluated in this report by comparing test case results from uncertainty assessments conducted using a simplified, one-dimensional, statistical modeling approach and a complex, three-dimensional, stochastic modeling approach. We use the results from the complex, three-dimensional stochastic model as our best estimate of the “actual” mean and uncertainty. Comparisons between the two modeling approaches include the probability distribution of peak dose, the relative importance of parameters, and the value of site-specific data in reducing uncertainty.

The test case described in the current report used subsurface properties derived from data obtained in the Las Cruces Trench experiments (Wierenga et al., 1989; 1990) with a source term and exposure scenario loosely based on that used in NUREG/CR-6695. The Las Cruces Trench site was chosen because the characterization of the unsaturated zone at the site was excellent, tracer experimental data and modeling results were available, and the NRC sponsored the experiments.

The simplified modeling approach used the RESRAD code (v. 6.1). Although our conclusions are specific to the RESRAD code, we believe similar analyses using other simplified codes (such as DandD and MEPAS) would highlight analogous concerns. RESRAD was chosen because it is a familiar code to NRC staff and NRC licensees. The more complex modeling approach used the STOMP[1] code in a stochastic framework of Monte Carlo simulations. STOMP was chosen because of its flexibility and extensive feature set, its low price (free), and because the authors have experience with it. For comparisons between the two approaches, concentrations calculated by STOMP were converted to dose consistent with the procedures used in RESRAD.

Monte Carlo simulation was used in this analysis because of the complexity of the scenario, which included coupled unsaturated-saturated flow and transport and a pumped

[1] STOMP web page: http://www.pnl.gov/etd/stomp

well. Stochastic moment methods (Gelhar, 1993; Dagan and Neuman, 1997; Zhang, 2001) provide an alternative to Monte Carlo simulation for estimating flow and transport uncertainty. These methods have the potential to significantly reduce the computational requirements of the analyses discussed in this report. For our application, however, the available stochastic moment methods could not be used without unacceptable simplification of the modeled scenario. Recent improvements to address the effects of a coupled unsaturated-saturated system (Sun and Zhang, 2000; Zhang and Lu, 2002) suggest that stochastic moment methods may be a viable alternative in the near future.

The following chapter describes the setting of the test case and the exposure scenario used to provide relative equivalence in the simplified and complex approaches. Probabilistic simulation results are then presented followed by results from a limited sensitivity analysis.

The emphasis in this report series, including the current report, is on prediction uncertainty resulting from uncertainty in parameter values. This emphasis is not intended to downplay the importance of uncertainty arising from other sources such as model structure and future scenarios. The importance of conceptual model uncertainty was recognized in the first report of this series and played a role in the analysis of the test case results discussed in the second report. Conceptual model uncertainty is the subject of an NRC research project currently being conducted at the University of Arizona. Our test case analyses indirectly include model uncertainty since we compare results from a three-dimensional model and a one-dimensional model, a significant difference in problem conceptualization. Other uncertainties in model structure investigated in this project (through sensitivity analyses) include variations in pumping well location and discharge rates, boundary conditions (affecting ambient mean gradient), and variations in geostatistical parameters. The NRC staff have also recognized the importance of scenario uncertainty. Although this topic is not addressed in detail in this report series, it is touched on in this report as we looked at the sensitivity of model results to parameters related to the future exposure scenario.

In addition to discussing primarily parameter uncertainty, the analyses in this report series are limited to the hydrologic aspects of decommissioning cases. For buried contaminants, this means that the analysis is limited to the exposure pathway involving infiltration of water at the ground surface, leaching of contaminants, and transport of contaminants through the groundwater to a point of exposure. While other exposure pathways may be considered in a decommissioning analysis, subsurface water transport is likely to be a significant pathway for buried contaminants.

2 Test Case Scenario and Hydrogeologic Setting

This chapter describes the simulation domain, the exposure scenario, and the hydrogeologic setting of the test case. In all cases, decisions about the characteristics of the test case were made to result in RESRAD and STOMP models that looked as identical as possible, but at the same time allowed us to model the test case as realistically as feasible. The complex representation, which used the STOMP code, is discussed first. The simplified representation, which used the RESRAD code, is discussed at the end of this chapter.

2.1 Complex Representation

The test case was based on the hydrogeology at the site of the Las Cruces Trench Experiments, New Mexico (Wierenga, et al., 1989, 1990). We did not adhere strictly to the regional hydrogeology, however, but enforced a water table seven meters below the ground surface. In addition, we assumed a five-meter-thick aquifer. The region modeled in STOMP was a three-dimensional domain of 20 m by 20 m by 12m deep, as shown in Figure 2-1. In our coordinate system, groundwater flow occurred along the x-axis. These assumptions about the hydrogeology were done to make the test case more comparable to that in NUREG/CR-6695. These assumed conditions likely also reduced the differences between the simplified and complex modeling approaches.

To fit the conceptual model embodied in the RESRAD code, it was assumed that a source existed as a contaminant buried in the top 1 m of soil and that this contaminant would leach down with the percolating water when exposed to infiltrating precipitation. The near-surface contamination

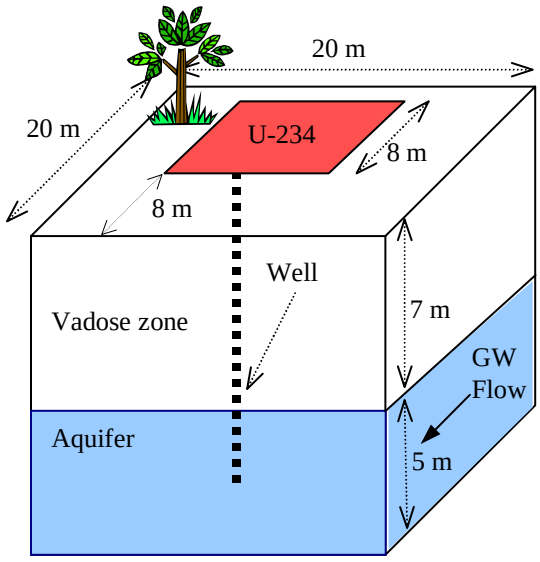

Figure 2-1. The domain for the test case simulations

covered an area 8 m by 8 m and was located 4 m from the upstream boundary along the X axis (centered with respect to the Y axis). The contaminated zone was 1-m thick. For simplicity, the source consisted of U-234 only with an initial concentration of 122 pCi/g in the solid phase. A uniform distribution coefficient of K_d = 15 cm^3/g was used. This is the same value used in NUREG/CR-6695 for this soil type. The source was leached over time according to the source-term model used in RESRAD. The resulting solid and liquid phase concentrations of the source as a function of time are shown in Figure 2-2. Following the RESRAD manual, we assigned a half-life time of 2.45 x 10^5 years for U-234 in the STOMP simulations.

To conform with RESRAD it was assumed that a well tapped the aquifer on the downstream boundary of the contaminated zone. This well was assumed to supply domestic water needs only and the sole route of exposure was assumed to be through the drinking water pathway. It was also assumed that 100% of the drinking water was derived from the well and that drinking water ingestion was 2 l/day. The pumping rate from the well was 118 m^3/yr, the approximate median of the distribution for this quantity given in the DandD documentation (Beyeler, et al., 1999).

2.1.1 Las Cruces Trench Data, Domain, and Geostatistics

We started with data and the geostatistics of soil hydraulic properties at the Las Cruces site, as presented by Rockhold et al. (1996). Based on their findings, we assumed the existence of Miller's similarity principle, particularly with the assumption of identical scaling factors for saturated hydraulic conductivities and for pressure heads. We adopted the scaling factor statistics described in Table 1, Figure 6, and Equation 18 of Rockhold et al. (1996). We used the Brooks and Corey (B-C) water retention model with the Burdine hydraulic conductivity model (Eqs. 1 and 2 in Rockhold et al., 1996). We used the mean-scaled parameters as determined by Rockhold et al. (1996), that is, K_s^* = 4.16 m/day (mean saturated hydraulic conductivity), ψ_e^* = 5 cm (mean air-entry value), θ_s = 0.32 (saturated water content or porosity), θ_r = 0 (residual water content), b = 0.267 (B-C exponent parameter). The last three parameters were assumed uniform over the whole domain (as done in Rockhold et al., 1996). The scaling theory implies the following relationships:

$$\psi = \psi^*/\alpha, \text{ hence, } \psi_e = \psi_e^*/\alpha \qquad (2\text{-}1)$$

$$K = \alpha^2 K^*, \text{ hence, } K_s = \alpha^2 K_s^* \qquad (2\text{-}2)$$

where α is the scaling factor. α does not depend on saturation, but it is heterogeneous or random in a similar manner to K or K_s. Hence, rather than generating random fields of K_s and ψ_e, we generated a random field of α based on the geostatistics presented in Rockhold et al. (1996), and then

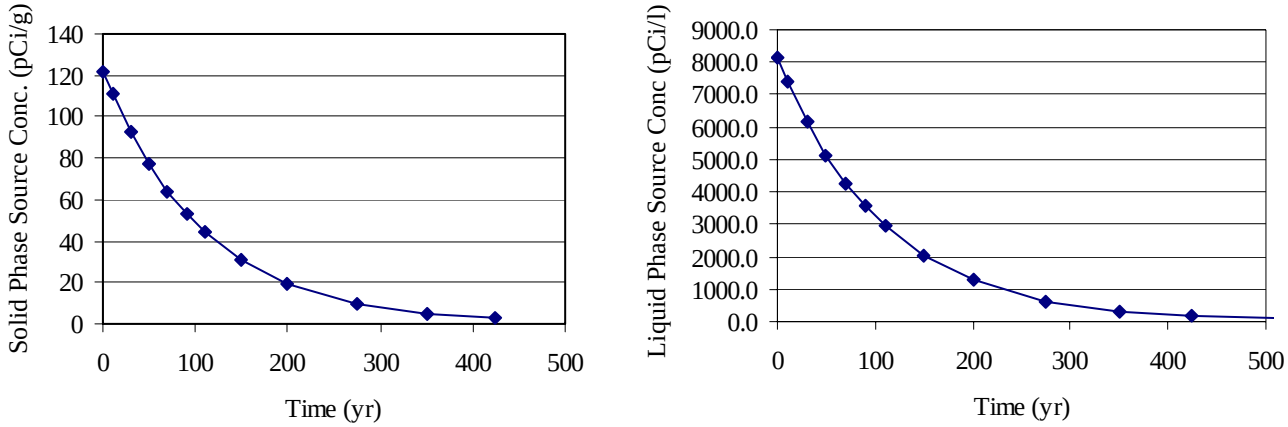

Figure 2-2. Contaminant source (U-234) concentrations in the solid phase (left) and the liquid phase (right)

translated it to fields of K_s and ψ_e (the necessary input parameters) using the above relationships (Eqs. 2-1 and 2-2).

The particle density was also assumed uniform at 2.65 g/cm^3, which implied a bulk density of 1.8 g/cm^3.

2.1.2 Choice of Random Field Generator, Resulting Geostatistics of α and K_s and Spatial Distribution of Permeabilities

There are several methods to generate correlated random fields. The most commonly used are methods based on Turning Bands, LU decomposition, fast Fourier transform (FFT), and sequential simulations (also called the method of conditional distribution). We chose SGSIM, a sequential Gaussian random field generator from GSLIB (Deutsch and Journel, 1997) because it allows nested, anisotropic, conditional simulations. At the core of each random field generator there is a random number generator, which generates independent pseudo random numbers based on three deterministic parameters, including a seed – the only random number generator parameter that can be changed by the user. A good discussion on random number generators is presented in Press et al. (1986). The random field generator uses the uncorrelated numbers generated by the random number generator and transforms them into correlated values in space (or time), based on a correlation structure (in the form of a covariance function or a variogram) provided by the user. Descriptions of the different random field generators can be found in Deutsch and Journel (1997), and an extensive comparison between different random field generators and random number generators can be found in Orr (1993).

We used SGSIM to generate random realizations of log-α using the normalized variogram model defined by Eq. 18 of Rockhold et al. (1996) (after correction), that is:

$$\gamma(h) = 0.132 + 0.543(1 - e^{-h_1}) + 0.325(1 - e^{-h_2}) \quad (2\text{-}3)$$

where

$$h_1 = [(h_0/6.347)^2 + (h_{90}/0.039)^2]^{1/2}$$
$$h_2 = [(h_0/1.089)^2 + (h_{90}/1.129)^2]^{1/2}$$

and h_0 and h_{90} are lag distances in the horizontal and vertical directions, respectively. Simulations were carried out on a 1-m grid over the domain of Figure 2-1. (See Section 2.1.4 for a discussion of the numerical grid.)

The resulting variograms are presented in Figure 6 of Rockhold et al. (1996) and Figure 2-3 below (after translating the integral scales into effective ranges by multiplying them by 3). Eq. 2-3 implies a nested variogram with statistical anisotropy expressed by principal vertical and horizontal directions, with statistical isotropy in the horizontal plane. In Figure 2-3, note the relatively good fit between experimental and theoretical variograms for a single realization; however, the experimental variogram is presumed isotropic, horizontally, while in reality, generated single realizations whose size is less than 40 correlation scales almost always exhibit anisotropy (apparently, due to imperfection of all random field generators). Note also that the vertical variogram shows practically no correlation between block values in the vertical direction. Sample statistics of a single realization of α are given in Table 2-1.

Next, we used Eqs. 2-1 and 2-2 (above) to generate realizations of K_s and ψ_e, a different value for each block (or element). Figure 2-4 shows the geostatistics of log(K_s). As expected, the normalized variograms almost resemble those of log(α). Sample statistics of log(K_s) and K_s for a single realization are given in Table 2-2.

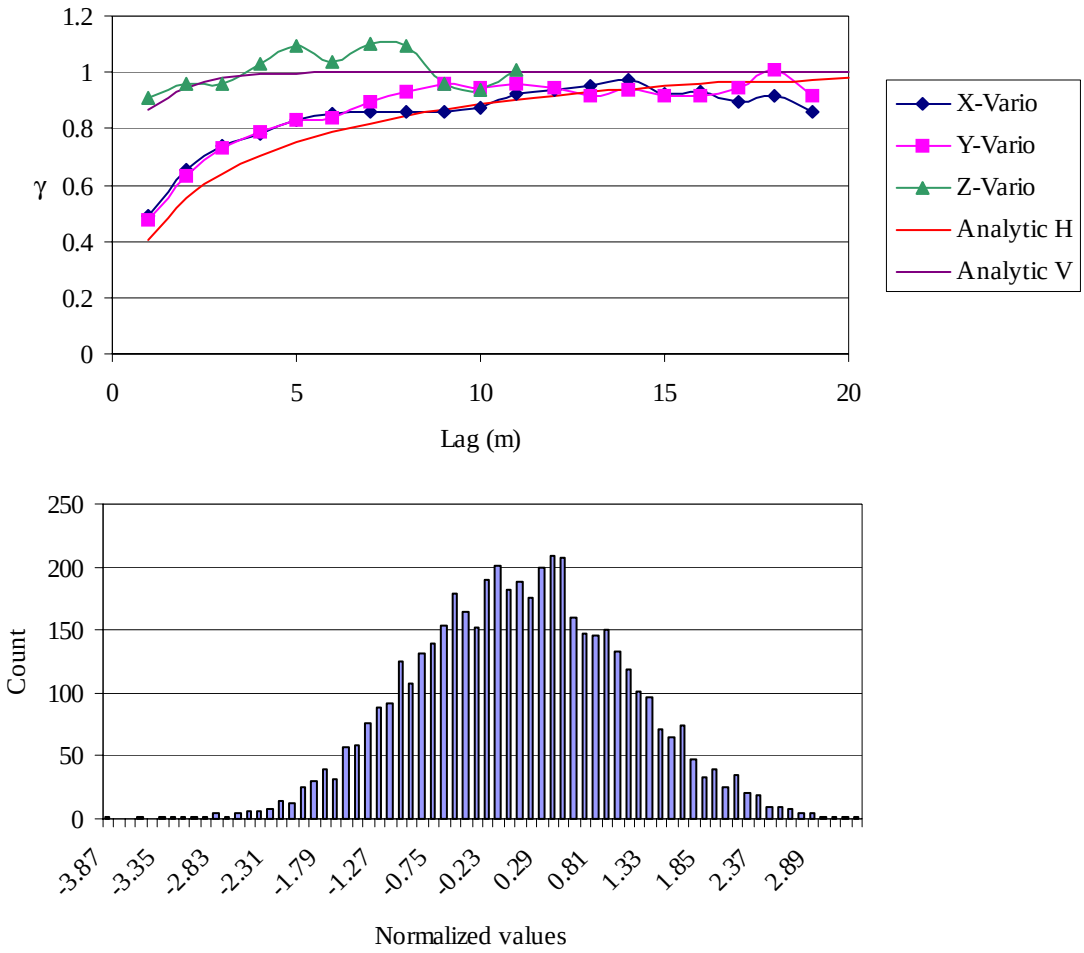

Figure 2-3. Variograms (top) and histogram (bottom) of log(α) for a single realization with the analytical directional variograms shown for comparison (H=horizontal, V=vertical)

Typically, in Monte Carlo simulations every element is considered a zone. Consequently, each element (or basic block) possesses its own hydraulic and transport properties. Figure 2-5 shows one realization of the permeability field. These values, as well as values of ψ_e and the other (uniform) parameters, were written into STOMP's input file in a generic way that enables us to regenerate the input automatically (4,800 values for each parameter) for each new realization. Our sample statistics started with 300 simulations for each case we analyzed. After examining the results, particularly the (sample) ensemble variances vs. number of simulations, we concluded that the number of simulations could be reduced to 200 with relatively insignificant reduction in accuracy (of ensemble mean and variance) and significant savings in computer time. We checked the output at different locations and particularly at the location of the pumping well.

2.1.3 Flow and Transport Parameters

Table 2-3 presents the hydraulic and transport parameters used in our models, following the parameters presented by Rockhold et al. (1996) for the Las Cruces Trench site. For each realization, different K_s and ψ_e values were assigned to each element, while other flow parameters, such as porosity, were assigned uniformly. This is due to the dominating variability of the saturated hydraulic conductivity as indicated by the statistics presented by Rockhold et al. (1996). The coefficient of variation of porosity, for example, is smaller than the coefficient of variation of K_s by an order of magnitude, implying negligible variations in porosity. Other transport parameters included longitudinal and transverse dispersivities of 0.5 m and 0.1 m, respectively.

A recharge rate of 25.4 cm/yr (or 10 inch/yr) was imposed as a Neumann boundary condition at the top of the domain.

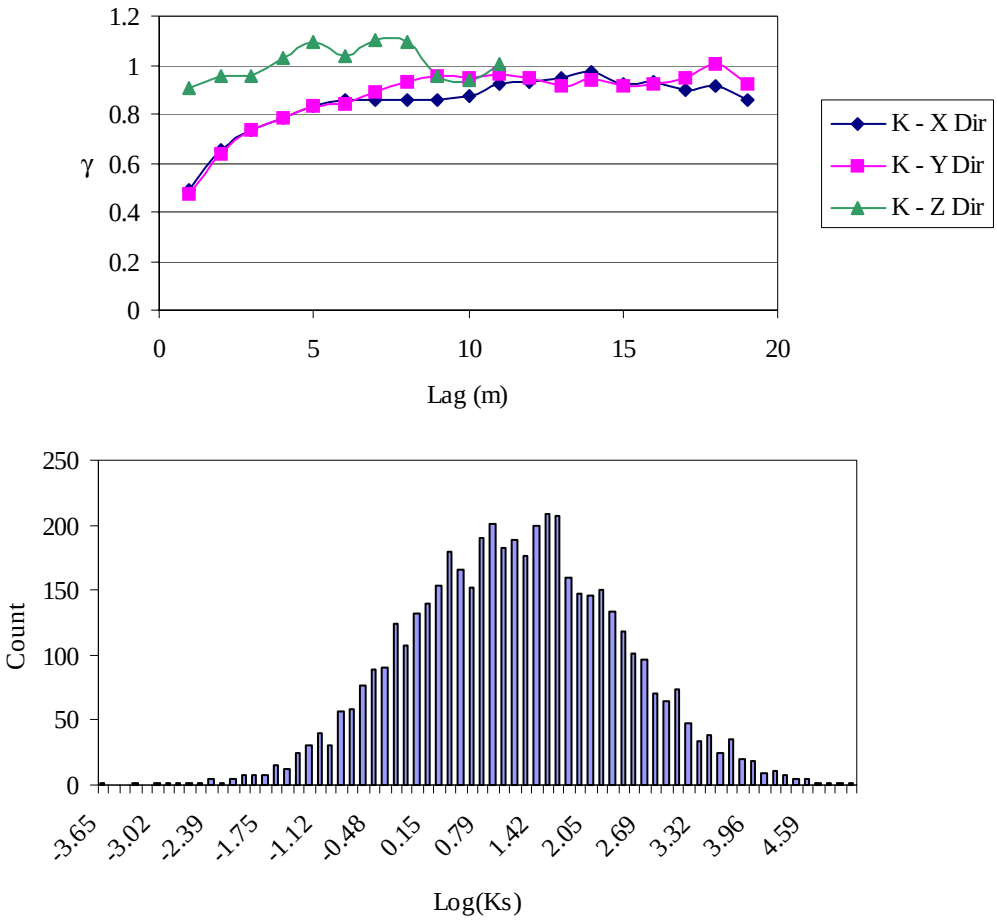

Figure 2-4. Variograms (top) and histogram (bottom) of log(K_s) (m/day) (single realization)

Initial conditions assumed gravitational/static conditions in the vadose zone and steady state flow in the aquifer. Boundary conditions included prescribed heads on aquifer boundaries, creating a gradient of 0.02. All other boundaries were considered no-flow. In terms of transport, we assumed boundary conditions of zero concentration gradient on all the vertical side surfaces, implying no dispersive transport (only advective transport). A time-varying concentration Dirichlet condition was imposed over the 8 m x 8 m contaminated zone. Liquid phase concentration as a function of time was presented above.

We ran flow simulations with STOMP until steady state was reached (in less than 1000 years), and then used the steady velocity fields as the basis for transport simulations, using STOMP. This was done in order to save computation time, keeping in mind (a) this is not too far from reality (natural recharge had been there long before contamination started), and (b) the goal of finding long-term effects. This is not a recommended shortcut in cases where short-term predictions are desired and variations in recharge events dominate the flow.

2.1.4 Numerical Modeling Considerations with STOMP: Grid Resolution, Time Step, and Solver

The basic block (element) size for the STOMP modeling was a 1-m cube. With a domain size of 20 m x 20 m x 12 m, this translates to 4800 blocks with different hydraulic properties (K_s and ψ_e). These generated properties were fed into STOMP for flow and transport simulations. The choices of domain size and block size were a compromise between a desire for high resolution of the randomly varying parameters (including adequate representation of the geostatistics) and the need to be able to conduct Monte Carlo simulations in a reasonable amount of time on the available computers. The chosen mesh size imposes certain numerical considerations as discussed below.

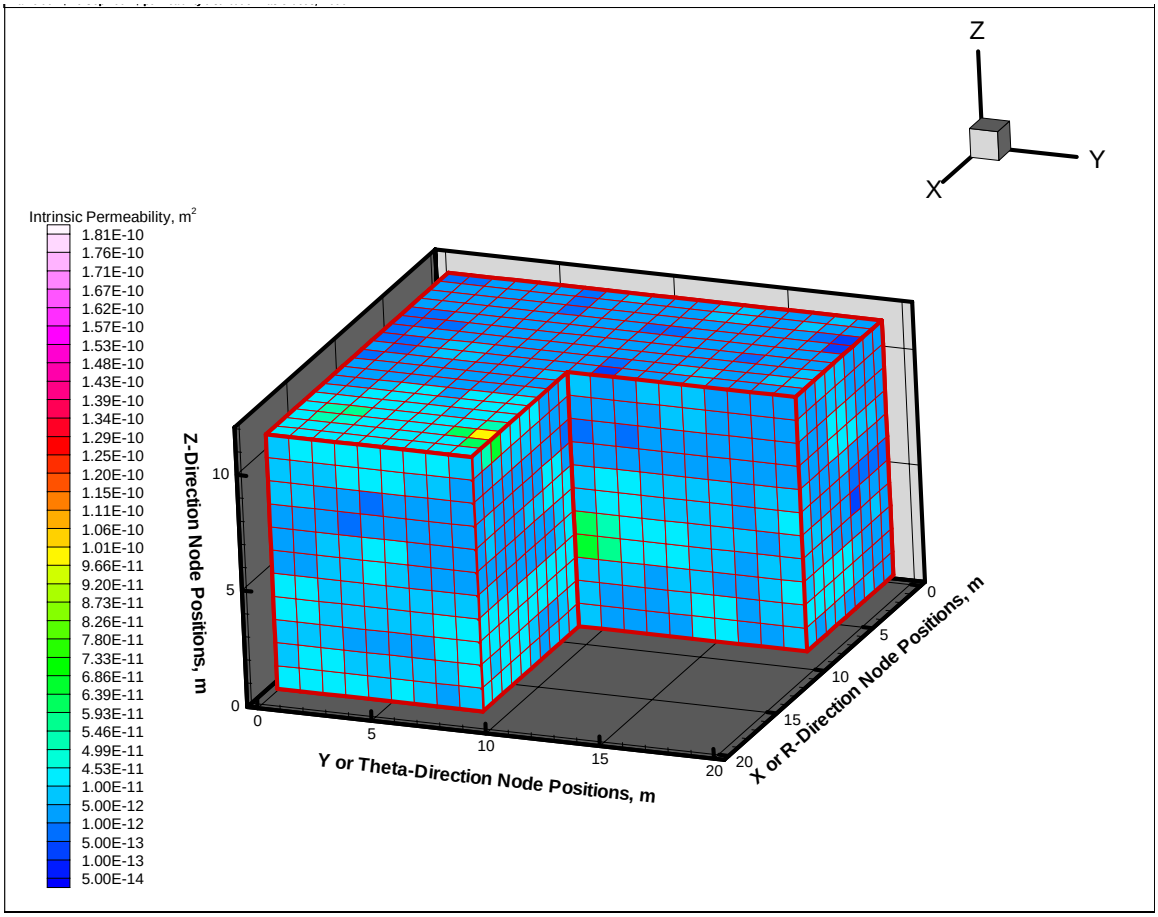

Figure 2-5. Permeability distribution of a single realization (Las Cruces geostatistics)

Table 2-1. Statistics of log(α) for a single realization

Mean	0.0341
Median	0.0344
Standard Deviation	1.01
Kurtosis	-0.0595
Skewness	0.000947
Range	7.17
Minimum	-3.87
Maximum	3.31
Count	4800

Table 2-2. Statistics of log(K_s) and K_s (m/day) for a single realization

	log(K_s)	**K_s**
Mean	1.10	6.38
Median	1.10	3.02
Standard Deviation	1.23	10.7
Kurtosis	-0.06	47.2
Skewness	0.00	5.47
Range	8.75	163.6
Minimum	-3.65	0.03
Maximum	5.10	163.59
Count	4800	4800

Peclet Number (Pe): According to the scheme and solver used in STOMP, the maximum Peclet number allowed is Pe = 2. Since Pe = v dx / D = dx / α_L = ratio of grid spacing to longitudinal dispersivity, the minimum allowed dispersivity is half the cell size. Following Bear (1979, p. 261-263), the numerical dispersivity equals half the mesh size, which also corresponds to Pe = 2. Given the chosen block

Table 2-3. Model parameters used in the STOMP simulations

Parameter	Value (deterministic or stochastic)
Block size	1 m (X, Y, and Z)
Recharge	254 mm/yr (10 inch/yr)
GW gradient	0.02
Pumping rate	118 m^3/yr
Log α - mean	0
Log α - Std. Dev.	0.61
θ_s	0.32
θ_r	0
β (Brooks-Corey)	0.267
Initial source concentration	122 pCi/g (solid) = 8133 pCi/l (liquid)
U-234 Half-life	2.45 x 105 years
K_d	15 cm^3/g
Mean-scaled K_s* (geometric mean)	4.16 m/day = 4.8E-3 cm/s
Mean air entry ψ_e*	5 cm
Particle density	2.65 g/cm^3
Longitudinal dispersivity	0.5 m
Transverse dispersivity	0.1 m

size, this Peclet number constraint determined the longitudinal dispersivity of $\alpha_L = 0.5$.

Courant Number (Co): The Courant number condition imposes a limit on the maximum size of the time step in a numerical simulation. Co = v (dt/dx) = (q/θ)(dt/dx) < 4 was suggested by El-Kadi and Ling (1993) and El-Kadi (1995). For the STOMP code, Co = q (dt/dx) < 1 has been suggested.[1] The largest flux (q) we encountered in our simulations is about 4 cm/hr in the saturated zone (θ = 0.32). Following El-Kadi's formulation, since dz = dx = 1 m = 100 cm, dt < (0.32/4)x100x4 = 32 hours. However, such high flux rates are limited to the vicinity of the pumping well, while fluxes in the vadose zone are dominated by the recharge (the boundary condition), which is q ≅ 0.0029 cm/hr. Statistics of the vertical flux are given in Table 2-4 for a uniform domain and two different random realizations, one with a low variance (of α) and one with a high variance. A histogram of the vertical flux for the low-variance random realization is shown in Figure 2-6. The mean and median values given in Table 2-4 are smaller than the local maximum rate around the well by three orders of magnitude, implying much higher allowable time steps.

Table 2-4. Statistics of vertical fluxes (cm/hr) in uniform and random realizations (Las Cruces statistics)

	Uniform	Low Variance	High Variance
Mean	0.00208	-0.00662	-0.00498
Median	0.00288	-0.00297	-0.00277
Std. Dev.	0.00107	0.0667	0.0577
Kurtosis	-0.872	32.4	63.8
Skewness	-0.878	-1.40	1.26
Range	0.00299	1.74	1.78
Minimum	0	-0.933	-0.805
Maximum	0.00299	0.812	0.973
Count	4800	4400	4800

[1] M.D. White, personal communication, May 2001.

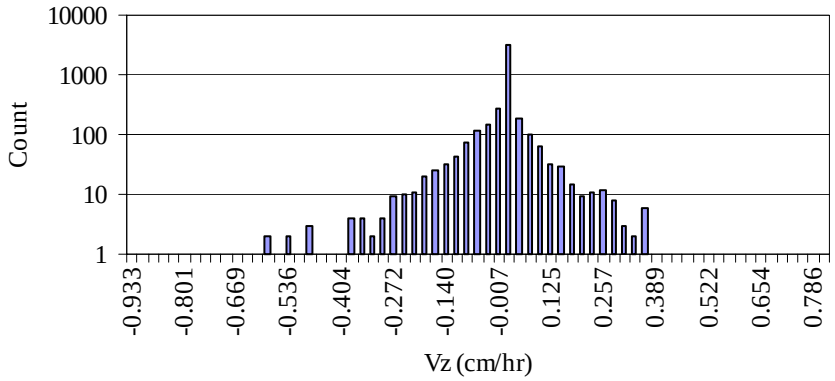

Figure 2-6. Histogram of vertical flux in a low-variance, random realization

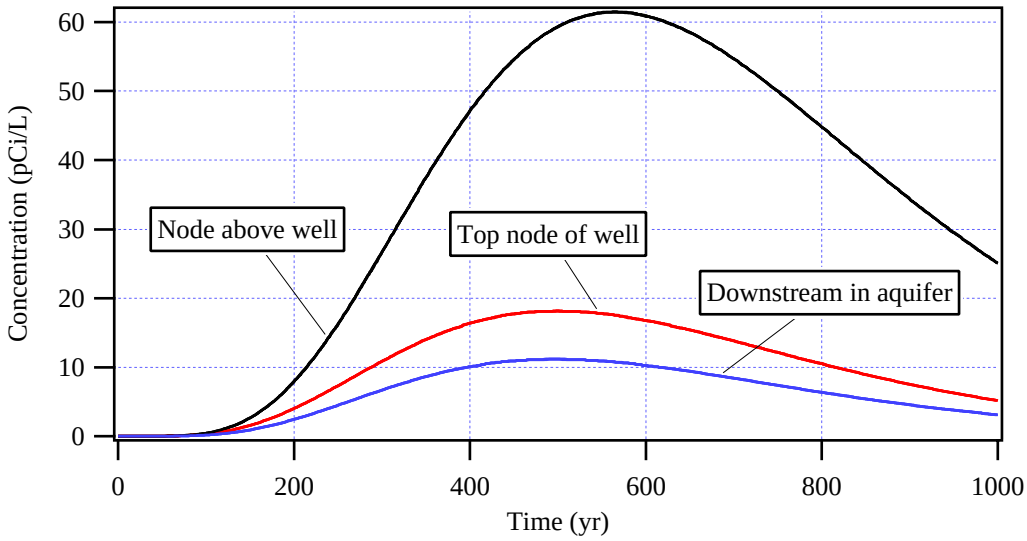

Figure 2-7. Comparison of concentrations at three locations in the domain using three different maximum time step sizes (300, 900, and 2600 years) for a random realization (#81). Note, concentration differences are negligible.

We experimented with transport simulations, incrementing time steps from dt = 30 up to dt = 5000 hours. A few results using an extreme random realization are shown in Figure 2-7. These are concentrations over time at the top node of the well screen, at the node just above the water table at the well location, and at a node downstream from the well, 2.5-m from the aquifer bottom, half way between the contaminated zone and the outflow boundary. The results indicate practically identical transport at least up to dt = 2600 hours. We found similar results from simulations of a more variable random field (with twice the standard deviation). Nevertheless, we selected the value of 600 hours as the maximum time step allowed in most transport simulations.

As was stated earlier, the choice of grid resolution of 1 m^3 was a compromise. High resolution is desirable for two reasons: (a) to avoid upscaling of parameters obtained from core samples, and (b) to include as many elements as possible within an integral scale, such that the spatial variability is captured and is represented correctly by the spatial variogram. Several studies (e.g., Orr, 1993) have shown the need for at least 5 elements, preferably 10, per integral scale. A block size of 1 m implies upscaling of hydraulic properties from the smaller core size. The 1-m block size still provides a fair representation of lateral correlation, with an integral scale of about 6.4 m (from Eq. 2-3), but misses the vertical correlation, with almost one block per integral scale. This is not too disturbing because the short correlation scale implies almost no correlation vertically anyway. Note that within blocks there is perfect vertical correlation. Another important factor is the effect of boundary conditions governed by the distance of stresses and responses in the aquifer from the boundaries. A distance of at least three to five integral scales is needed in order to ignore boundary effects (Orr, 1993). Our random fields are generally below this threshold with about three correlation scales across the domain.

Due to the limited size of the domain, we do not expect it to be ergodic; this means that we cannot imply ensemble statistics from spatial statistics and vice versa. Nevertheless, the univariate statistics and spatial (experimental) variograms were shown (in Section 2.1.1) to be close to the theoretical (ensemble) values. The Monte Carlo simulation results presented in Chapters 3 and 4 are all sample-ensemble quantities (mean, variance, covariance).

In order to have an idea about possible deviations from a more rigorous resolution, we ran a few simulations with double the grid resolution, i.e., 40 x 40 x 24 blocks (block size of 0.5-m on each side). Figure 2-8 shows results as concentration profiles with depth at the (x, y) location of the well for the two resolutions using a uniform domain. The bottom 5 m in each plot represents the well (and the saturated zone). The similarity between the results leads us to the conclusion that the 1-m block size is acceptable. The difference in the location of the peak is due to the effective difference in the location of the bottom of the contaminated zone: 1.0 m for the low resolution grid and 0.5 m for the high resolution grid. Note that this comparison does not address the question of domain size relative to the correlation scale and the overall effects of boundary conditions.

The matrix solver of preference in STOMP for large and complex domains is SPLIB – a preconditioned conjugate gradient solver. STOMP also includes different weighting

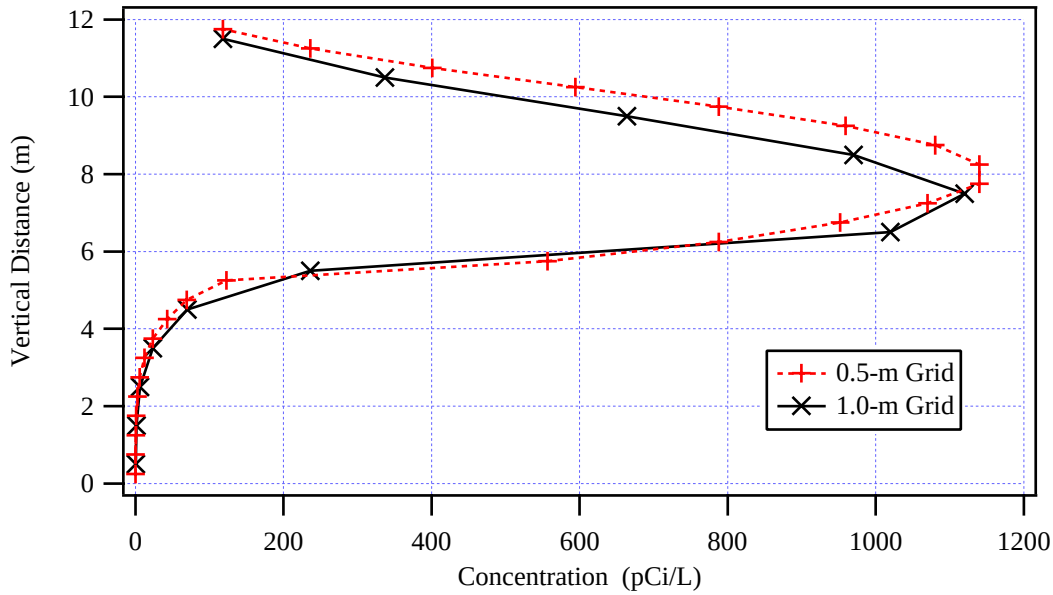

Figure 2-8. Concentration depth profiles at the (x, y) location of the well using a 1-m grid and a 0.5-m grid for a uniform domain after 500 years

schemes for transport calculations, namely Patankar (the default), TVD, and Superbee. We experimented and compared the performances of these schemes in an attempt to maximize time step size, minimize dispersion, and optimize grid resolution. Results from our experiments are shown in Figure 2-9. The figure shows concentrations of U-234 over time (breakthrough curves) at three different locations – the top node of the well screen, one node just above the well, and one point downstream, half way between the well and the outflow boundary. A close look at the breakthrough curves, and a comparison with breakthrough curves generated by simulations with different maximum time steps revealed high sensitivity of the TVD and Superbee schemes to the maximum time step, while the Patankar scheme showed robustness and consistency over a large range of maximum time steps. Therefore, we used the Patankar scheme in all our STOMP simulations.

2.1.5 Sample Results from Single Realizations

This section shows a sample of some of the results obtained from single realization simulations with STOMP. Figures 2-10 and 2-11 show distributions of saturation, pressure head, and total head resulting from steady state flow (imposed by steady recharge) in a nonuniform realization (of hydraulic conductivities and air-entry values) from the random field described above. The heterogeneous nature of the domain is clearly illustrated along with the location of the water table. Figure 2-12 shows the evolution of the U-234 plume within the nonuniform domain over 900 years in 100-year increments. For this particular plume realization, it can be seen that there is a significant concentration gradient with depth in the aquifer and that a portion of the contaminant is not captured by the pumping well. In addition, concentrations are highest in the unsaturated zone.

Breakthrough curves resulting from flow and transport simulations in a single random realization are shown in Figure 2-13. Concentrations at four locations in the domain are shown: in the unsaturated zone directly above the well, at the top and bottom nodes of the well, and downstream at the top of the aquifer, half-way between the source and the boundary. The average concentration in the five nodes comprising the well is also shown. The behavior observed in Figure 2-12 is seen here in detail. The concentration in the unsaturated zone is significantly larger than in the aquifer. In addition, the concentration at the top of the well is much larger than at the bottom of the well. The peak average well concentration for this realization was about 30 pCi/l.

To provide additional detail on the complex model results, Figure 2-14 shows a series of concentration profiles with depth at the location of the well as obtained from a STOMP simulation for a single random realization. These profiles illustrate the limited vertical mixing in the aquifer and the significant dilution in the aquifer due to horizontal flow.

2.2 Simplified Representation

The simplified representation of the test case site was made as close to the complex representation discussed above as

possible. The primary differences were required by the conceptual model embodied in RESRAD and are summarized here.

- One-dimensional flow and transport. RESRAD is limited to a one-dimensional analysis.
- Uniform domain. RESRAD allows for multiple layers in the domain, but since there were no distinct layers observed at the Las Cruces Trench site, the test case was modeled as statistically homogeneous in the complex representation and as homogeneous in the simplified representation.
- Unit hydraulic gradient in the unsaturated zone. RESRAD makes the unit gradient assumption to simplify the unsaturated flow solution. This assumption is not required by STOMP, which solves the Richards equation for flow in the unsaturated zone.
- Simplified aquifer mixing model. RESRAD uses a simplified analysis to estimate mixing and dilution in the aquifer. The primary reason a three-dimensional analysis was adopted for the complex representation was to more accurately represent the effect of the pumping well.

The RESRAD domain consisted of a 1-m thick contaminated zone above a 6-m unsaturated zone (7 m total of unsaturated soil) and a 5-m saturated zone. There was no cover over the contaminated zone, which was 8 m x 8 m in area. Based on the characterization of the Las Cruces Trench site soils, all soils in the test case (contaminated zone, unsaturated zone, and aquifer) were classified as a sand. Precipitation was set at 25.4 cm/y with irrigation, evapotranspiration, and runoff set to zero, resulting in the required recharge rate. As discussed above, the source term was calculated using RESRAD.

In the RESRAD Monte Carlo simulations, the hydraulic properties of the unsaturated zone and the aquifer were modeled as random parameters. This is the corollary of the three-dimensional Monte Carlo simulations carried out with STOMP. Note that statistically, however, the Monte Carlo simulations have different meanings for the two representations. The RESRAD model (1-D) assumes univariate statistics, i.e., either multiple scenarios (an ensemble) of uniform domains, or multiple parallel non-interacting columns averaged in space. The STOMP model (3-D) assumes a multivariate joint distribution, i.e., multiple scenarios of spatially correlated random realizations (a spatially correlated random field).

Two sets of distributions of the soil hydraulic parameters were used for the RESRAD simulations. One of these was a set of generic distributions taken from NUREG/CR-6565 (Meyer et al., 1997). Distributions for the sand classification were selected. For the saturated hydraulic conductivity, log-normal distributions with the mean and standard deviation given in NUREG/CR-6565 were used instead of the specified beta distributions. These parameter distributions are given in Tables 2-5. Correlations between parameters greater than 0.6 as given in NUREG/CR-6565 were included in the simulations.

The second set of distributions used with RESRAD was based on data from the Las Cruces Trench site. These parameter distributions are given in Table 2-6. Compared to the generic distributions, the following changes were made. Mean bulk density was set to the value implied by the

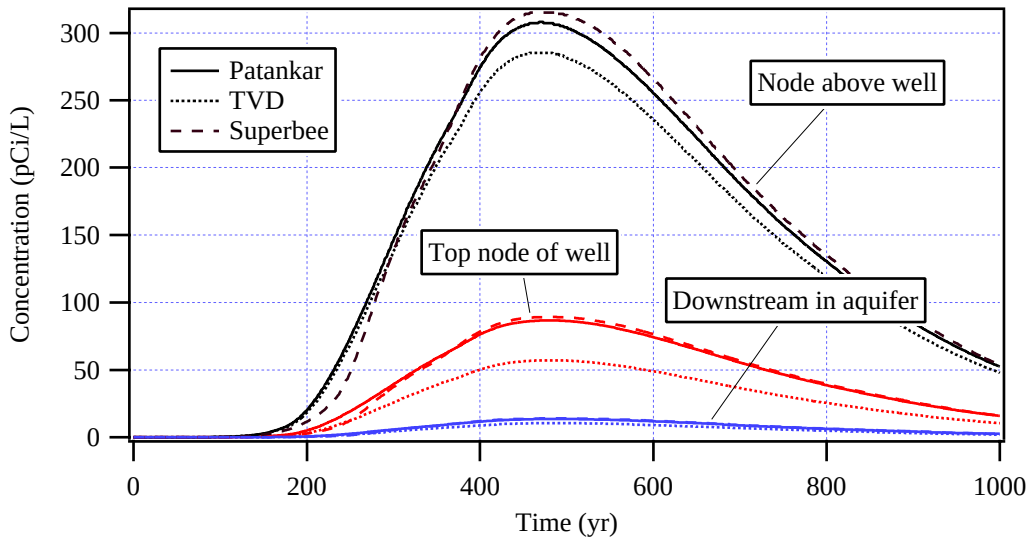

Figure 2-9. Comparison between different weighting schemes for transport simulations at three locations in the domain

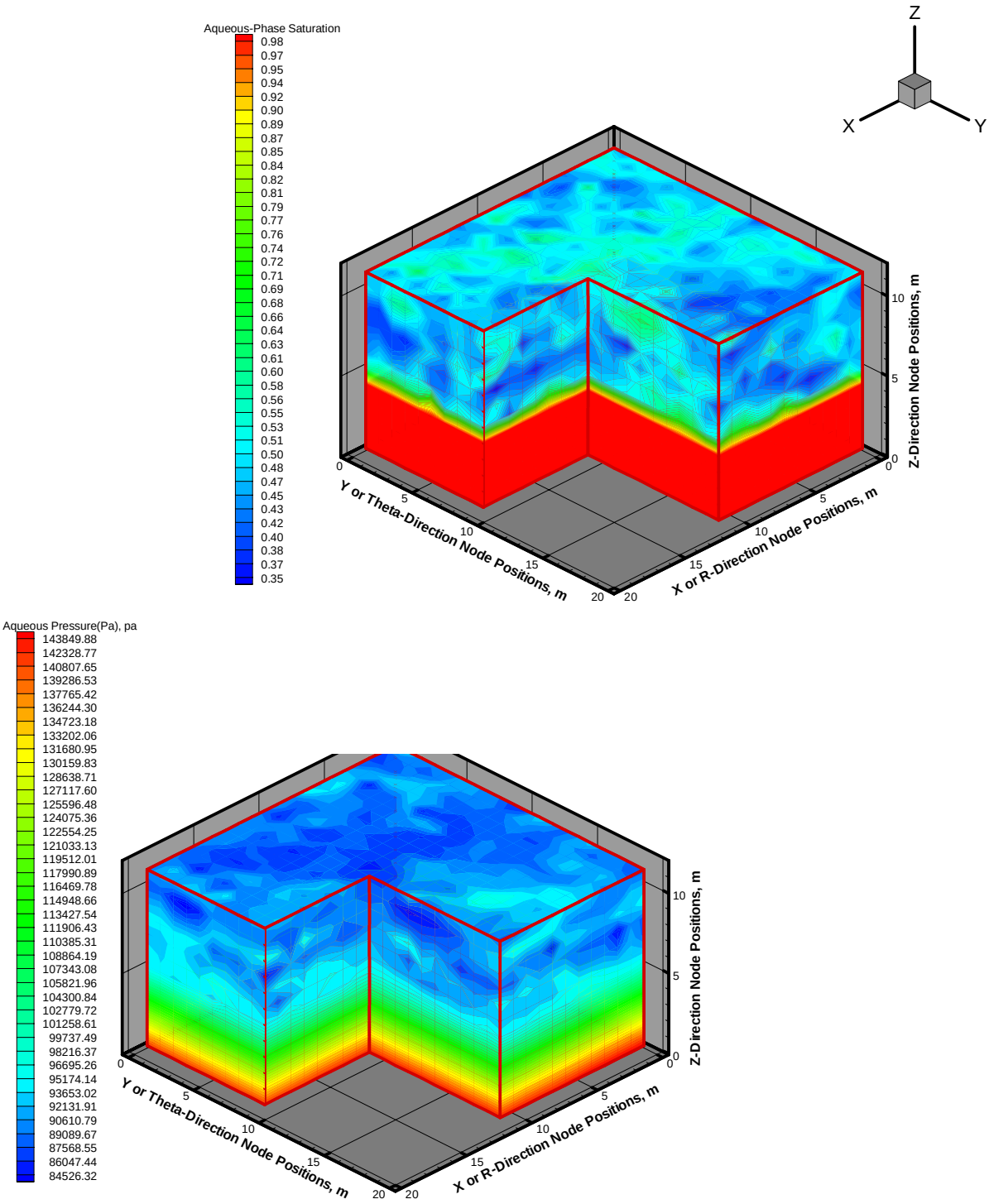

Figure 2-10. Saturation (top) and pressure (bottom) distributions in a nonuniform (random) realization (Var[ln(K_s)] = 1.5)

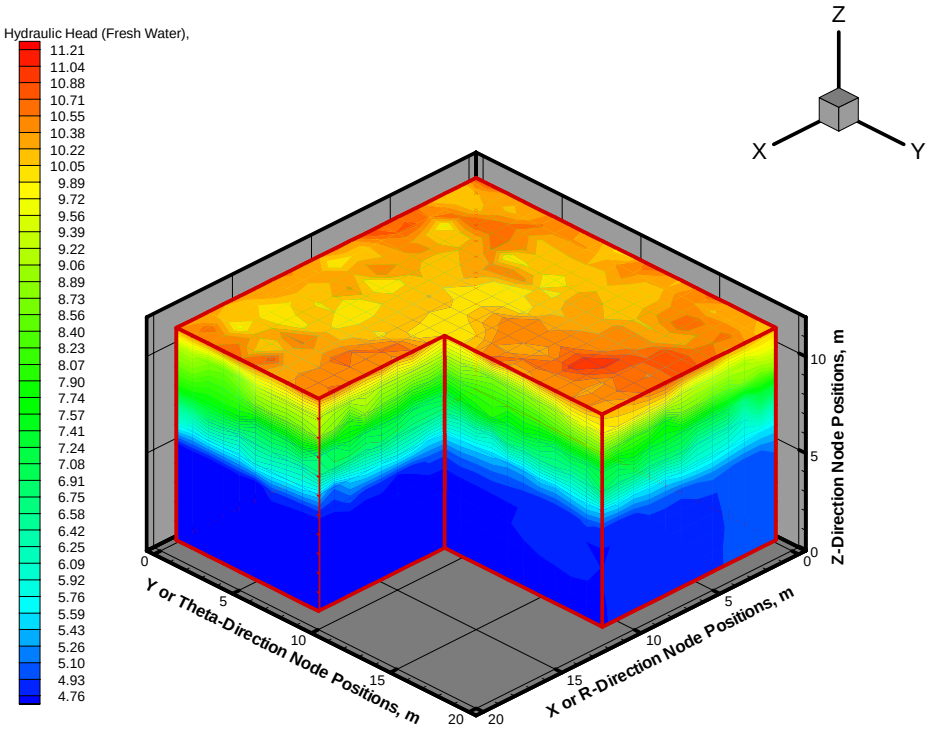

Figure 2-11. Total head distribution for the same realization as Figure 2-10

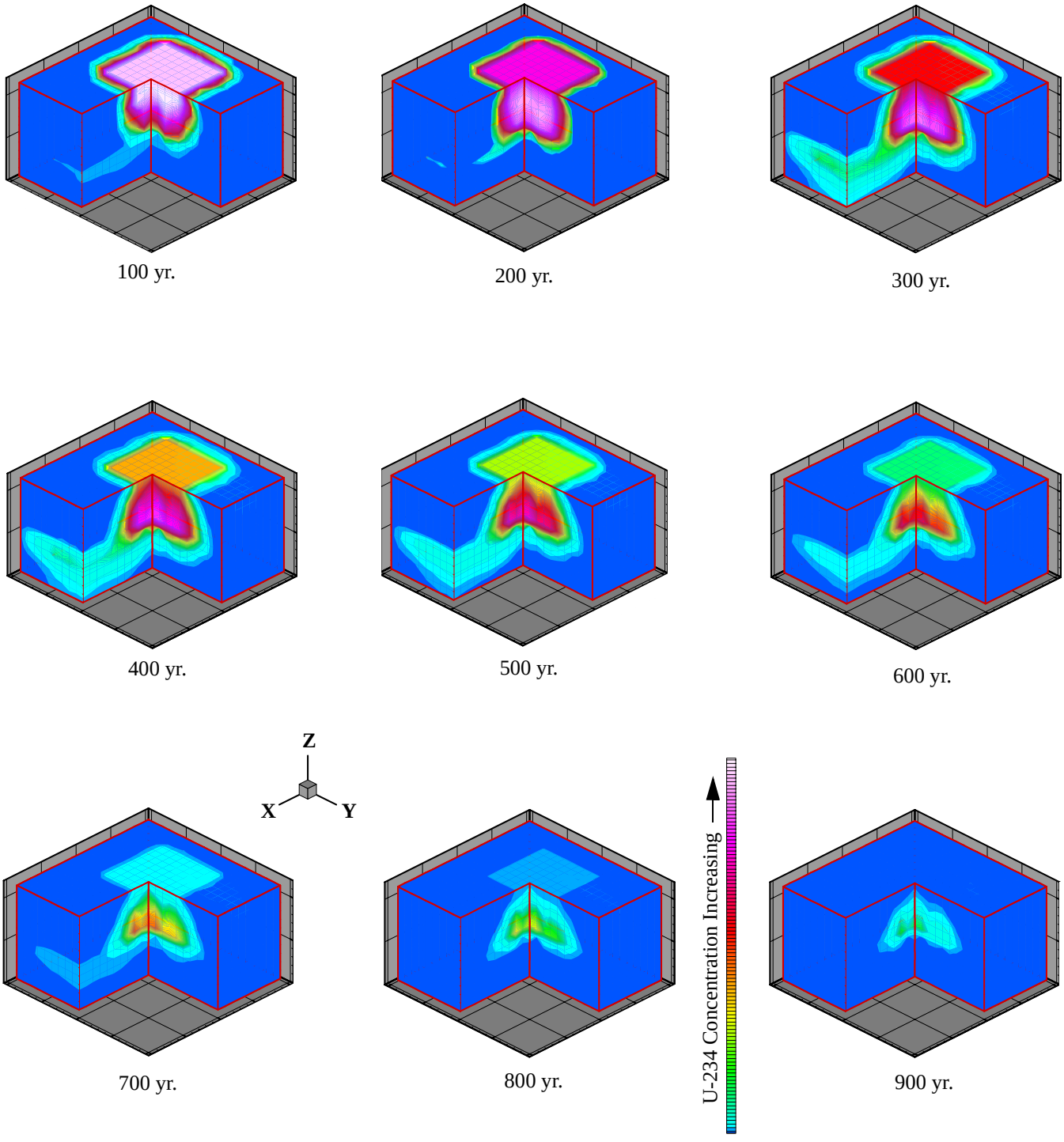

Figure 2-12. Snapshots of the simulated U-234 plume including transport from the source, extraction from the well, and radioactive decay. The snapshots are in 100-year increments, from 100 years to 900 years after the initial release.

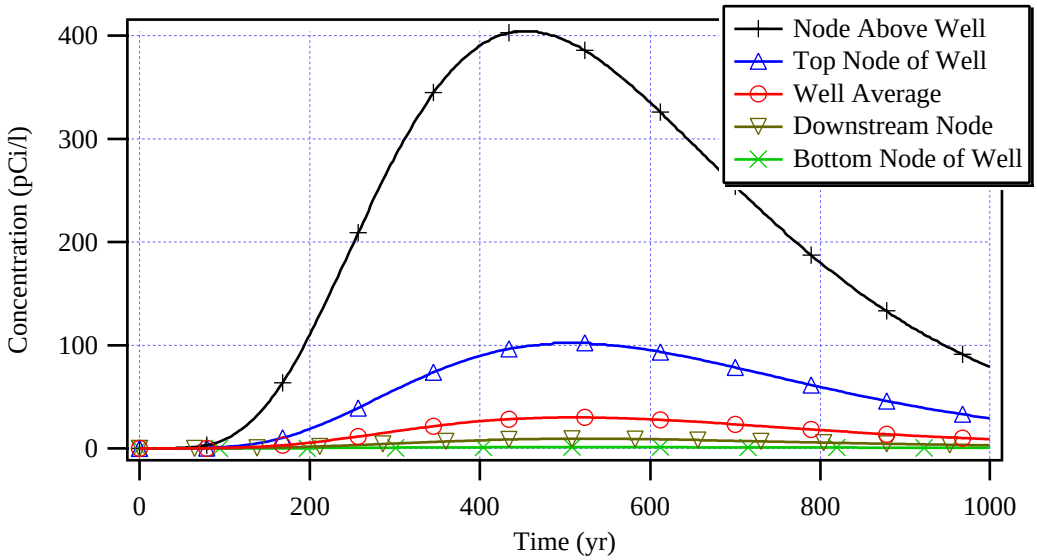

Figure 2-13. Breakthrough curves from a single random realization at four locations in the domain and for the average of the five well nodes

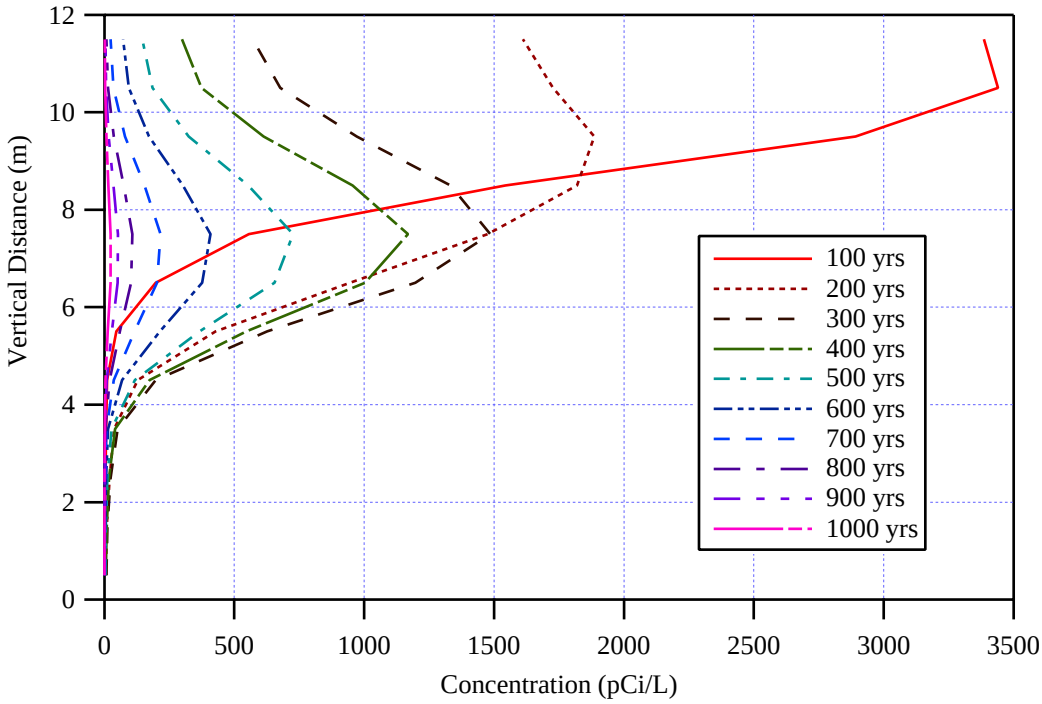

Figure 2-14. Vertical profiles of concentration at the (x, y) location of the well as calculated by STOMP for a randomly heterogeneous realization

measured average porosity of 0.32 and a particle density of 1.8 g/cm^3. The Las Cruces Trench sample mean and variance of the saturated water content were used for the porosity moments. The effective porosity distribution was set equal to the total porosity distribution. The distribution of the unsaturated zone soil-type exponent was based on the van Genuchten water retention parameters derived from the Las Cruces Trench data. The soil-type exponent (b) was calculated from the van Genuchten parameters using the relationship presented in NUREG/CR-6565 (Appendix C). Field-measured values of saturated hydraulic conductivity were used as the basis for the K_s distributions. Lognormal distributions were assumed for both b and K_s. The sample mean values of ln(b) and ln(K_s) were taken as the geometric mean values of the parameter distributions. The variance of the ln(b) and ln(K_s) parameter distributions were determined from a relationship presented in Gilbert (1987; Eq. 4.14) for the variance of the mean.

$$Var(\bar{x}) = \frac{\sigma^2}{n}\{1 + \rho_c(n-1)\} \qquad (2\text{-}4)$$

where

$Var(\bar{x})$ =the variance of the estimated mean site value for ln(b) or ln(K_s)

σ^2 = 0.2768^2 and 1.2134^2, the sample variances of the ln(b) and ln(K_s) measurements, respectively

n = 448, the number of measurements

ρ_c = 0.033, the average cross-correlation between the measurement locations

This relationship considers the multitude of samples at the Las Cruces Trench site and the spatial correlation of those samples. The value of ρ_c was derived from the spatial covariance of K_s (discussed above) and the known measurement locations from the Las Cruces Trench. The same value of ρ_c was used for ln(b). The means and standard deviations listed in Table 2-6 for the soil-type exponent and the saturated hydraulic conductivity parameter distributions were calculated from the estimated mean and variance of the mean for ln(b) and ln(K_s) (see, for example, NUREG/CR-6565, Appendix A). The same correlations between parameters used with the generic distributions were applied to the site-specific distributions.

Table 2-5. Generic stochastic parameter inputs used in RESRAD simulations - default distributions from NUREG/CR-6565 for a sand soil

Parameter	Distribution	Mean	Std. Dev.	Min.	Max.
Unsat. Zone Bulk Density (g/cm^3)	normal	1.58	0.158	1.092	2.068
Unsat. Zone Total Porosity	normal	0.43	0.06	0.245	0.615
Unsat. Zone Effective Porosity	normal	0.383	0.061	0.195	0.571
Unsat. Zone Field Capacity	normal	0.061	0.015	0.015	0.107
Unsat. Zone Sat. Hyd. Conductivity (m/yr)	lognormal	2604.5	1388.0	490.3	10775.2
Unsat. Zone Soil-Type Exponent	lognormal	0.998	0.218	0.500	1.901
Saturated Zone Bulk Density (g/cm^3)	normal	1.58	0.158	1.092	2.068
Saturated Zone Total Porosity	normal	0.43	0.06	0.245	0.615
Saturated Zone Effective Porosity	normal	0.383	0.061	0.195	0.571
Saturated Zone Sat. Hyd. Conductivity (m/yr)	lognormal	2604.5	1388.0	490.3	10775.2

RESRAD has two options for modeling mixing and dilution in the aquifer, referred to as the Mass Balance and the Nondispersion models. Based on the size of the contaminated zone (8 m x 8 m) and the guidance presented in the RESRAD documentation, the Mass Balance model would be recommended for this test case. Deterministic results using the site-specific mean parameter values are shown for both models in Figure 2-15. (Note that the scaled mean values for K_s and b=1/β from Table 2-3 were used in the deterministic RESRAD simulations, not the mean values from Table 2-6.) This figure shows well concentrations as a function of time and illustrates a number of points. Well concentrations from RESRAD reflect the shape of the source concentration (Figure 2-2) for a contaminant that experiences little decay over the time period of the simulation. In addition, the Mass Balance model results in a significantly larger peak concentration in the well, ten times larger in this case. By comparing the RESRAD results to the STOMP results in Figure 2-13, it can be seen that both RESRAD models predict a higher peak well concentration. The peak of the well concentration for this single STOMP realization was approximately 30 pCi/l, about one-third of the RESRAD Nondispersion model result. (As will be shown in Chapter 3, the ensemble average peak well concentration

Table 2-6. Site-specific stochastic parameter distributions used in the RESRAD simulations - based on the Las Cruces Trench dataset where applicable (compare to Table 2-5)

Parameter	Distribution	Mean	Std. Dev.	Min.	Max.
Unsat. Zone Bulk Density (g/cm^3)	normal	1.8	0.158	1.312	2.288
Unsat. Zone Total Porosity	normal	0.32	0.034	0.215	0.425
Unsat. Zone Effective Porosity	normal	0.32	0.034	0.215	0.425
Unsat. Zone Field Capacity	normal	0.061	0.015	0.015	0.107
Unsat. Zone Sat. Hyd. Conductivity (m/yr)	lognormal	1559.3	360.2	751.1	3073.3
Unsat. Zone Soil-Type Exponent	lognormal	3.239	0.169	2.755	3.799
Saturated Zone Bulk Density (g/cm^3)	normal	1.8	0.158	1.312	2.288
Saturated Zone Total Porosity	normal	0.32	0.034	0.215	0.425
Saturated Zone Effective Porosity	normal	0.32	0.034	0.215	0.425
Saturated Zone Sat. Hyd. Conductivity (m/yr)	lognormal	1559.3	360.2	751.1	3073.3

was approximately 25 pCi/l.) It can also be observed, however, that with RESRAD there is an inherent delay in arrival of contaminant at the well until the peak arrives. As a result of dispersion, STOMP predicts a much earlier first arrival of contaminant at the well.

The RESRAD Mass Balance model assumes instantaneous distribution of contaminant throughout the depth of the aquifer and that all contaminant is withdrawn through the well. Figures 2-12 to 2-14 illustrate that these conditions are not reflected in the complex representation results. Contaminant can be seen being transported out of the domain in this figure. Only limited vertical mixing in the aquifer is indicated by the results of the complex representation. Based on the observations from the single realization STOMP simulations, it was decided that the RESRAD Nondispersion model was more representative of the STOMP results. Only results from the Nondispersion model are reported in the remainder of this report.

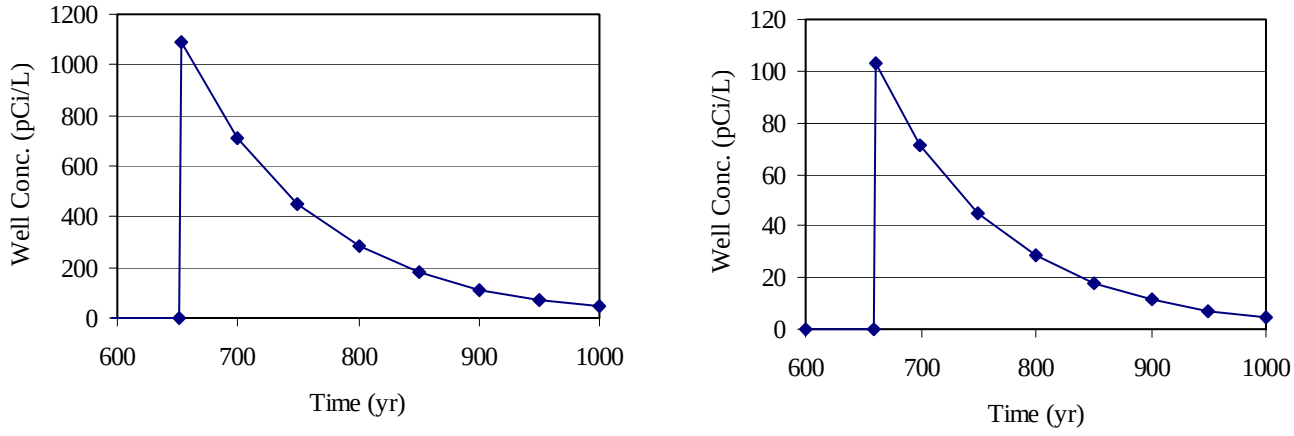

Figure 2-15. Concentration in the well for the RESRAD Mass Balance (left) and Nondispersion (right) models

3 Base Case Monte Carlo Simulation Results

This chapter presents the results of Monte Carlo simulations for the complex representation of the test case (using STOMP) and the simplified representation (using RESRAD). RESRAD v. 6.0 has a built-in Monte Carlo simulation capability. STOMP, however, required some additional work to allow it to be used in a Monte Carlo mode with minimal user interaction. Several programs and scripts in Fortran and C-Shell were written in order to perform a variety of tasks: translating generated random fields of scaling factors to other parameters (K_s and ψ_e); writing these to valid STOMP input files; extracting the required results from the STOMP output files; and calculating the ensemble statistics. STOMP simulations were run on a number of machines. Sequential runs were carried out on SGI and SUN Unix machines. In addition, a "task farm" script and a C++ program were written for parallel processing on one of the supercomputers at PNNL. Because of the independence of each realization, one of the available programs that utilize free processor time on a network of PCs or Unix machines could also be used.

3.1 STOMP Ensemble Mean Results

We started with the base case of mild variability, with variance of $\log(K_s)$ equal to 1.5. We generated 300 realizations of K_s and ψ_e and ran 300 simulations of flow and transport using STOMP. The resulting sample-ensemble mean concentrations of U-234 at different locations are shown in Figure 3-1. Average concentration at the five nodes comprising the well is shown along with plus and minus one standard deviation from this average. Maximum well concentrations are also shown. In addition, ensemble mean concentrations at the node immediately above the well and at a downstream node at the top of the aquifer are shown. Average well concentration and concentrations at individual nodes are also shown in the figure on a log scale to accentuate the differences, particularly between well nodes.

In Figure 3-1, well concentration is calculated as the arithmetic weighted average of the five well nodes (assuming mean uniform mixing within the pumping well). Note that ensemble mean concentrations 1 m above the well are 10 times higher than mean well concentrations. This is because this point is in the vadose zone, just above the capillary fringe, with a lower water content and no dilution from aquifer effects. Note also that the confidence intervals (defined here by ± one standard deviation of well concentration) seem relatively narrow due to relatively low concentration variance, implying overall low sensitivity of well doses to domain heterogeneity. The maximum well concentration (over 300 simulations) is about double the average well concentration.

Figure 3-2 shows the development of ensemble variance of well concentrations at a point in time (and space) as a function of the number of simulations. This is a measure of sample robustness, i.e., it shows how many simulations are needed to reach a stable, representative sample variance. The figure implies stabilization after 200 simulations. This prompted us to reduce the number of simulations in a later stage of our numerical experiments (a significant savings of computer time).

Figure 3-3 compares the well concentration obtained as the ensemble mean of the 300 realizations to the well concentration obtained from a single (deterministic) simulation using the scaled mean parameters (K_s* and ψ_e*), where K_s* also equals K_g, the geometric mean. The modest difference in peak concentration of only 20% is remarkable. If this difference was in hydraulic heads (rather than concentrations), it would be expected to shrink to zero under two-dimensional mean uniform, horizontal flow. In our case, despite the three-dimensional, mixed vertical, unsaturated flow and transport in the vadose zone and (essentially) horizontal, radial flow and transport in the aquifer, the geometric mean of saturated hydraulic conductivity is an acceptable rough estimate of the effective conductivity of the whole complex domain for transport calculations. The scaled mean parameters represent approximate equivalent uniform parameters in the sense that the well concentrations in the uniform case are an approximation of the ensemble average well concentrations. Calculations with the scaled mean parameters were done either as initial tests, or for comparison of numerical schemes (e.g., between solvers), or for sensitivity analyses (wherever permissible).

A rigorous analysis of equivalent parameters for this particular transport problem was beyond the scope of this project. However, since (a) the parameter distributions were based on the scaling assumption, (b) the geometric mean has been shown to be the expected effective hydraulic conductivity in two-dimensional domains and in slightly heterogeneous three-dimensional domains (with relatively small variance) (Orr, 1993; Neuman and Orr, 1993)[1], and (c) Figure 3-3 (and other results) show a fair similarity between mean breakthrough curves and breakthrough curves obtained with the geometric mean K_s, for the purpose of this study we consider the scaled mean parameter values to be acceptable equivalent uniform parameter values. Figure 3-3 demonstrates, however, that the use of the scaled mean parameters in a deterministic analysis will not completely match the ensemble mean well concentration (missing it by 20%) and that the deterministic results may not be conservative.

[1] Note that the formulations discussed in these publications are based on hydraulic responses in fully saturated domains; our case focuses on concentration/doses in a complex unsaturated-saturated domain.

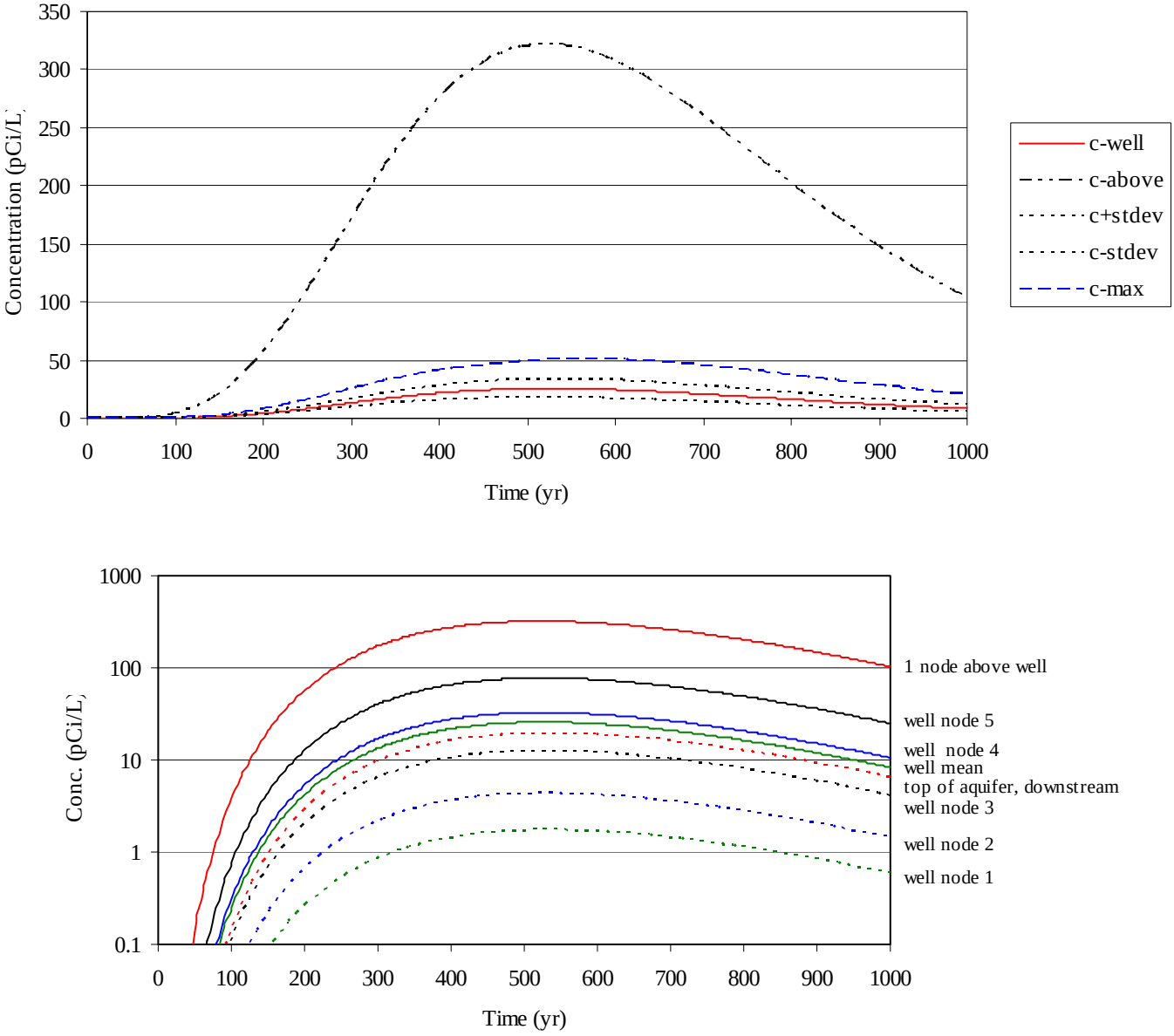

Figure 3-1. Top: Concentrations at the well with plus/minus one standard deviation, maximum well concentration, and concentration in the unsaturated zone immediately above the well, Bottom: Concentration on a log scale for the five nodes comprising the well (numbered from bottom to top of the aquifer), the node just above the well in the unsaturated zone, a downstream node, and the mean well concentration (bottom). Results are ensemble averages (except for c-max, c-stdev, and c+stdev) for the base case using 300 realizations.

3.2 Dose Distributions and Comparison

The base case RESRAD Monte Carlo simulation also consisted of 300 realizations. As discussed in the previous chapter, two sets of soil hydraulic parameter distributions were used in the RESRAD simulations. One was generic distributions and the other set had several mean and variance values based on the data from the Las Cruces Trench site. Because well concentrations are not available from the results of a RESRAD Monte Carlo simulation, comparisons between the two models were made using dose. Well concentrations from STOMP were converted to total effective

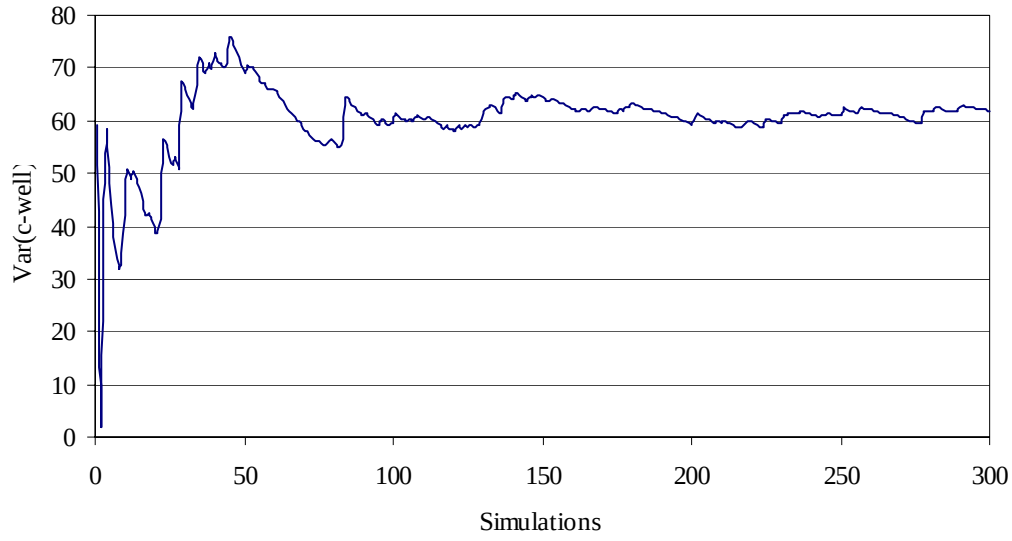

Figure 3-2. Variance of well concentration at 579 years after start of release, as a function of the number of simulations

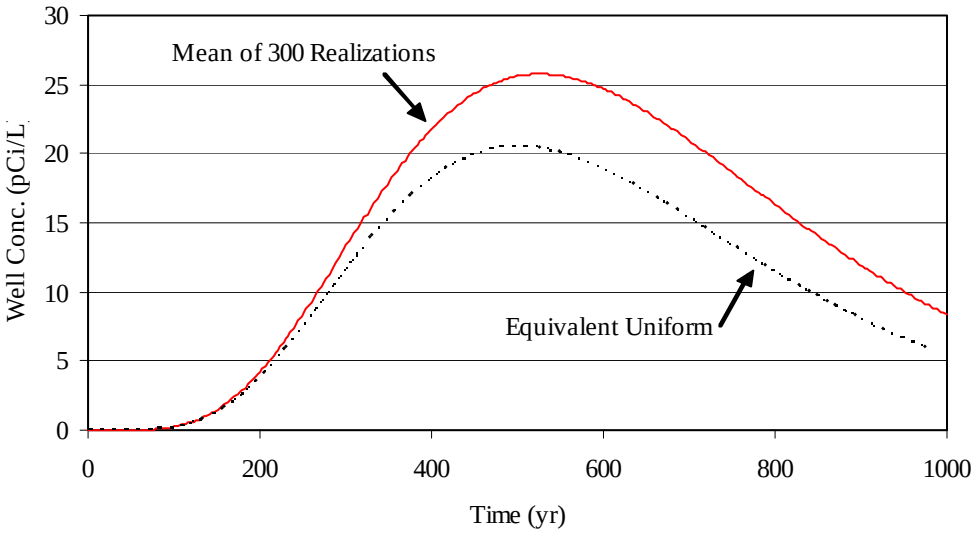

Figure 3-3. Ensemble mean concentration from the STOMP Base Case Monte Carlo simulation compared to the deterministic concentration using equivalent uniform (scaled mean) parameter values. The concentration shown is the arithmetic average of the five well nodes.

dose equivalent by applying the same drinking water ingestion rate and dose conversion factor for U-234 that were used in RESRAD. Limiting the test case simulation to the drinking water pathway simplified this comparison.

Figure 3-4 shows the cumulative distribution functions for peak dose and the time of the peak dose for the STOMP base case simulation and the two RESRAD simulations. Statistics of the peak dose and the time of the peak dose are given in Table 3-1 for the three cases. The STOMP simulations result in a significantly smaller variance, and hence, smaller uncertainty, than the RESRAD simulations for both peak dose and time to peak. This result is not unexpected for the generic case since the variance of the RESRAD parame-

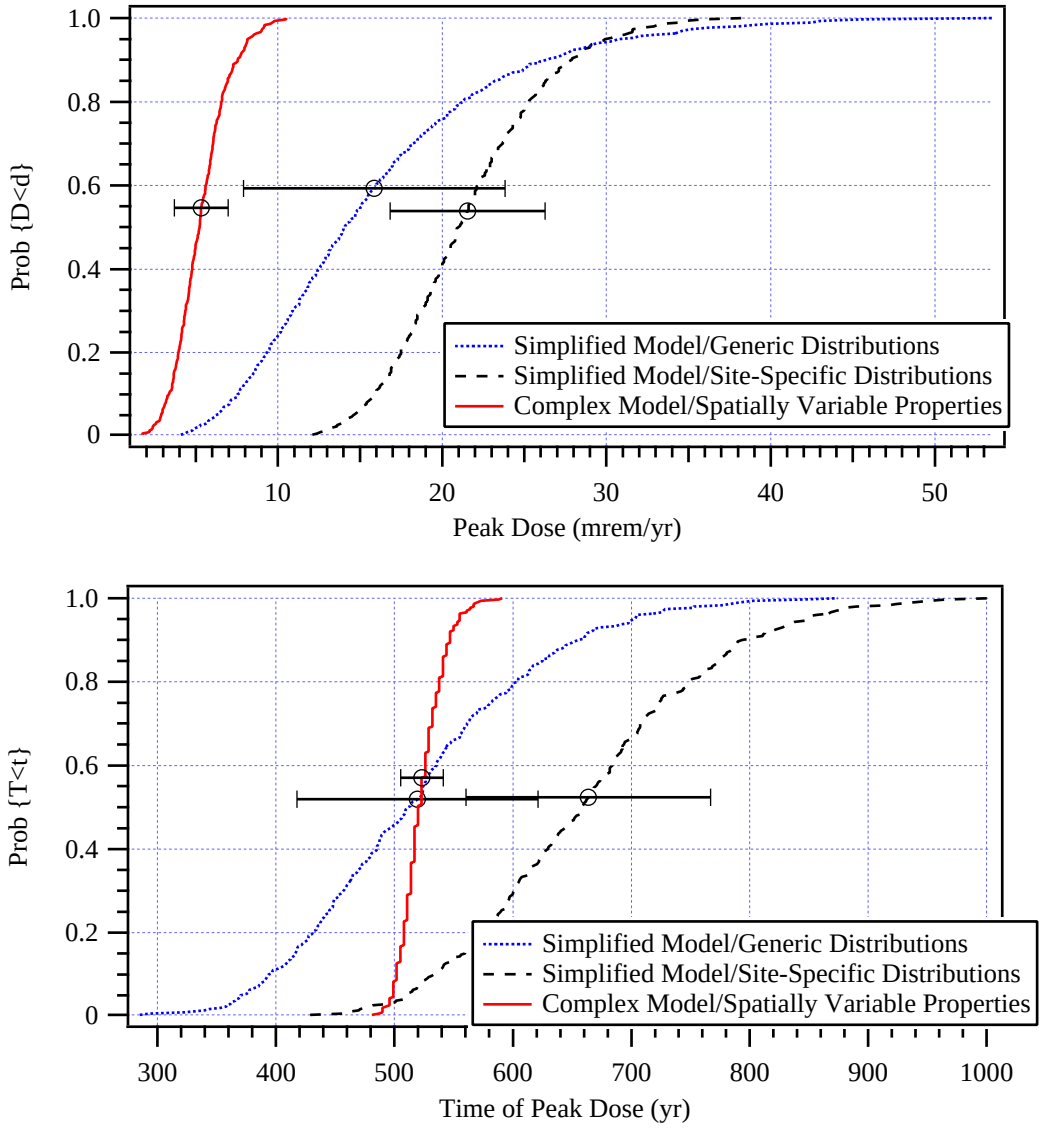

Figure 3-4. Empirical cumulative distribution functions for the peak dose (top) and time of peak (bottom) over 300 simulations for the complex model using STOMP and the simplified model using RESRAD. Error bars represent the mean value and plus/minus one standard deviation.

ters represents the variability over a large number of sites across the United States, while the covariances of the STOMP parameters (K_s and ψ_e) and resulting concentrations/doses represent the variability at a single site. The larger dose variance from the RESRAD simulation reflects the intended conservativeness of the generic parameter distributions. For the site-specific RESRAD simulation the parameter variances are a mix of generic values and values specific to the Las Cruces Trench site. The reduction in the site-specific peak dose variance relative to the generic case reflects the site-specific K_s data. The lack of a similar reduction in the variance of the time of the peak dose primarily reflects the use of generic parameter values (for the unsaturated zone bulk density in particular).

The mean dose predicted from the RESRAD simulations is larger than the mean dose from STOMP, reflecting the deterministic results presented in Chapter 2. The larger mean dose predicted by RESRAD would be expected if the RESRAD code represented a conservative analysis of the test case.

Table 3-1. Statistics of peak dose and the time of the peak dose for the simplified model with generic parameter distributions, the simplified model with site-specific parameter distributions, and the complex model with spatially varying properties

	Peak Dose (mrem/yr)			Time of Peak Dose (yr)		
	Generic	**Site-Specific**	**Complex**	**Generic**	**Site-Specific**	**Complex**
Number	300	300	300	300	300	300
Minimum	3.2	12.1	1.73	333	429	481
Maximum	56.5	38.3	10.5	729	1003	591
Mean	15.9	21.6	5.3	513	664	523
Std. Deviation	8.2	4.7	1.6	67	103	18
Median	14.2	21.0	5.2	515	659	520

An unexpected result of the simulations is that the use of the site-specific parameter distributions results in a mean dose (and a mean time to peak dose) from RESRAD that is less similar to the STOMP results than when using generic parameter distributions with RESRAD. An explanation for this behavior requires a detailed look at the models (see the following chapter). In the simplest terms, however, the peak dose predicted by RESRAD is primarily a function of the hydraulic conductivity in the saturated zone and the time of the peak dose is primarily a function of the unsaturated zone bulk density (considering only the soil hydraulic parameters listed in Tables 2-5 and 2-6). The differences between the generic and site-specific mean values for these two parameters explain the differences in generic and site-specific mean peak dose and time of peak dose. The relative accuracy of the generic results is thus fortuitous. The behavior displayed in Figure 3-4 reflects the significant structural differences in the simplified and complex models.

The RESRAD distributions of peak dose are highly skewed whereas the peak dose distribution from the STOMP simulation appears closer to normal. The large degree of skewness in the RESRAD results indicates a potential sensitivity to parameter values, particularly to the 1D hydraulic conductivity that constitutes the flow path in the simplified model, an issue that will be discussed in the following chapter.

The mean dose as a function of time is shown in Figure 3-5 for the two RESRAD cases (simplified model) and for the STOMP base case (complex model). The peaks of these mean doses are similar, particularly in magnitude. This result contrasts with the means of the peak dose distributions shown in Figure 3-4, which are significantly different for the three simulations. For the STOMP model, the peak of the mean dose and the mean of the peak dose distribution are almost the same because of the smoothness of the breakthrough curve(s). The RESRAD results for the same quantities are very different for this test case because of the sharpness of the breakthrough curve, which is a result of the lack of dispersion in the model and the form of the contaminant source release function. Differences between the two RESRAD cases shown in Figure 3-5 reflect the higher peak dose and longer time to peak displayed for these same cases in Figure 3-4. Note that doses are underestimated by RESRAD prior to 550-600 years. Note also that similarity of the simulated peak mean and mean peak doses implies robustness and reliability of the complex model, in contrast to the simplified approach. These results are specific to the test case considered and the relationship between the two models' results for the peak of the mean and the mean of the peak doses can be expected to vary with the problem specification, particularly when additional exposure pathways are considered.

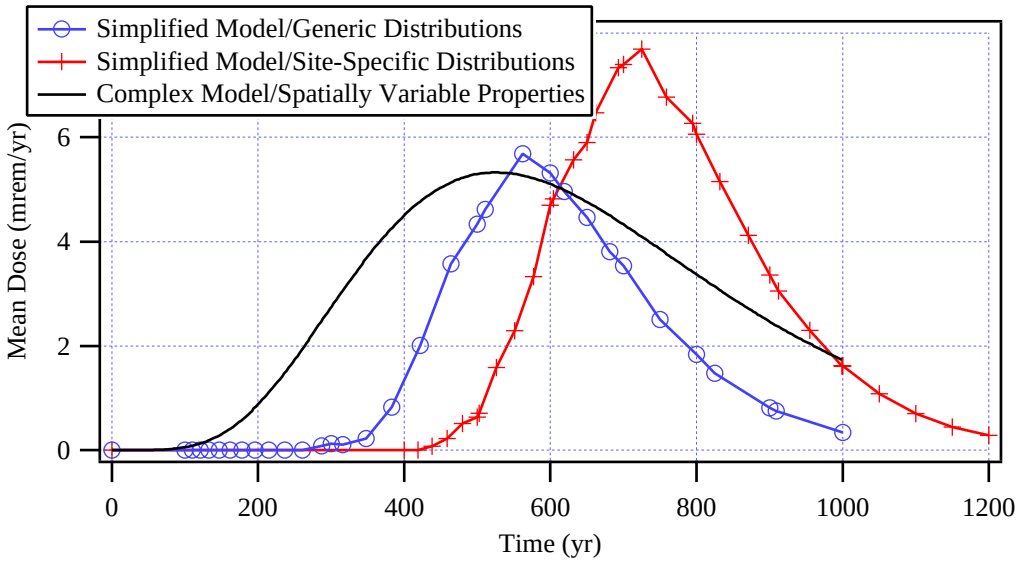

Figure 3-5. Mean dose as a function of time for the complex model using STOMP and the simplified model using RESRAD

4 Sensitivity Cases

An important part of the evaluation of uncertainty estimates as predicted by the simplified and complex models is a comparison of the sensitivity to parameter values. Models that are highly sensitive to certain parameters are worrisome because even small uncertainty in these parameters translates to large uncertainty in predictions. Too much robustness (very low sensitivity) may indicate model weakness or a deficiency in model structure, such as over- or under-parameterization or strong boundary effects. Since the complex model is more representative of reality, ideally we would also like to see that the simplified and complex models are sensitive to the same parameters, thus providing evidence that they represent the flow and transport processes in a physically similar way.

This chapter describes the sensitivity analyses that were carried out with the STOMP and RESRAD models and draws some conclusions from the results.

4.1 Sensitivity to Geostatistical Parameters

The geostatistical characterization of the soil hydraulic properties used in the complex representation requires parameters that have no corollary in the simplified representation. The sensitivity of the STOMP model to these parameters is discussed in this section.

4.1.1 Variance of K_s and ψ_e

Sensitivity of the STOMP model to the degree of heterogeneity was evaluated by conducting a Monte Carlo simulation for a case with double the variance of log conductivity and air entry pressure. This simulation was carried out using the same realizations of the scaling factor, α, but translating the values to double the variance of K_s and ψ_e. This translates to fluctuations in conductivity at least an order of magnitude larger than in the base case. Figure 4-1 shows the resulting ensemble mean breakthrough curves. The figure shows that mean concentrations in the well are slightly smaller than the concentrations simulated in the base case. The variance of the well concentration increased for the high variance case as reflected in the plots of well concentration plus and minus one standard deviation, shown in Figure 4-1. The magnitude of the concentration variance increase was less significant than anticipated, however.

Figure 4-2 shows the variance of well concentration at a point in time as a function of the number of realizations for the high variance case. The well variance is much less stable than for the base case due to the higher variability (compare to Figure 3-2). Here, 200 simulations are not sufficient. Variability of the peak dose and the time of the peak dose did not increase significantly, however. These results indicate relatively low sensitivity of the dose to the degree of heterogeneity in the subsurface. This conclusion may be the result of the small domain used in the simulation, a possibility that was not explored.

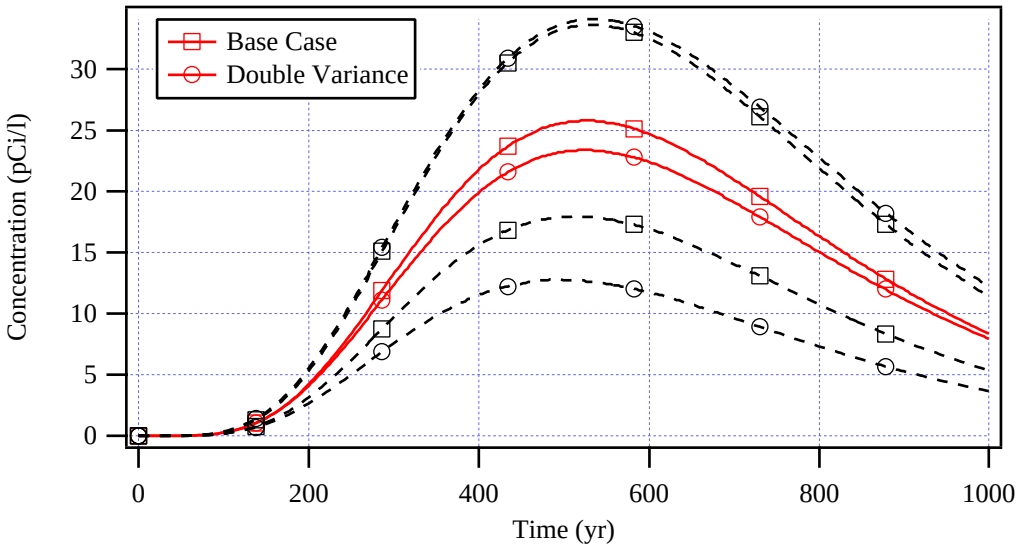

Figure 4-1. Ensemble mean concentration in the well (solid lines) and plus/minus one standard deviation about the mean well concentration (dashed lines) for the base case and a Monte Carlo simulation consisting of 300 realizations with double the variance of log[K_s] and ψ_e

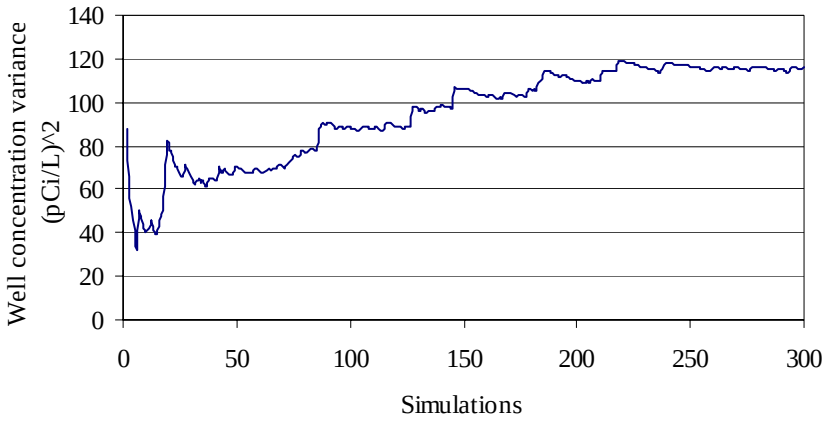

Figure 4-2. Evolution of the variance of the well concentration at 579 years with the number of Monte Carlo realizations - variance of log[K_s] two times the base case value

4.1.2 Correlation Scale

Monte Carlo simulations were also carried out to evaluate the sensitivity to correlation scale. Two simulations consisting of 200 realization each were run, one with the correlation scale doubled and one with it cut in half, relative to the base case value. Figure 4-3 shows the effect of the horizontal correlation scale on ensemble mean concentrations at the pumping well, plus/minus one standard deviation about this mean, and the maximum well concentration. Differences in the mean well concentration are small. The figure shows, however, an increase in the variability/uncertainty of the well concentrations as the correlation scale increases, as evidenced by the increasing difference between the plus/minus one standard deviation curves and between the mean and the maximum curves. This result suggests that the presence of larger structures within the domain tends to increase the well concentration variability.

4.2 Sensitivity to Other Hydrologic Parameters

Sensitivity analyses were carried out for a number of parameters that have a representation in both the complex and the simplified models. The results for the hydrologic parameters are presented here, with comparisons between the STOMP and RESRAD sensitivities. One parameter not considered in the sensitivity analyses was the contaminant distribution coefficient. Previous studies have demonstrated the importance of the contaminant distribution coefficient in simplified and complex representations.

For the sake of reducing computer time, a number of the STOMP sensitivity analyses presented in this section were performed on “equivalent uniform” domains. That is, a small number of deterministic simulations were carried out with K_s and ψ_e assigned their scaled mean values and with a single parameter value varied incrementally. Based on earlier results (e.g., Figure 3-3), we concluded that the differences between variations in ensemble mean responses and variations in responses from an equivalent uniform domain would be insignificant for sensitivity analysis purposes, with the exception of variations in geostatistical parameters discussed in the previous section.

4.2.1 Recharge Rate

Additional Monte Carlo simulations were carried out to evaluate the sensitivity of the STOMP model to the recharge rate. Two simulations consisting of 300 realizations each were run, one with the recharge rate increased by 40% and the other with recharge cut to one-half the base case value. Figure 4-4 shows the effect of the higher and lower recharge rates on the mean breakthrough curves. As expected, high recharge translates to higher concentrations at the well and a shorter time to peak. The 40% increase in recharge resulted in about a 30% shorter time to peak and about a 20% higher peak concentration. Reducing recharge by half (50%) resulted in almost doubling the time to peak and about a 45% reduction in peak concentration. This sensitivity to the recharge rate is on a par with that observed in RESRAD simulations and reflects the fact that the recharge rate controls the contaminant flux through the unsaturated zone.

Results from recharge sensitivity calculations for the complex and simplified models are compared in Figure 4-5. The complex model results were obtained from the ensemble mean well concentrations shown in Figure 4-4. The simplified model results were obtained by running RESRAD with the recharge rate as the only variable parameter (other parameters were set to the site-specific mean values). The effects of recharge on the peak dose and the time of the peak

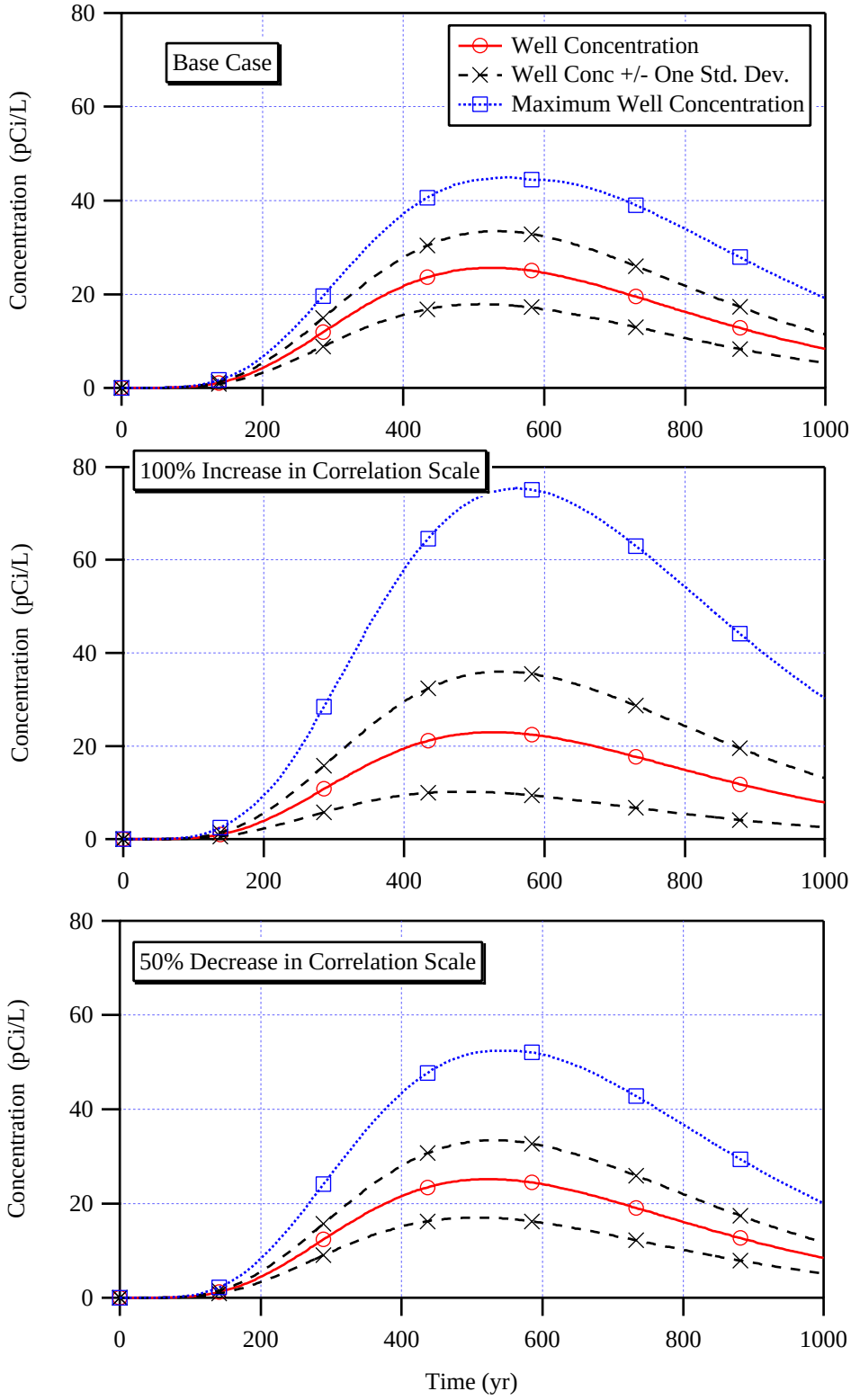

Figure 4-3. Effect of correlation scale on breakthrough concentrations at the pumping well. Mean concentration, mean +/- one standard deviation, and maximum concentration are shown for 200 realizations.

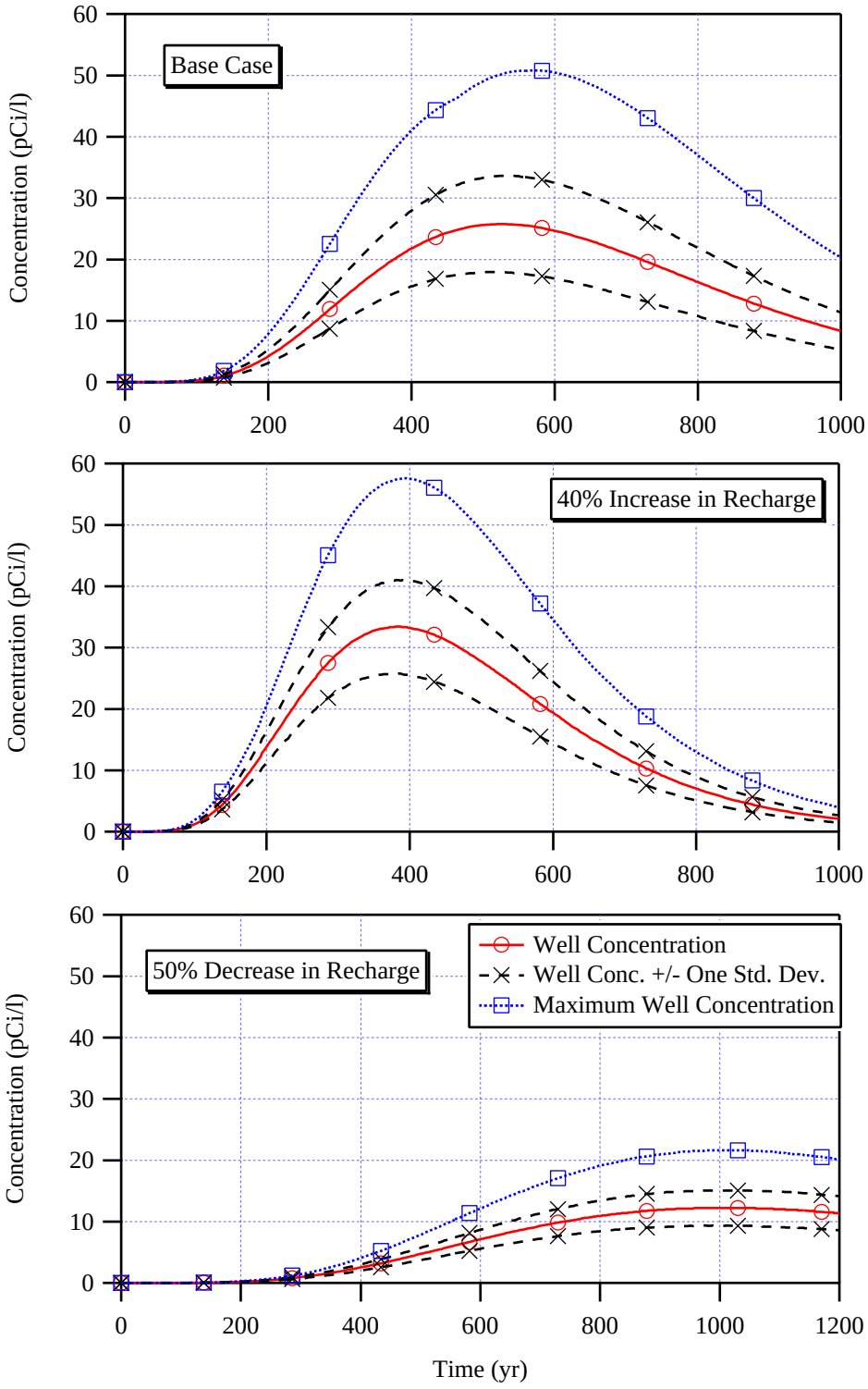

Figure 4-4. Effect of recharge on breakthrough concentrations at the pumping well. Mean concentration, mean +/- one standard deviation, and maximum concentration are shown for 300 realizations.

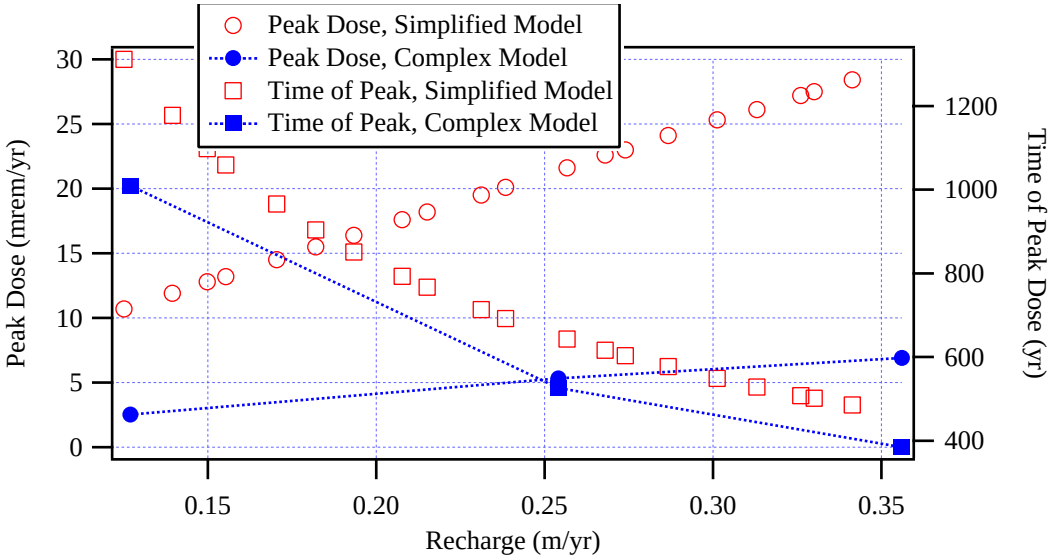

Figure 4-5. Effect of the recharge rate on peak dose and on the time of the peak dose for the simplified (RESRAD) and the complex (STOMP) models

dose are shown in Figure 4-5. Other than the previously noted differences in magnitudes, the primary difference is the greater sensitivity of the RESRAD peak dose results to the recharge rate. The slope of the peak dose relationship for RESRAD is more than three times the slope for the STOMP results. This stems from differences in model structure (one vs. three dimensions).

4.2.2 Mean Air Entry Pressure

Sensitivity to the air entry pressure was evaluated by conducting two simulations on uniform domains using air entry pressures that were twice and one-half the base case value. Concentration results for the two sensitivity cases are shown in Figure 4-6. There is little sensitivity to air-entry values. This is, again, due to the imposed boundary conditions on the top surface. Air-entry variations translate to variations in pressure head in the unsaturated zone, but mass flux in the vadose zone is fixed by the specified source concentration and recharge rate. The air-entry value does not apply to saturated flow in the aquifer.

4.2.3 Mean Hydraulic Conductivity

Two additional Monte Carlo simulations, each consisting of 200 realizations, were carried out to examine the sensitivity to the mean hydraulic conductivity. One simulation used a mean K_s an order of magnitude larger than the base case value and one used a mean K_s an order of magnitude smaller. Figure 4-7 shows the well concentration results for the two simulations with the base case results also shown for comparison. Reducing the mean hydraulic conductivity by an order of magnitude resulted in more than a five-fold increase in the peak concentration and a 20% increase in the time of the peak. Increasing the mean conductivity by an order of magnitude resulted in nearly a 90% reduction in well concentration and a 10% decrease in the time to peak.

At first glance, the variations in concentrations caused by varying mean conductivities seem counter-intuitive, and the variations in peak time are much smaller than expected. This is apparently due to the boundary conditions imposed on the system. In particular, the prescribed water flux and source concentrations at the surface imply a steady flux of solute mass in the vadose zone regardless of mean K_s. Since the majority of the travel time is in the unsaturated zone, these boundary conditions limit the sensitivity of the time of the peak dose to the mean K_s. On the other hand, with prescribed heads on upstream and downstream boundaries of the aquifer, a higher mean conductivity in the aquifer entails higher flow rates. This implies greater mixing and flushing in the aquifer, which leads to lower concentrations at the well. Similarly, lower flow rates in the aquifer result in less mixing and hence higher concentrations at the well.

Note that if the contaminant source boundary condition on top was defined as solute mass rather than solute concentrations, the results would be different. In that case, since a lower mean K_s implies an apparent increase in water content in the unsaturated zone (in order to maintain the same water flux)[1], lower source concentrations would result. By the same reasoning, a finite concentration at the surface

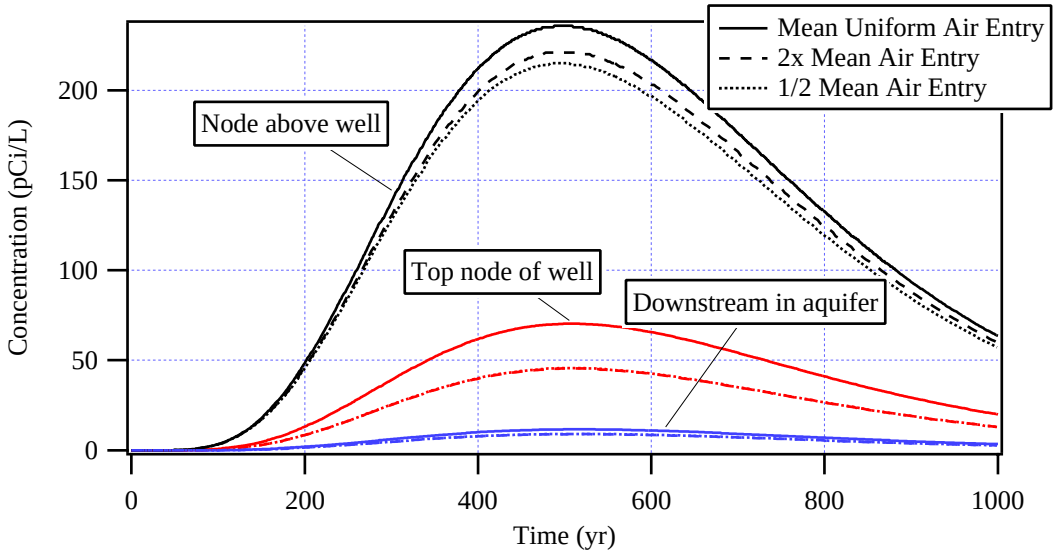

Figure 4-6. Effect of air-entry value on breakthrough curves at the unsaturated node above the well, at the top well node, and downstream mid-depth in the aquifer. All simulations are single deterministic runs with uniform properties.

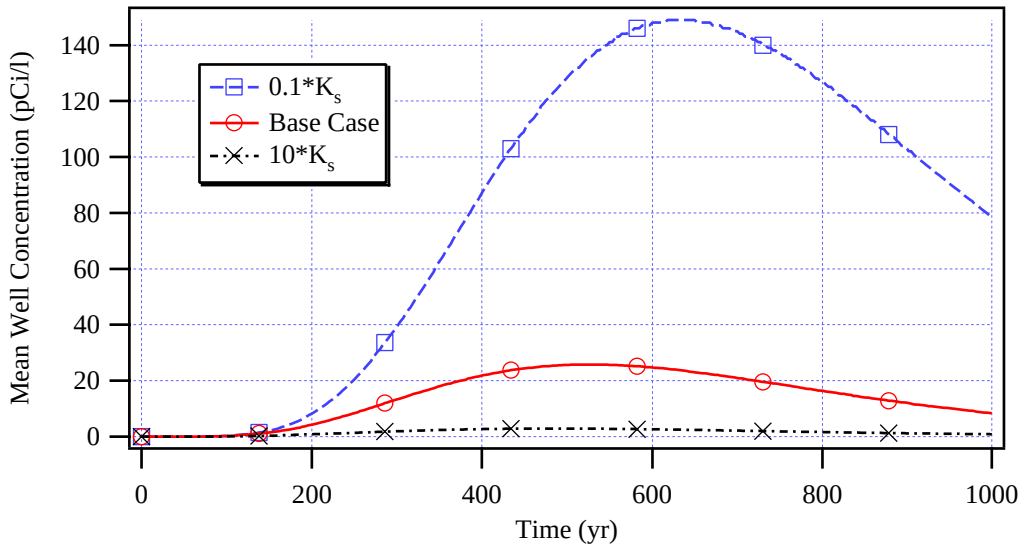

Figure 4-7. Effect of mean saturated conductivity on the ensemble mean well concentration for 200 realization Monte Carlo simulations

[1] The constant recharge at the surface entails mean steady gravitational flow (in all simulations), implying uniform pressure head (plus random variations in the random fields) and unsaturated hydraulic conductivity approximately equal to the imposed flux.

implies a higher solute mass in the vadose zone, which augments the increase in well concentrations caused by the lower aquifer flow. Careful examination of the results from the mean K_s sensitivity simulations (not shown) indicates that concentration variations in the unsaturated zone are more pronounced than the concentration variations within

the nodes comprising the well. These are important differences in model structure (of otherwise the same model) that one has to keep in mind when comparing different models.

For the simplified representation, the hydraulic conductivity in the aquifer dominated the variability in peak dose. This can be seen most clearly by looking at scatter plots derived from the RESRAD Monte Carlo simulation results. Figure 4-8 (upper plot) shows the peak dose as a function of the values of aquifer hydraulic conductivity and unsaturated zone bulk density used in the RESRAD simulation. The lack of correlation between the dose and the bulk density is representative of the scatter plots for the remaining random parameters. In fact, virtually all the variability in the peak dose was due to the variability in the aquifer hydraulic conductivity. The lower plot in Figure 4-8 shows the same RESRAD results for the peak dose as a function of the aquifer hydraulic conductivity and includes the STOMP results for comparison. The STOMP results were taken from the breakthrough curves presented in Figure 4-7 for the three values of mean hydraulic conductivity. Although the range of hydraulic conductivities used in the STOMP simulations was significantly larger than that used in RESRAD, the overall sensitivity of peak dose to hydraulic conductivity appears similar for the two models.

The quantities compared in Figure 4-8 (lower plot) are not strictly the same. Each point of the complex model results represents an ensemble mean peak dose and an ensemble mean hydraulic conductivity. Each point of the simplified model curve represents a peak dose and a spatial average hydraulic conductivity for a particular realization. Averaging all the results for the simplified model would give a single point equivalent to the central point (of three) from the complex model. In order to provide the most direct comparison to the RESRAD sensitivity results shown in Figure 4-8, a similar plot was prepared from the results of one of the STOMP simulations (the high recharge simulation). The spatial geometric mean hydraulic conductivity in the aquifer was calculated for each realization. This was then plotted versus the peak dose for each realization (calculated from average well concentrations). The resulting scatter plot is shown in Figure 4-9 and demonstrates that there is no correlation between the spatial geometric mean conductivity of a single realization and peak concentration at the pumping well as simulated by STOMP. This result is in sharp contrast to the RESRAD results. Note that in Figure 4-9 the spatial geometric mean hydraulic conductivity varies over approximately the same range as the three ensemble mean values used to obtain the STOMP results shown in Figures 4-7 and 4-8.

It's possible that the effect of variation in other parameters obscures the relationship between peak dose predicted by STOMP and the spatial average aquifer hydraulic conductivity. More likely, in single bounded realizations the generated parameter values (K_s and ψ_e) tend to be statistically anisotropic, implying preferred continuity in certain directions, and hence, preferential flow and transport. Rather than an isotropic spatial average of hydraulic conductivities, the patterns in which these parameters are distributed in each realization determines the transport both in the vadose zone and in the aquifer. Orr (1993) showed how these patterns of hydraulic conductivities in single bounded realizations are reflected by anisotropic spatial covariances and variograms, implying a non-ergodic behavior and preferred directions. Orr (1993) also showed how these irregularities are themselves random, disappearing as the number of realizations increases and generated parameter values are averaged over the ensemble of realizations. Indeed, this is why generating and simulating a sufficient number of realizations in Monte Carlo simulations is essential for reliable analyses. This is consistent with the ensemble averaging we perform in order to obtain unbiased estimates of predicted values (i.e., the expected values).

The results shown in Figures 4-8 and 4-9 demonstrate that although the complex model ensemble results and the simplified model results behave similarly, the individual realizations from the complex model behave quite differently. The results have implications for the value of hydraulic conductivity data. Adopting the homogeneous parameterization of RESRAD leads to a conclusion that reducing the uncertainty in the value of the aquifer hydraulic conductivity parameter will have a significant impact on the uncertainty in peak dose. Looking at the individual realization results from the STOMP model suggests that characterization of the average aquifer hydraulic conductivity is relatively unimportant in reducing uncertainty in peak dose. Sensitivity of the ensemble mean peak dose to the ensemble mean hydraulic conductivity is not significant in this case because the actual aquifer is a single realization. Characterizing the pattern of aquifer heterogeneity is likely to be more important than simply obtaining a value for the spatial mean hydraulic conductivity.

4.2.4 Aquifer Hydraulic Gradient

Sensitivity to the aquifer hydraulic gradient was evaluated by conducting several additional STOMP simulations using the equivalent uniform parameters (scaled mean parameter values for K_s and ψ_e) with the aquifer gradient reduced from the base case value of 0.02. Well concentration results are shown in the upper plot of Figure 4-10. Peak dose is inversely related to the aquifer gradient, increasing approximately seven times with a ten-fold decrease in the aquifer gradient. A smaller gradient results in less mixing of uncontaminated groundwater with the contaminated water recharging the aquifer from the unsaturated zone. Peak dose calculated from these results of the complex model are compared to the equivalent simplified model results in the lower plot of Figure 4-10. The relationship between peak dose and the aquifer gradient is similar for the two models. Although

peak dose for the simplified model is significantly higher, both models produce about a seven-fold increase in the peak dose over the range of aquifer gradients considered. This similarity occurs in spite of the fact that RESRAD uses a relatively simplified aquifer dilution model.

4.3 Sensitivity to Scenario Parameters

There are a number of parameters related to the exposure scenario that might contribute to the uncertainty in the dose. A comprehensive study of these parameters deserves further consideration, but was not undertaken for this report. We examined the sensitivity of the two models to only the depth of the well penetration. Our choice of three-dimensional modeling for the complex representation was made primarily to allow for realistic representation of the pumping well. We thus had an opportunity to compare the effect of well depth to the simpler representation used in RESRAD.

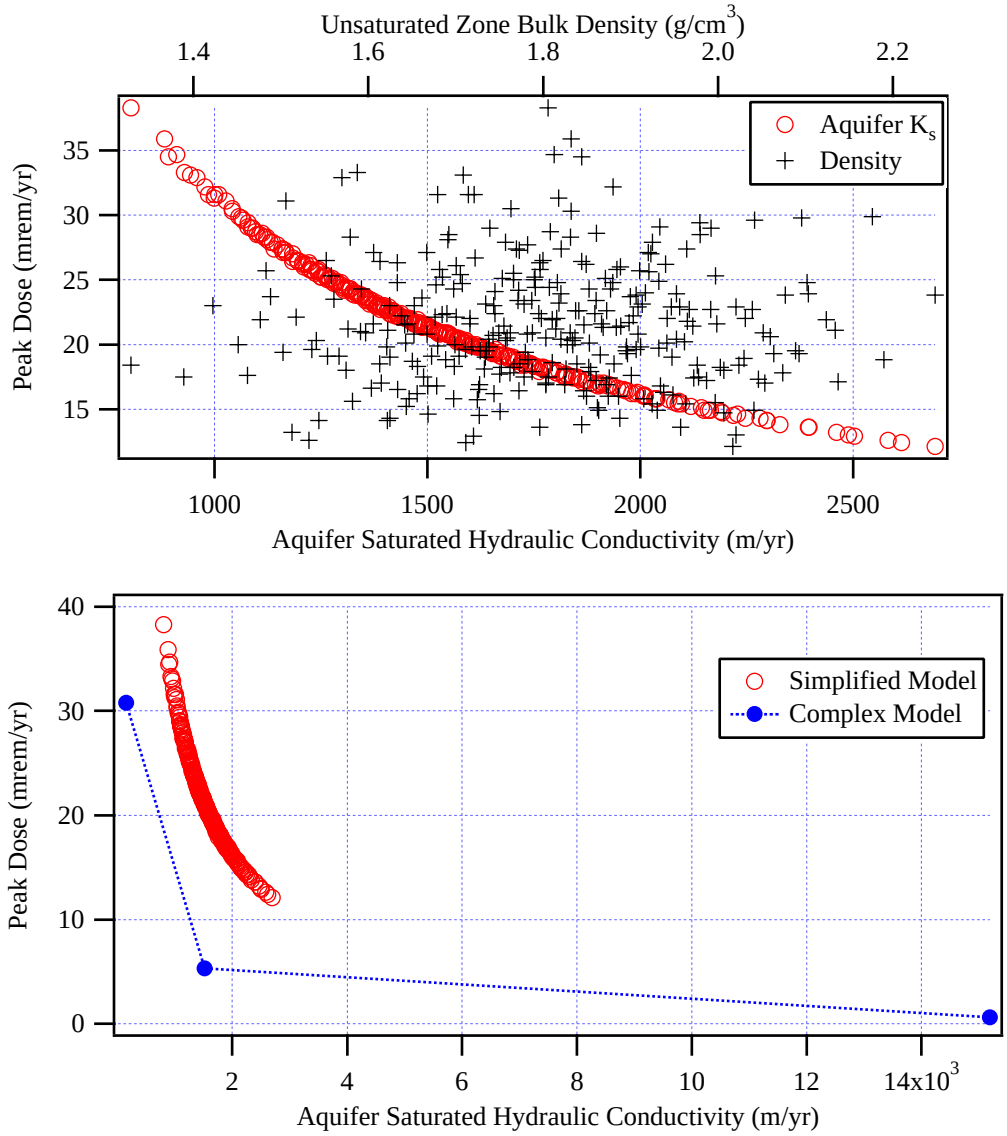

Figure 4-8. RESRAD sensitivity to aquifer hydraulic conductivity and unsaturated zone bulk density from the base case simulation (top) and a comparison of the RESRAD (simplified) and STOMP (complex) results for peak dose sensitivity to aquifer hydraulic conductivity (STOMP results from Figure 4-7)

4.3.1 Depth of Well Penetration into the Aquifer

The base case results for the STOMP model showed a sharp decrease in concentration with depth within the well (see Figure 3-1, well nodes 1 to 5). This suggests that the average well concentrations may be sensitive to the depth of well penetration. In order to explore this issue, we ran an additional Monte Carlo simulation with the STOMP model using only the three uppermost well nodes as an active well screen, with the same total discharge (or pumping rate). Figure 4-11 shows the results with the base case (five well nodes) shown for comparison. The ensemble mean well concentration is actually slightly lower for the three-node well, while the variance of the well concentration increased somewhat. Overall, however, the differences in well concentrations are insignificant. This result is not entirely unexpected because ultimately, well concentrations are dominated by pumping and ambient flow, two quantities that remained the same in the two simulations.

Results from deterministic STOMP simulations using the equivalent uniform parameter values are shown in Figure 4-12 (upper plot). Well concentrations are shown for well depths of one to five meters (one to five nodes). Sensitivity to the well depth is significant for these simulations, with the peak well concentration increasing from 20 pCi/l to over 30 pCi/l as the well depth is reduced from 5 to 3 m and increasing to more than 50 pCi/l for a well depth of 1 m. This sensitivity to the well depth is in contrast to the Monte Carlo ensemble mean results presented in Figure 4-11. Peak dose results for the deterministic STOMP simulations are compared to equivalent results from RESRAD in the lower plot of Figure 4-12. The peak dose predicted by RESRAD appears to be more sensitive to the depth of the well penetration, particularly for well depths less than 3 m.

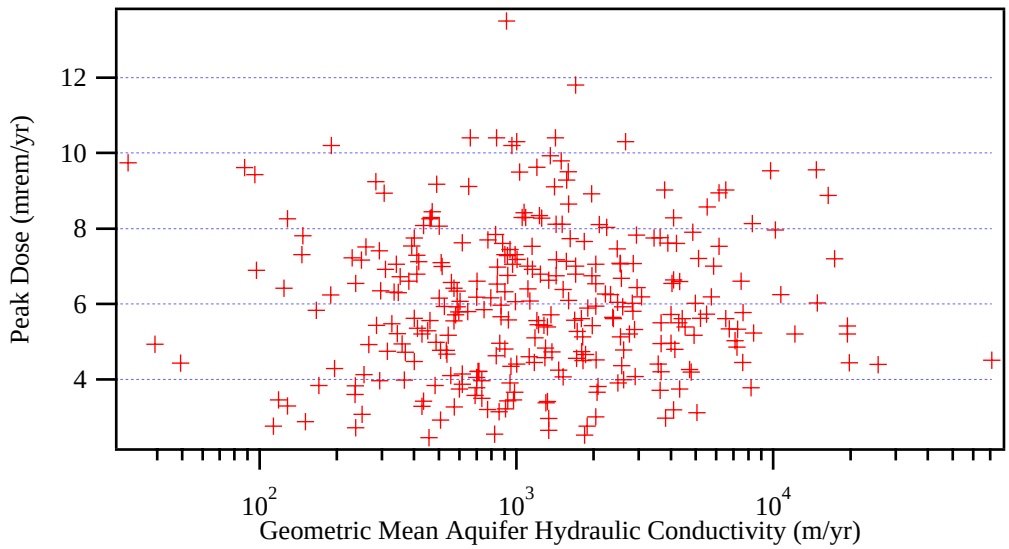

Figure 4-9. STOMP sensitivity to the spatially averaged (geometric mean) aquifer hydraulic conductivity using the high recharge case

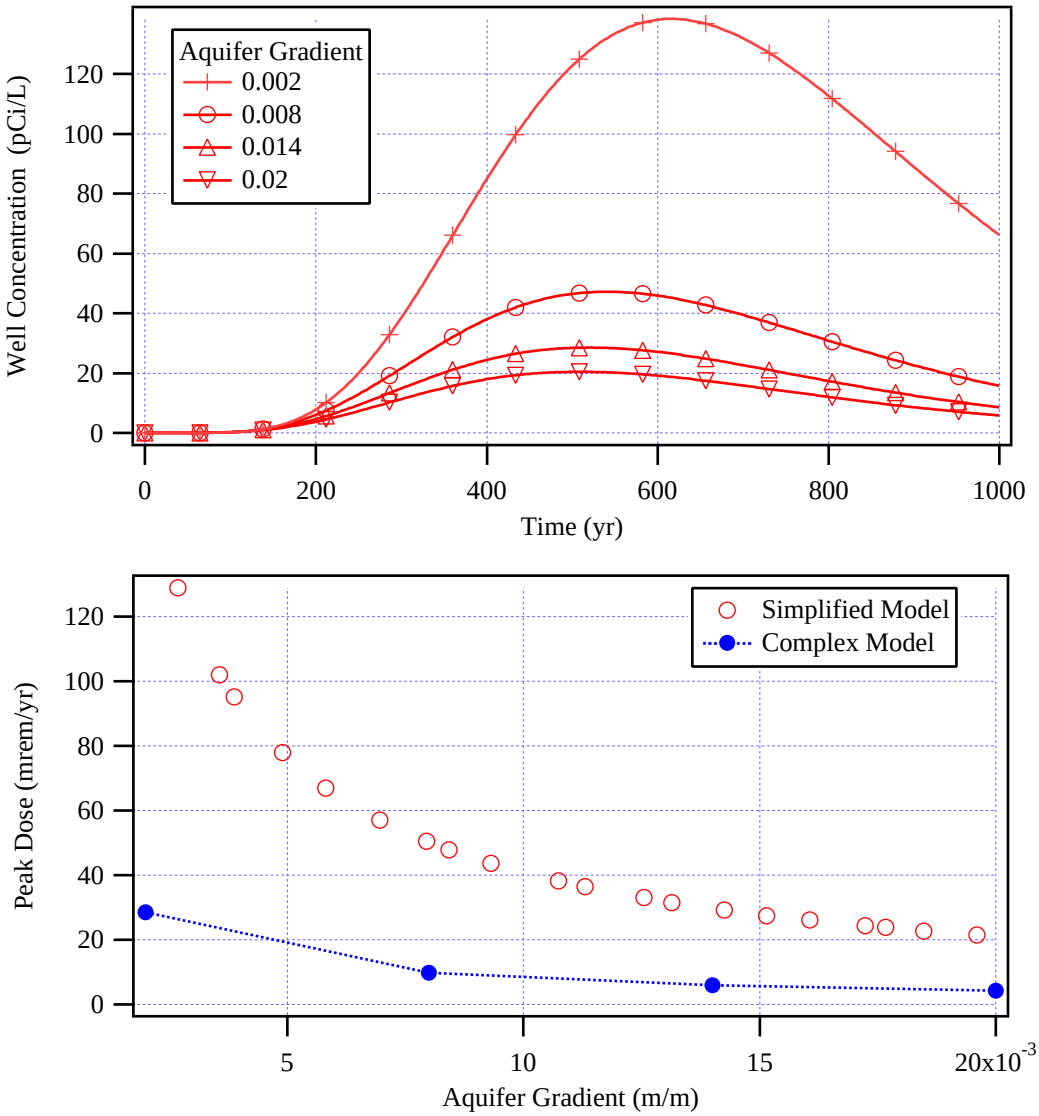

Figure 4-10. Well concentration over time for aquifer hydraulic gradients of 0.002 to 0.02 from the complex model (STOMP) using equivalent uniform hydraulic properties (top) and a comparison of peak dose for the complex and simplified models as a function of aquifer hydraulic gradient using equivalent uniform properties in both cases (bottom).

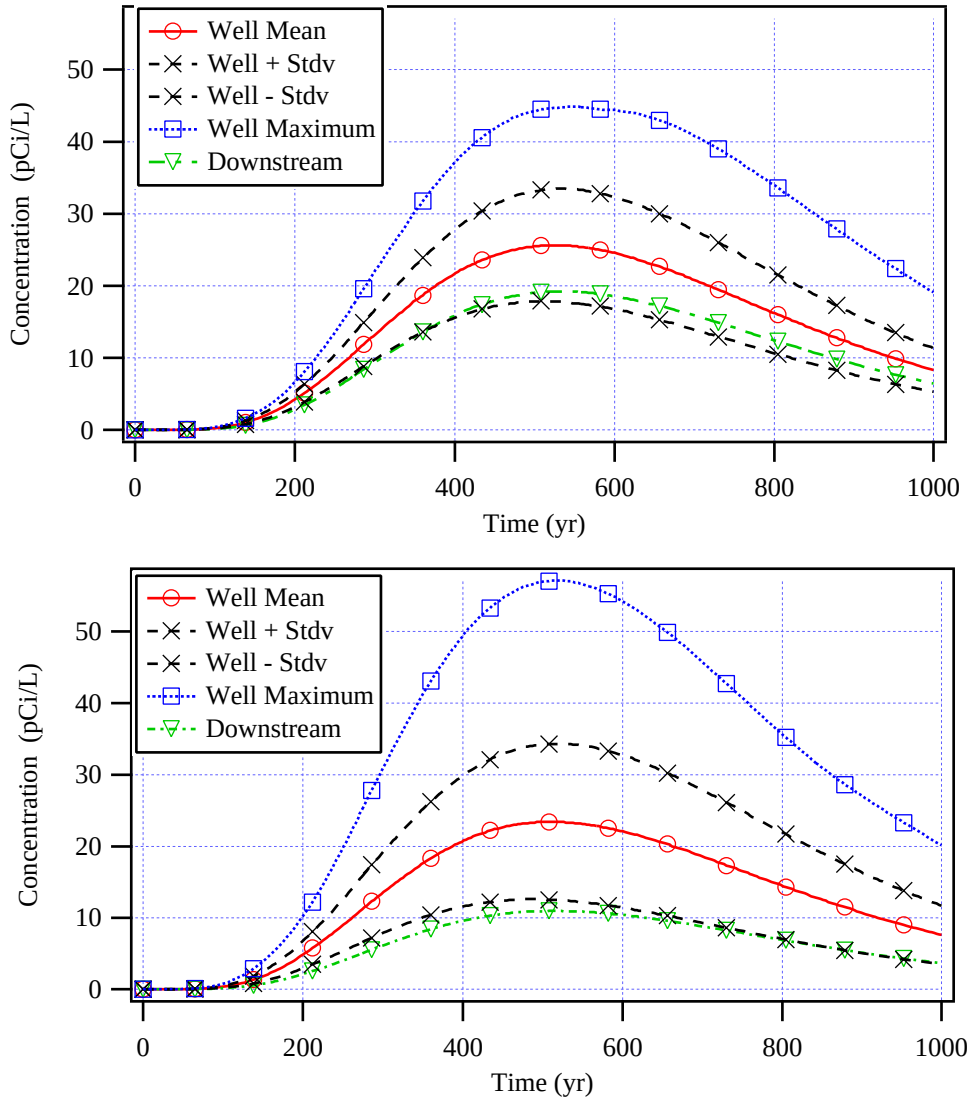

Figure 4-11. STOMP model base case results (top) with a fully penetrating well (5-m well depth) and results from a simulation with a 3-m deep well (bottom). Results are shown for the ensemble mean well concentration, plus/minus one standard deviation, the maximum well concentration, and a downstream aquifer node for a 200 realization Monte Carlo simulation.

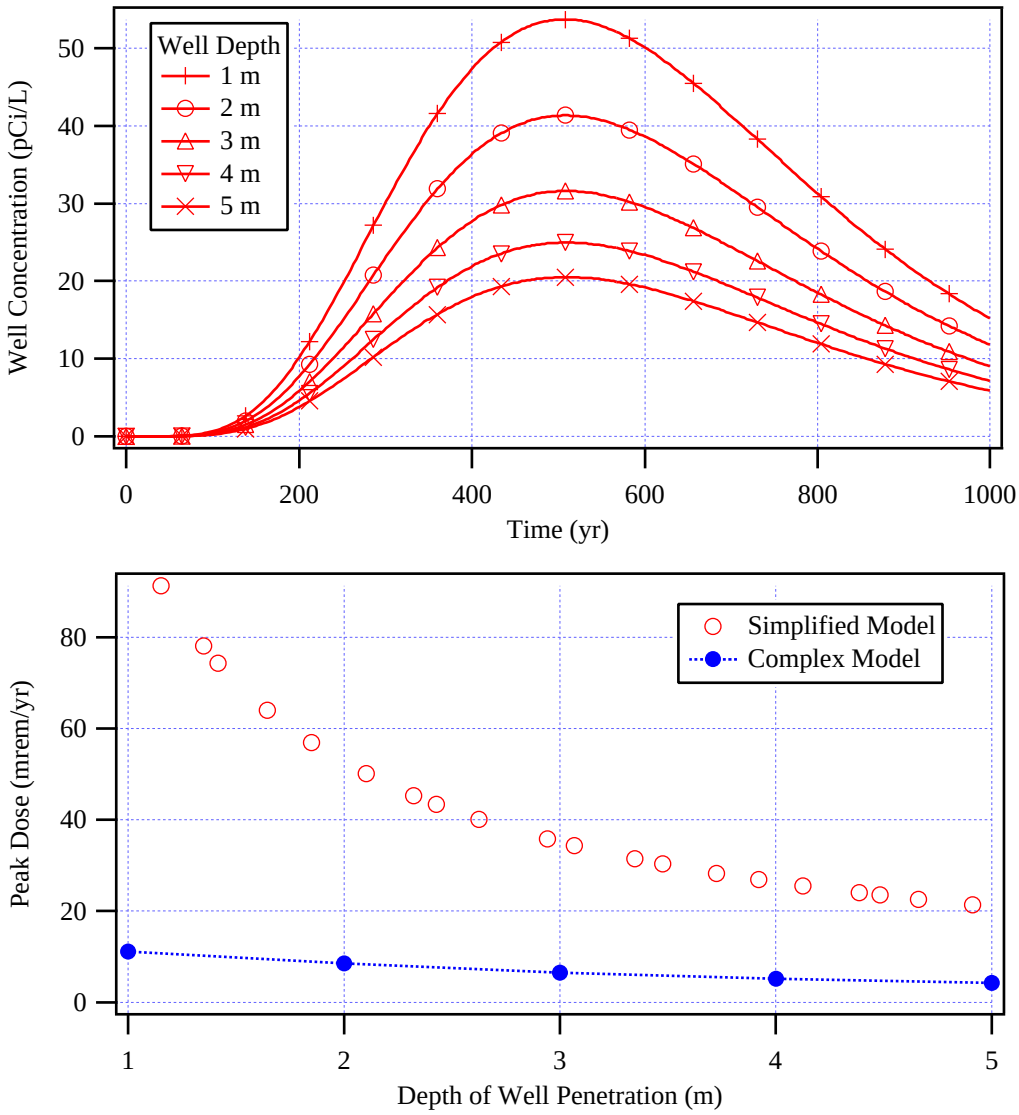

Figure 4-12. Well concentration over time for well depths of 1 m to 5 m from the complex model (STOMP) using equivalent uniform hydraulic properties (top) and a comparison of peak dose for the complex and simplified models as a function of well depth using equivalent uniform properties in both cases (bottom).

5 Conclusions

This report has evaluated an uncertainty assessment as carried out using RESRAD by comparing the results to similar analyses conducted using a more complex code, STOMP. A test case was developed for the evaluation using data from the Las Cruces Trench site. Characteristics of the test case were set to eliminate many differences between the codes and to highlight the differences due to the underlying conceptualization and parameterization of subsurface flow and transport.

Mean peak dose predicted by the simplified model (RESRAD) for a base case Monte Carlo simulation was several times higher than the mean peak dose predicted by the complex model (STOMP). This difference was attributed to the lack of dispersion in the RESRAD model and differences in the mixing and dilution in the aquifer. For this test case, RESRAD provided conservative results in the sense that the peak dose was higher than that predicted by STOMP. The RESRAD concentration breakthrough curves exhibited a sharp peak, however, with essentially no contaminant in the well until the time of the peak. This could be interpreted as nonconservative behavior since the STOMP simulations predicted a much earlier arrival of contaminants and, prior to the arrival of the RESRAD peak, the well concentrations from the STOMP model were larger than those predicted by RESRAD. This point is particularly relevant because the regulatory criteria include a time limit: 1000 years from the time of decommissioning. If the RESRAD predicted peak had occurred after 1000 years, the RESRAD results would have been nonconservative in every sense of the word.

The complex model assumed the availability of an extensive dataset on which to base the random field characterization of the subsurface. Uncertainty in predicted dose was correspondingly small, with the peak dose coefficient of variation being 30%. When the variances of parameters in the simplified model were based on a generic dataset, the uncertainty in predicted peak dose was much larger; the coefficient of variation was 52% in this case. When the variances of parameters in the simplified model were based on the available site-specific data, the coefficient of variation for the peak dose was reduced to 22%. In this case, however, the mean peak dose was actually less similar to the STOMP results than the generic case. This unexpected result occurred because the site-specific mean aquifer hydraulic conductivity was significantly smaller than the generic value and because of the strong dependence of the RESRAD peak dose on aquifer hydraulic conductivity. The lognormal distribution of the hydraulic conductivity accentuated the effect.

For the STOMP model, the peak of the mean dose as a function of time and the mean of the peak dose distribution were almost the same because of the smoothness of the breakthrough curve(s). The RESRAD results for the same quantities were very different for this test case because of the sharpness of the breakthrough curves, which was a result of the lack of dispersion in the model. Similarity of the simulated peak mean and mean peak doses implies robustness and reliability of the complex model, in contrast to the simplified approach

Sensitivity analyses illustrated the relative importance of parameters. For the RESRAD Monte Carlo simulations involving random soil hydraulic properties, the variability of peak dose was entirely attributed to variability in the aquifer hydraulic conductivity. Sensitivity to other parameters was examined by varying one parameter at a time. These results indicated that the recharge rate, the aquifer gradient, and the depth of penetration of the well would be significant contributors to uncertainty in peak dose and also the time of the peak dose.

Sensitivity analyses of the complex model showed that stochastic predictions of mean dose over time exhibited low sensitivity to parameter variability (expressed by their variances), including to the variance of log hydraulic conductivity. This may have been due to the use of a relatively small simulation domain. Uncertainty in dose predictions, however, was directly (linearly) dependent on the variance of hydraulic conductivity. Ensemble mean dose was insensitive to the correlation scales of the hydraulic properties. Uncertainty in dose, however, increased somewhat with an increase in the correlation scale. Overall, the complex model showed robustness with respect to geostatistical parameters.

Ensemble mean peak dose predicted by the complex model was strongly sensitive to the ensemble mean hydraulic conductivity. Reducing the ensemble mean hydraulic conductivity by an order of magnitude resulted in more than a fivefold increase in the peak dose. Increasing the ensemble mean conductivity by an order of magnitude resulted in nearly a 90% reduction in peak dose. It was noted, however, that for a single ensemble mean hydraulic conductivity, the complex model showed no correlation between the spatial geometric mean aquifer conductivity of individual realizations and the resulting peak dose. This was in contrast to the simplified model in which the dose from individual realizations was strongly correlated with the aquifer conductivity. This result has implications for the value of hydraulic conductivity data. Adopting the homogeneous parameterization of RESRAD leads to a conclusion that reducing the uncertainty in the value of the aquifer hydraulic conductivity parameter will have a significant impact on the uncertainty in peak dose. Looking at the individual realization results from the STOMP model suggests that characterization of the average aquifer hydraulic conductivity is relatively unimportant in reducing uncertainty in peak dose. Characterizing the pattern of aquifer heterogeneity is likely to be more important than obtaining a value for the spatial mean hydraulic conductivity.

RESRAD predicted peak dose was more sensitive to the parameter values than was the STOMP predicted peak dose

for the aquifer hydraulic conductivity, aquifer gradient, and depth of well penetration. Sensitivity to the recharge rate appeared to be comparable for the two codes, perhaps a result of the boundary condition constraints imposed on the STOMP model. Differences in model sensitivities may lead to different conclusions about which parameters are critical to the analysis and about the importance of site-specific data.

Finally, some observations on computational issues. Flow and transport in single realizations of the complex model showed strong dependence on the spatial structure of generated hydraulic properties. These large variations in results, however, diminished sharply when averaged over the ensemble, as the number of realizations exceeded 200. A minimum of 200 realizations were thus conducted for each of the STOMP Monte Carlo simulations. STOMP model results showed some sensitivity to mesh resolution, particularly near the water table, where concentration gradients were extremely high. The relatively coarse mesh size was a calculated compromise without which the Monte Carlo simulations could not be performed. The variety of numerical consideration required by the application of a complex, three-dimensional model was clearly illustrated. No such considerations were required to execute RESRAD as its internal conceptual-mathematical model is fixed. The complex model required many hours of computational time to execute a Monte Carlo simulation. RESRAD, on the other hand required no more than a few minutes.

We note here that our results are specific to the application of RESRAD to the test case we simulated. It may be valuable to conduct similar studies with other multimedia models (e.g. MEPAS/FRAMES, DandD) and for other test cases. The complex representation of the test case was less complex than reality at many sites. The impact of such processes as preferential flow or chemical heterogeneity were not investigated. Our application also did not make use of monitoring data and calibration/inversion. A similar test case comparison using such data would be instructive.

6 References

Bear, J., *Hydrauics of Ground Water,* McGraw-Hill Book Co., New York, NY, 569 pp., 1979.

Beyeler, W. E., P. A. Davis, F. A Duran, M. C. Daily, and T. A. Feeney, "Residual Radioactive Contamination from Decommissioning: Parameter Analysis," Draft *NUREG/CR-5512, Vol. 3,* Sandia National Laboratories, Albuquerque, New Mexico, October, 1999.

Buck, J. W., G. Whelan, J. G. Droppo Jr., D. L. Strenge, K.J. Castleton, J. P. McDonald, C. Sato, G. P. Streile, "Multimedia Environmental Pollutant Assessment System (MEPAS) Application Guidance," *PNL-10395,* Pacific Northwest National Laboratory, Richland, WA, 1995.

Carsel, R. F., and R. S. Parrish, "Developing joint probability distributions of soil water retention characteristics," *Wat. Resour. Res.,* 24(5):755-770, 1988.

Dagan, G., and S. P. Neuman (eds.), *Subsurface Flow and Transport: A Stochastic Approach,* Cambridge University Press, New York, 1997.

Deutsch, C.V., and A.G. Journel, *GSLIB – Geostatistical Software Library and User's Guide,* Second Ed., Applied Geostatistical Series, Oxford University Press, New York – Oxford, 369 pp., 1997.

El-Kadi, A.I (ed.), *Groundwater Models for Resources Analysis and Management,* CRC/Lewis Pub., Boca Raton, Florida. 384pp., 1995.

El-Kadi, A.I. and G. Ling, "The Courant and Peclet criteria for numerical solution of the Richards equation," *Water Resources Research,* 29(10):3485-3494, 1993.

Fayer, M.J., J.B. Sisson, W.A. Jordan, A.H. Lu, and P.R. Heller, "Subsurface Injection of Radioactive Tracers – Field experiment for model validation testing," *NUREG/CR-5996* (PNL-8499), U.S. Nuclear Regulatory Commission, Washington, DC, 1993.

Gelhar, L. W., *Stochastic Subsurface Hydrology,* Prentice-Hall, Englewood Cliffs, New Jersey, 1993.

Gilbert, R. O. *Statistical Methods for Environmental Pollution Monitoring,* Van Nostrand Reinhold, New York, NY, 320 pp., 1987.

Kennedy, J.D., and D.L. Strenge, "Residual Radioactive Contamination from Decommissioning: Technical Basis for Translating Contamination Levels to Annual Total Effective Dose Equivalent," *NUREG/CR-5512,* (PNL-7994), U.S. Nuclear Regulatory Commission, Washington, D.C., 1992.

Kincaid, C.T., M.P. Bergeron, C.R. Cole, M.D. Freshley, N.L. Hassig, V.G. Johnson, D.I. Kaplan, R.J. Serne, G.P. Streile, D.L. Strenge, P.D. Thorne, L.W. Vail, G.A. Whyatt, S.K. Wurstner, "Composite Analysis for Low-Level Waste Disposal in the 200 Area Plateau of the Hanford Site," *PNNL-11800,* Pacific Northwest National Laboratory, Richland, WA, 1998.

Khaleel, R., and E.J. Freeman, "Variability and Scaling of Hydraulic Properties for 200 Area Soils, Hanford Site," *WHC-EP-0883, UC-900,* Westinghouse Hanford Company, Richland, WA, 1995.

Leij, F. J., W. J. Alves, M. Th. van Genuchten, and J. R. Williams, "The UNSODA Unsaturated Soil Hydraulic Database User's Manual Version 1.0," *EPA/600/R-96/095,* U.S. Environmental Protection Agency, Washington, D.C., 1996.

Meyer, P.D., M.L. Rockhold, and G.W. Gee, "Uncertainty Analyses of Infiltration and Subsurface Flow and Transport for SDMP Sites," *NUREG/CR-6565,* U.S. Nuclear Regulatory Commission, Washington, DC, 1997.

Meyer, P. D. and G. W. Gee, "Information on Hydrologic Conceptual Models, Parameters, Uncertainty Analysis, and Data Sources for Dose Assessments at Decommissioning Sites," *NUREG/CR-6656,* U.S. Nuclear Regulatory Commission, Washington, D.C., 1999.

Meyer, P. D. and R. W. Taira, "Hydrologic Uncertainty Assessment for Decommissioning Sites: Hypothetical Test Case Applications," *NUREG/CR-6695,* U.S. Nuclear Regulatory Commission, Washington, D.C., 2001.

Neuman, S.P., and S. Orr, "Prediction of steady state flow in nonuniform geologic media by conditional moments: exact nonlocal formalism, effective conductivities, and weak approximation", *Water Resources Research,* 29(2):341-364, 1993.

Neuman, S.P., S. Orr, O. Levin, and E. Paleologos, "Theory and High Resolution Finite Element Analysis of Two Dimensional and Three Dimensional Effective Permeability in Strongly Heterogeneous Porous Media," in *Computational Methods in Water Resources IX, Vol. 2: Mathematical Modeling in Water Resources,* edited by T.F. Russell, R.E. Ewing, C.A. Brebbia, W.G. Gray, and G.F. Pinder, Elsevier, New York, 1992.

NRC, "Decision Methods for Dose Assessments to Comply with Radiological Criteria for License Termination," Draft *NUREG-1549,* U.S. Nuclear Regulatory Commission, Washington, DC, February 3, 1998

NRC, "NMSS Decommissioning Standard Review Plan," *NUREG-1727,* U.S. Nuclear Regulatory Commission, Washington, DC, September, 2000.

Orr, S., *Stochastic Approach to Steady State Flow in Nonuniform Geologic Media,* Ph.D. Dissertation, Department of Hydrology and Water Resources, University of Arizona, Tucson, AZ, 356 pp., 1993.

Press, W.H., B.P. Flannery, S.A. Teukolsky, and W.T. Vetterling, *Numerical Recipes – The Art of Scientific Computing*, Cambridge University Press, Cambridge, 818 pp., 1986.

Rockhold, M.L., R.E. Rossi, and R.G. Hills, "Applications of similar media scaling and conditional simulations for modeling water flow and tritium transport at the Las Cruces Trench Site," *Wat. Resour. Res.*, Vol. 32, No. 3, pp 595-609, 1996.

Schaap, M. G. and F. J. Leij, "Database-related accuracy and uncertainty of pedotransfer functions," *Soil Science*, 163(10):765-779, 1998.

Sisson, J.B., and A. Lu, "Field Calibration of Computer Models for Applications to Buried Liquid Discharges: A Status Report," *RHO-ST-46P,* Rockwell Hanford Operations, Richland, WA, 1984.

Smoot, J.L., and R.E. Williams, "A Geostatistical Methodology to Assess the Accuracy of Unsaturated Flow Models," *NUREG/CR-6411* (PNL-10866), Richland, WA, 1996.

Sun, A. Y. and D. Zhang, "Prediction of solute spreading during vertical infiltration in unsaturated, bounded heterogeneous porous media," *Water Resour. Res.*, 36(3):715-723, 2000.

Wierenga, P. J., A. F. Toorman, D. B. Hudson, J. Vinson, M. Nash, and R. G. Hills, "Soil Physical Properties at the Las Cruces Trench Site," *NUREG/CR-5441*, U.S. Nuclear Regulatory Commission, Washington, DC, 1989.

Wierenga, P. J., D. B. Hudson, R. G. Hills, I. Porro, J. Vinson, and M. R. Kirkland, "Flow and Transport Experiments at the Las Cruces Trench Site: Experiments 1 and 2," *NUREG/CR-5607*, U.S. Nuclear Regulatory Commission, Washington, DC, 1990.

Yu, C., C. Loureiro, J.-J. Cheng, L. G. Jones, Y. Y. Wang, Y. P. Chia, and E. Faillace, "Data Collection Handbook to Support Modeling the Impacts of Radioactive Material in Soil," *ANL/EAIS-8*, Argonne National Laboratory, Argonne, IL, 1993.

Zhang, D., *Stochastic Methods for Flow in Porous Media: Coping with Uncertainties*, Academic Press, San Diego, California, 2001.

Zhang, D. and Z. Lu, "Stochastic analysis of flow in a heterogeneous unsaturated-saturated system," *Wat. Resour. Res.*, 38(2), 10.1029/2001WR000515, 2002.

Appendix A: Recommended Soil Parameter Distributions

Probability distributions of three types (normal, lognormal, and beta) were used to approximate the soil hydraulic parameter distributions generated from the Carsel and Parrish (1988) statistics. This appendix provides a summary of these distributions and presents tables of recommended distributions for selected soil hydraulic parameters. The information provided in Sections A.1 – A.3 can be found in many good probability or statistics textbooks (e.g., Ang and Tang, 1975). Definitions of parameters can be found in Appendix D.

This appendix was originally presented in NUREG/CR-6565 (Meyer et al., 1997).

A.1 The Normal Distribution

The normal distribution has a density function given by

$$f(x) = \frac{1}{\sqrt{2\pi}\sigma'} \exp\left[\frac{1}{2}\left(\frac{x-\mu'}{\sigma'}\right)^2\right] \quad \text{(A-1)}$$

where x is the soil parameter being modeled and μ' and σ' are the parameters of the distribution. The mean, μ, and the variance, σ^2, are related to the parameters of the normal distribution as follows.

$$\mu = \mu' \quad \text{(A-2)}$$

$$\sigma^2 = \sigma'^2 \quad \text{(A-3)}$$

Although the normal distribution is unbounded, soil parameters modeled by a normal distribution often have physical limits. These limits can be enforced by specifying that the soil parameter values fall between given quantiles of the normal distribution. In the tables below, the lower (A) and upper (B) limits of each normal distribution are the 0.001 and 0.999 quantiles calculated as follows.

$$A = \mu' - 3.09\sigma' \qquad B = \mu' + 3.09\sigma' \quad \text{(A-4)}$$

A.2 The Lognormal distribution

The lognormal distribution has a density function given by

$$f(x) = \frac{1}{\sqrt{2\pi}\zeta x} \exp\left[\frac{1}{2}\left(\frac{\ln(x)-\gamma}{\zeta}\right)^2\right] \quad \text{(A-5)}$$

where γ and ζ are the parameters of the distribution. The mean and variance of the lognormal distribution are related to the parameters as follows.

$$\mu = \exp(\gamma + \tfrac{1}{2}\zeta^2) \quad \text{(A-6)}$$

$$\sigma^2 = \mu^2[\exp(\zeta^2) - 1] \quad \text{(A-7)}$$

These relationships can also be inverted.

$$\gamma = \ln\mu - \tfrac{1}{2}\zeta^2 \quad \text{(A-8)}$$

$$\zeta = \sqrt{\ln\left(\frac{\sigma^2}{\mu^2} + 1\right)} \quad \text{(A-9)}$$

The lognormal distribution is thus completely specified by either its parameters or its mean and variance.

The lognormal distribution is bounded below by zero, but has no upper bound. In the tables below, the lower and upper bound for the lognormal distributions are the 0.001 and 0.999 quantiles calculated as follows.

$$A = \exp(\gamma - 3.09\zeta) \qquad B = \exp(\gamma + 3.09\zeta) \quad \text{(A-10)}$$

A.3 The Beta Distribution

The beta distribution has a density function given by

$$f(x) = \frac{1}{\beta(q,r)} \frac{(x-A)^{q-1}(B-x)^{r-1}}{(B-A)^{q+r-1}} \quad \text{(A-11)}$$

where q and r are parameters controlling the shape of the distribution and A and B are the lower and upper limits of the distribution. $\beta(q,r)$ is the beta function, calculated through its relationship to the gamma function.

$$\beta(q,r) = \frac{\Gamma(q)\Gamma(r)}{\Gamma(q+r)} \quad \text{(A-12)}$$

where $\Gamma(\,)$ indicates the gamma function.

The mean and variance of the beta distribution are related to the parameters as follows.

$$\mu = A + \frac{q}{q+r}(B-A) \quad \text{(A-13)}$$

$$\sigma^2 = \frac{qr}{(q+r)^2(q+r+1)}(B-A)^2 \quad \text{(A-14)}$$

With some algebraic manipulation, these relationships can be inverted to provide the shape parameters as a function of the mean, variance, and limits.

$$q = \left(\frac{(B-\mu)(\mu-A)}{\sigma^2} - 1\right)\left(\frac{\mu-A}{B-A}\right) \quad \text{(A-15)}$$

$$r = q\left(\frac{B-\mu}{\mu-A}\right) \quad \text{(A-16)}$$

The beta distribution can thus be completely specified by its lower and upper limits and either its mean and variance or its shape parameters.

In the tables below, the lower and upper limits for the beta distributions are the actual limits, A and B.

A.4 Recommended Probability Distributions for Soil Hydraulic Parameters by Soil Texture

Tables A-1 to A-12 contain the recommended distributions for the selected soil hydraulic parameters. Each table represents a particular USDA soil textural classification. Observed correlations between parameters are given in Appendix B.

Table A-1. Recommended distributions for Sand

Parameter	Distribution[1]	Mean	Std. Deviation	Lower Limit[2]	Upper Limit[2]
θ_s	Normal	0.430	0.0600	0.245	0.615
θ_r	LN(-3.09,0.224)*	0.0466	0.0106	0.0228	0.0907
p_e	Normal	0.383	0.0610	0.195	0.572
f_c	LN(-2.83,0.241)	0.0607	0.0150	0.0280	0.124
w_p	LN(-3.09,0.224)	0.0466	0.0106	0.0227	0.0907
awc	LN(-4.34,0.387)	0.0141	6.12E-03	3.95E-03	0.0431
α [cm^{-1}]	Normal	0.147	0.0255	0.0687	0.226
n	LN(0.978,0.0998)*	2.67	0.267	1.95	3.62
h_b	LN(1.93,0.183)	7.02	1.38	3.92	12.1
λ	LN(0.502,0.161)	1.67	0.267	1.00	2.72
b	LN(-0.0253,0.216)	0.998	0.226	0.501	1.90
K_s [cm/s]	Beta(1.398,1.842)	8.22E-03	4.39E-03	3.50E-04	0.0186

Table A-2. Recommended distributions for Loamy Sand

Parameter	Distribution[1]	Mean	Std. Deviation	Lower Limit[2]	Upper Limit[2]
θ_s	Normal	0.410	0.0900	0.132	0.688
θ_r	Normal	0.0569	0.0145	0.0121	0.102
p_e	Normal	0.353	0.0913	0.0711	0.635
f_c	LN(-2.55,0.281)	0.0809	0.0224	0.0327	0.186
w_p	Normal	0.0570	0.0146	0.0119	0.102
awc	LN(-3.85,0.491)	0.0239	0.0125	4.65E-03	0.0966
α [cm^{-1}]	Normal*	0.125	0.0404	2.03E-04	0.250
n	LN(0.816,0.0910)	2.27	0.209	1.71	3.00
h_b	LN(2.15,0.401)	9.58	8.59	2.48	29.5
λ	LN(0.226,0.164)	1.27	0.209	0.756	2.08
b	LN(0.305,0.258)	1.40	0.397	0.610	3.01
K_s [cm/s]	Beta(0.7992,1.910)	3.99E-03	3.17E-03	3.90E-05	0.0134

Table A-3. Recommended distributions for Sandy Loam

Parameter	Distribution[1]	Mean	Std. Deviation	Lower Limit[2]	Upper Limit[2]
θ_s	Normal	0.410	0.0899	0.132	0.688
θ_r	Beta(2.885,2.304)	0.0644	0.0169	0.0173	0.102
p_e	Normal	0.346	0.0915	0.0629	0.628
f_c	LN(-2.21,0.314)	0.116	0.0369	0.0417	0.291
w_p	Normal	0.0659	0.0179	0.0106	0.121
awc	LN(-3.12,0.489)	0.0498	0.0256	9.75E-03	0.200
α [cm^{-1}]	Beta(1.816,3.412)	0.0757	0.0368	8.72E-03	0.202
n	LN(0.634,0.0818)*	1.89	0.155	1.46	2.43
h_b	LN(2.71,0.538)	17.7	12.0	2.85	79.4
λ	Normal	0.892	0.155	0.412	1.37
b	LN(0.632,0.282)	1.96	0.597	0.786	4.50
K_s [cm/s]	LN(-7.46,1.33)	1.17E-03	1.37E-03	9.62E-06	0.0347

Table A-4. Recommended distributions for Sandy Clay Loam

Parameter	Distribution[1]	Mean	Std. Deviation	Lower Limit[2]	Upper Limit[2]
θ_s	Normal	0.390	0.0700	0.174	0.606
θ_r	Beta(2.202,2.010)	0.101	6.09E-03	0.0860	0.114
p_e	Normal	0.289	0.0703	0.0723	0.507
f_c	LN(-1.59,0.254)	0.212	0.0568	0.0933	0.449
w_p	LN(-2.14,0.158)	0.120	0.0214	0.0724	0.193
awc	Beta(1.890,3.817)	0.0920	0.0393	0.0204	0.237
α [cm^{-1}]	LN(-3.04,0.639)	0.0572	0.0337	6.62E-03	0.343
n	LN(0.388,0.0858)*	1.48	0.127	1.13	1.92
h_b	LN(3.04,0.639)	26.2	21.3	2.92	151.
λ	Normal	0.479	0.127	0.0865	0.872
b	LN(1.41,0.275)	4.27	1.39	1.75	9.57
K_s [cm/s]	LN(-9.30,1.75)	3.23E-04	5.98E-04	4.12E-07	0.0202

Table A-5. Recommended distributions for Loam

Parameter	Distribution[1]	Mean	Std. Deviation	Lower Limit[2]	Upper Limit[2]
θ_s	Normal	0.430	0.0998	0.122	0.738
θ_r	Beta(3.639,2.652)	0.0776	0.0127	0.0374	0.107
p_e	Normal	0.352	0.101	0.0414	0.663
f_c	LN(-1.68,0.300)	0.194	0.0609	0.0735	0.468
w_p	LN(-2.40,0.250)	0.0935	0.0246	0.0418	0.196
awc	LN(-2.40,0.462)	0.101	0.0454	0.0218	0.380
α [cm^{-1}]	Beta(1.576,3.625)	0.0367	0.0202	3.51E-03	0.113
n	LN(0.442,0.0730)	1.56	0.114	1.24	1.95
h_b	LN(3.470,0.598)	38.9	29.3	5.05	203.
λ	Normal	0.560	0.114	0.209	0.911
b	LN(1.08,0.271)	3.07	0.900	1.28	6.82
K_s [cm/s]	LN(-9.26,1.66)	2.92E-04	4.91E-04	5.51E-07	0.0159

Table A-6. Recommended distributions for Silt Loam

Parameter	Distribution[1]	Mean	Std. Deviation	Lower Limit[2]	Upper Limit[2]
θ_s	Normal	0.45	0.0800	0.203	0.697
θ_r	Beta(3.349,2.566)	0.0670	0.0142	0.0243	0.0998
p_e	Normal	0.383	0.0813	0.132	0.634
f_c	Normal	0.252	0.0776	0.0119	0.491
w_p	LN(-2.22,0.397)	0.117	0.0471	0.0318	0.368
awc	Normal	0.135	0.0402	0.0107	0.259
α [cm^{-1}]	LN(-4.10,0.554)*	0.0193	0.0115	2.99E-03	0.0919
n	LN(0.343,0.0851)	1.41	0.120	1.08	1.83
h_b	LN(4.10,0.554)	70.3	41.9	10.9	335.
λ	Normal	0.414	0.120	0.0417	0.786
b	LN(1.28,0.334)	3.80	1.42	1.28	10.1
K_s [cm/s]	LN(-10.4,1.49)*	9.33E-05	2.24E-04	3.12E-07	3.11E-03

Table A-7. Recommended distributions for Silt

Parameter	Distribution[1]	Mean	Std. Deviation	Lower Limit[2]	Upper Limit[2]
θ_s	Normal	0.456	0.110	0.1206	0.799
θ_r	Beta(1.717,1.072)	0.0352	8.97E-03	0.0131	0.0490
p_e	Normal	0.425	0.110	0.0839	0.766
f_c	Normal	0.236	0.0578	0.0575	0.415
w_p	LN(-2.46,0.295)	0.0890	0.0268	0.0342	0.212
awc	Normal	0.147	0.0395	0.0252	0.269
α [cm^{-1}]	Normal*	0.0178	5.73E-03	3.91E-05	0.0355
n	Normal*	1.38	0.0369	1.27	1.49
h_b	LN(4.10,0.403)	68.1	74.8	17.3	209.
λ	Normal	0.380	0.0369	0.266	0.494
b	LN(1.16,0.140)	3.21	0.465	2.06	4.89
K_s [cm/s]	LN(-10.0,0.475)*	4.89E-05	2.76E-05	9.95E-06	1.87E-04

Table A-8. Recommended distributions for Clay Loam

Parameter	Distribution[1]	Mean	Std. Deviation	Lower Limit[2]	Upper Limit[2]
θ_s	Normal	0.410	0.0900	0.132	0.688
θ_r	Normal	0.0954	9.68E-03	0.0655	0.125
p_e	Normal	0.315	0.0905	0.0349	0.594
f_c	LN(-1.27,0.297)	0.292	0.0862	0.112	0.700
w_p	LN(-1.84,0.257)	0.164	0.0468	0.0714	0.350
awc	Beta(2.986,4.318)	0.128	0.0497	9.34E-03	0.301
α [cm^{-1}]	LN(-4.22,0.719)*	0.0190	0.0153	1.59E-03	0.136
n	Normal	1.32	0.0973	1.02	1.62
h_b	LN(4.22,0.719)	88.0	71.3	7.37	628.
λ	Normal	0.318	0.0973	0.0170	0.618
b	LN(1.73,0.323)	5.97	2.37	2.08	15.3
K_s [cm/s]	LN(-11.3,2.17)	9.93E-05	2.51E-04	1.42E-08	9.76E-03

Table A-9. Recommended distributions for Silty Clay Loam

Parameter	Distribution[1]	Mean	Std. Deviation	Lower Limit[2]	Upper Limit[2]
θ_s	Normal	0.430	0.0699	0.214	0.646
θ_r	Normal*	0.0880	9.00E-03	0.0602	0.116
p_e	Normal	0.342	0.0705	0.124	0.560
f_c	Normal	0.347	0.0710	0.127	0.566
w_p	LN(-1.61,0.233)	0.205	0.0508	0.0970	0.410
awc	Normal	0.142	0.0333	0.0387	0.245
α [cm^{-1}]	LN(-4.72,0.563)	0.0104	6.08E-03	1.57E-03	0.0508
n	Normal*	1.23	0.0610	1.04	1.42
h_b	LN(4.72,0.563)	132.	81.4	19.7	638.
λ	Normal	0.230	0.0610	0.0416	0.418
b	LN(1.96,0.265)	7.13	2.34	3.02	15.5
K_s [cm/s]	LN(-12.3,1.59)	1.54E-05	3.38E-05	3.44E-08	6.49E-04

Table A-10. Recommended distributions for Sandy Clay

Parameter	Distribution[1]	Mean	Std. Deviation	Lower Limit[2]	Upper Limit[2]
θ_s	Normal	0.380	0.0500	0.226	0.534
θ_r	Beta(4.000,1.487)	0.0993	0.0116	0.0508	0.117
p_e	Normal	0.281	0.0513	0.122	0.439
f_c	LN(-1.23,0.210)	0.299	0.0623	0.153	0.559
w_p	Beta(1.142,4.640)	0.165	0.0344	0.121	0.346
awc	Normal	0.134	0.0356	0.0238	0.244
α [cm^{-1}]	LN(-3.77,0.562)*	0.0270	0.0164	4.06E-03	0.131
n	LN(0.241,0.0653)*	1.28	0.0834	1.04	1.56
h_b	LN(3.77,0.562)	50.7	30.5	7.64	246.
λ	Normal	0.275	0.0834	0.0177	0.533
b	LN(1.89,0.260)	6.90	2.27	2.97	14.8
K_s [cm/s]	LN(-12.2,2.02)*	3.55E-05	1.48E-04	9.59E-09	2.50E-03

Table A-11. Recommended distributions for Silty Clay

Parameter	Distribution[1]	Mean	Std. Deviation	Lower Limit[2]	Upper Limit[2]
θ_s	Normal	0.360	0.0698	0.144	0.576
θ_r	Normal*	0.0706	0.0228	1.47E-04	0.141
p_e	Normal	0.289	0.0735	0.0623	0.517
f_c	Normal	0.334	0.0678	0.124	0.543
w_p	LN(-1.49,0.220)	0.230	0.0512	0.114	0.444
awc	Normal	0.103	0.0303	9.63E-03	0.197
α [cm^{-1}]	LN(-5.66,0.584)*	4.13E-03	2.60E-03	5.73E-04	0.0211
n	LN(0.145,0.0430)	1.16	0.0499	1.01	1.32
h_b	LN(5.66,0.584)	340.	216.	47.3	1743.
λ	Beta(2.591,3.268)	0.157	0.0499	0.0404	0.304
b	LN(2.29,0.259)	10.2	2.96	4.43	22.0
K_s [cm/s]	LN(-13.9,1.31)*	2.19E-06	4.08E-06	1.64E-08	5.37E-05

Table A-12. Recommended distributions for Clay

Parameter	Distribution[1]	Mean	Std. Deviation	Lower Limit[2]	Upper Limit[2]
θ_s	Normal	0.380	0.0900	0.102	0.658
θ_r	Beta(1.501,1.580)	0.0685	0.0344	8.36E-04	0.140
p_e	Normal	0.311	0.0963	0.0138	0.609
f_c	Normal	0.340	0.0893	0.0638	0.615
w_p	Beta(2.751,4.921)	0.263	0.0770	0.0939	0.567
awc	LN(-2.66,0.429)	0.0761	0.0299	0.0186	0.263
α [cm^{-1}]	LN(-5.54,0.893)	6.18E-03	7.59E-03	2.50E-04	0.0621
n	Beta(0.8857,2.400)	1.13	0.0697	1.04	1.36
h_b	Beta(0.8002,1.546)	353.	257.	14.1	1007
λ	Beta(0.8854,2.399)	0.127	0.0697	0.0397	0.365
b	Beta(1.751,11.61)	14.1	6.24	4.93	75.0
K_s [cm/s]	LN(-12.36,2.269)	3.65E-05	1.08E-04	3.87E-09	4.76E-03

1. LN(,) = Lognormal(γ,ζ); see Section A.2. Beta(,) =Beta(q,r); see Section A.3.

2. Lower Limit and Upper Limit are 0.001 and 0.999 quantiles for Normal and Lognormal distributions.

* Indicates that the recommended distribution is the same type as used by Carsel and Parrish (1988). This applies to the parameters θ_r, α, n, and K_s only.

A.5 References

Ang, A. H-S. and W. H. Tang, *Probability Concepts in Engineering Planning and Design, Volume 1, Basic Principles,* John Wiley & Sons, New York, 409 pp., 1975.

Carsel, R. F., and R. S. Parrish, "Developing joint probability distributions of soil water retention characteristics," *Water Resources Research,* 24(5):755-770, 1988.

Meyer, P.D., M.L. Rockhold, and G.W. Gee, "Uncertainty Analyses of Infiltration and Subsurface Flow and Transport for SDMP Sites," *NUREG/CR-6565,* U.S. Nuclear Regulatory Commission, Washington, DC, 1997.

Appendix B: Soil Parameter Correlation Coefficients

The correlation coefficient is a measure of the strength of a linear relationship between two random variables (i.e., soil parameters), *X* and *Y*. Sample correlation coefficients were calculated as follows [e.g., Ang and Tang (1975)].

$$\hat{\rho} = \frac{1}{N-1}\frac{\sum_{i=1}^{N} x_i y_i - N\bar{x}\bar{y}}{s_x s_y} \quad \text{(B-1)}$$

where

$\hat{\rho}$ = sample correlation coefficient

x_i, y_i = sample values for parameters *X* and *Y*

$\bar{x}$, $\bar{y}$ = sample mean values calculated as

$$\bar{x} = \frac{1}{N}\sum_{i=1}^{N} x_i \quad \text{(B-2)}$$

s_x, s_y = sample standard deviations calculated as

$$s_x^2 = \frac{1}{N-1}\sum_{i=1}^{N} (x_i - \bar{x})^2 \quad \text{(B-3)}$$

N = the number of sample values

Correlations between parameters were induced by applying the correlations between θ_r, α, n, and K_s given in Carsel and Parrish (1988). The rank correlation method of Iman and Conover (1982) as embodied in the Latin hypercube sampling code of Iman and Shortencarier (1984) was used. Note that the correlations given in the tables below do not necessarily appear to be the same as those of Carsel and Parrish (1988) since their correlations were calculated after the parameters were transformed to normal distributions. The correlations given below were calculated on the untransformed parameters. Definitions of parameters in the tables can be found in Appendix D.

This appendix was originally presented in NUREG/CR-6565 (Meyer et al., 1997).

Table B-1. Correlation coefficients for Sand

	θ_s	θ_r	p_e	f_c	w_p	awc	α	n	h_b	λ	b	K_s
θ_s	1	-0.01	0.99	0.15	-0.01	0.38	0.00	0.00	-0.02	0.00	-0.29	0.00
θ_r		1	-0.18	0.94	1	0.59	0.12	-0.84	-0.12	-0.84	0.91	-0.50
p_e			1	-0.02	-0.18	0.27	-0.02	0.15	0.01	0.15	-0.44	0.08
f_c				1	0.94	0.82	-0.11	-0.91	0.11	-0.91	0.89	-0.67
w_p					1	0.59	0.12	-0.84	-0.12	-0.84	0.91	-0.50
awc						1	-0.49	-0.79	0.49	-0.79	0.59	-0.78
α							1	0.29	-0.97	0.29	-0.09	0.73
n								1	-0.28	1	-0.88	0.84
h_b									1	-0.28	0.09	-0.68
λ										1	-0.88	0.84
b											1	-0.65
K_s												1

Table B-2. Correlation coefficients for Loamy Sand

	θ_s	θ_r	p_e	f_c	w_p	awc	α	n	h_b	λ	b	K_s
θ_s	1	-0.01	0.99	0.27	0.00	0.49	0.00	0.01	-0.03	0.01	-0.50	0.01
θ_r		1	-0.16	0.85	1	0.34	-0.29	-0.58	0.16	-0.58	0.71	-0.34
p_e			1	0.13	-0.16	0.42	0.05	0.10	-0.05	0.10	-0.60	0.07
f_c				1	0.85	0.79	-0.53	-0.76	0.33	-0.76	0.57	-0.58
w_p					1	0.35	-0.30	-0.58	0.17	-0.58	0.72	-0.35
awc						1	-0.60	-0.68	0.39	-0.68	0.19	-0.63
α							1	0.38	-0.57	0.38	-0.29	0.88
n								1	-0.22	1	-0.64	0.65
h_b									1	-0.22	0.17	-0.38
λ										1	-0.64	0.65
b											1	-0.41
K_s												1

Table B-3. Correlation coefficients for Sandy Loam

	θ_s	θ_r	p_e	f_c	w_p	awc	α	n	h_b	λ	b	K_s
θ_s	1	0.00	0.98	0.38	0.03	0.54	0.01	0.00	0.01	0.00	-0.44	0.01
θ_r		1	-0.19	0.72	1	0.34	0.14	-0.79	-0.17	-0.79	0.77	-0.22
p_e			1	0.24	-0.16	0.46	-0.02	0.15	0.04	0.15	-0.57	0.05
f_c				1	0.78	0.90	-0.35	-0.85	0.35	-0.85	0.51	-0.51
w_p					1	0.42	0.08	-0.82	-0.10	-0.82	0.77	-0.25
awc						1	-0.56	-0.65	0.57	-0.65	0.20	-0.56
α							1	0.36	-0.77	0.36	-0.11	0.82
n								1	-0.28	1	-0.78	0.60
h_b									1	-0.28	0.05	-0.51
λ										1	-0.78	0.60
b											1	-0.33
K_s												1

Table B-4. Correlation coefficients for Sandy Clay Loam

	θ_s	θ_r	p_e	f_c	w_p	awc	α	n	h_b	λ	b	K_s
θ_s	1	0.00	1	0.48	0.21	0.58	-0.01	0.00	-0.02	0.00	-0.43	-0.01
θ_r		1	-0.09	-0.02	0.23	-0.16	0.37	-0.11	-0.36	-0.11	0.21	0.16
p_e			1	0.48	0.19	0.59	-0.04	0.01	0.01	0.01	-0.45	-0.03
f_c				1	0.88	0.97	-0.67	-0.81	0.66	-0.81	0.42	-0.50
w_p					1	0.73	-0.51	-0.81	0.68	-0.81	0.65	-0.33
awc						1	-0.69	-0.73	0.58	-0.73	0.24	-0.54
α							1	0.77	-0.70	0.77	-0.49	0.82
n								1	-0.65	1	-0.76	0.71
h_b									1	-0.65	0.57	-0.39
λ										1	-0.76	0.71
b											1	-0.38
K_s												1

Table B-5. Correlation coefficients for Loam

	θ_s	θ_r	p_e	f_c	w_p	awc	α	n	h_b	λ	b	K_s
θ_s	1	0.00	0.99	0.55	0.18	0.63	0.03	0.00	0.04	0.00	-0.46	0.03
θ_r		1	-0.13	0.29	0.79	-0.03	-0.04	-0.70	0.07	-0.70	0.67	0.14
p_e			1	0.50	0.08	0.63	0.03	0.09	0.03	0.09	-0.54	0.01
f_c				1	0.75	0.93	-0.63	-0.71	0.70	-0.71	0.28	-0.41
w_p					1	0.47	-0.42	-0.87	0.56	-0.87	0.69	-0.16
awc						1	-0.62	-0.49	0.63	-0.49	0.00	-0.46
α							1	0.60	-0.73	0.60	-0.37	0.82
n								1	-0.55	1	-0.79	0.41
h_b									1	-0.55	0.39	-0.42
λ										1	-0.79	0.41
b											1	-0.21
K_s												1

Table B-6. Correlation coefficients for Silt Loam

	θ_s	θ_r	p_e	f_c	w_p	awc	α	n	h_b	λ	b	K_s
θ_s	1	-0.01	0.98	0.48	0.20	0.70	-0.02	-0.01	-0.02	-0.01	-0.20	-0.02
θ_r		1	-0.18	0.50	0.66	0.18	-0.29	-0.59	0.27	-0.59	0.63	-0.25
p_e			1	0.39	0.08	0.66	0.03	0.10	-0.06	0.10	-0.31	0.03
f_c				1	0.91	0.87	-0.72	-0.80	0.73	-0.80	0.63	-0.45
w_p					1	0.58	-0.63	-0.89	0.73	-0.89	0.86	-0.36
awc						1	-0.65	-0.50	0.54	-0.50	0.20	-0.44
α							1	0.74	-0.75	0.74	-0.56	0.80
n								1	-0.69	1	-0.88	0.48
h_b									1	-0.69	0.68	-0.39
λ										1	-0.88	0.48
b											1	-0.31
K_s												1

Table B-7. Correlation coefficients for Silt

	θ_s	θ_r	p_e	f_c	w_p	awc	α	n	h_b	λ	b	K_s
θ_s	1	-0.02	1	0.90	0.52	0.97	0.00	0.00	0.03	0.00	-0.39	0.02
θ_r		1	-0.10	0.25	0.57	-0.02	-0.19	-0.60	0.04	-0.60	0.70	-0.21
p_e			1	0.88	0.48	0.96	0.01	0.05	0.03	0.05	-0.44	0.04
f_c				1	0.81	0.92	-0.35	-0.37	0.16	-0.37	-0.03	-0.30
w_p					1	0.51	-0.60	-0.72	0.48	-0.72	0.44	-0.45
awc						1	-0.10	-0.06	-0.09	-0.06	-0.35	-0.14
α							1	0.55	-0.49	0.55	-0.41	0.89
n								1	-0.20	1	-0.84	0.44
h_b									1	-0.20	0.13	-0.29
λ										1	-0.84	0.44
b											1	-0.34
K_s												1

Table B-8. Correlation coefficients for Clay Loam

	θ_s	θ_r	p_e	f_c	w_p	awc	α	n	h_b	λ	b	K_s
θ_s	1	0.00	0.99	0.65	0.38	0.76	-0.02	0.00	-0.04	0.00	-0.40	0.01
θ_r		1	-0.11	-0.50	-0.46	-0.43	0.73	0.58	-0.74	0.58	-0.35	0.51
p_e			1	0.69	0.43	0.80	-0.10	-0.06	0.04	-0.06	-0.36	-0.04
f_c				1	0.89	0.90	-0.60	-0.71	0.55	-0.71	0.23	-0.42
w_p					1	0.60	-0.55	-0.84	0.75	-0.84	0.57	-0.33
awc						1	-0.52	-0.45	0.26	-0.45	-0.13	-0.42
α							1	0.79	-0.62	0.79	-0.42	0.89
n								1	-0.80	1	-0.73	0.58
h_b									1	-0.80	0.70	-0.36
λ										1	-0.73	0.58
b											1	-0.26
K_s												1

Table B-9. Correlation coefficients for Silty Clay Loam

	θ_s	θ_r	p_e	f_c	w_p	awc	α	n	h_b	λ	b	K_s
θ_s	1	0.00	0.99	0.73	0.46	0.85	-0.01	0.00	0.00	0.00	-0.19	-0.03
θ_r		1	-0.13	-0.42	-0.46	-0.21	0.72	0.55	-0.71	0.55	-0.37	0.47
p_e			1	0.77	0.51	0.87	-0.10	-0.07	0.10	-0.07	-0.15	-0.09
f_c				1	0.90	0.75	-0.62	-0.65	0.58	-0.65	0.35	-0.45
w_p					1	0.40	-0.68	-0.84	0.79	-0.84	0.69	-0.42
awc						1	-0.29	-0.11	0.02	-0.11	-0.30	-0.32
α							1	0.86	-0.75	0.86	-0.57	0.83
n								1	-0.84	1	-0.82	0.60
h_b									1	-0.84	0.80	-0.41
λ										1	-0.82	0.60
b											1	-0.32
K_s												1

Table B-10. Correlation coefficients for Sandy Clay

	θ_s	θ_r	p_e	f_c	w_p	awc	α	n	h_b	λ	b	K_s
θ_s	1	0.00	0.97	0.58	0.35	0.68	0.02	0.00	0.01	0.00	-0.23	0.05
θ_r		1	-0.23	-0.70	-0.82	-0.42	0.75	0.88	-0.92	0.88	-0.78	0.28
p_e			1	0.72	0.53	0.75	-0.15	-0.20	0.22	-0.20	-0.05	-0.02
f_c				1	0.89	0.89	-0.70	-0.78	0.68	-0.78	0.44	-0.33
w_p					1	0.58	-0.67	-0.85	0.87	-0.85	0.74	-0.24
awc						1	-0.58	-0.55	0.35	-0.55	0.05	-0.35
α							1	0.87	-0.74	0.87	-0.59	0.58
n								1	-0.86	1	-0.79	0.44
h_b									1	-0.86	0.83	-0.26
λ										1	-0.79	0.44
b											1	-0.23
K_s												1

Table B-11. Correlation coefficients for Silty Clay

	θ_s	θ_r	p_e	f_c	w_p	awc	α	n	h_b	λ	b	K_s
θ_s	1	0.00	0.95	0.94	0.74	0.84	-0.01	-0.01	-0.01	-0.01	-0.31	0.02
θ_r		1	-0.31	-0.29	-0.49	0.19	0.89	0.79	-0.88	0.79	-0.46	0.64
p_e			1	0.98	0.86	0.74	-0.28	-0.25	0.26	-0.25	-0.15	-0.18
f_c				1	0.91	0.70	-0.32	-0.33	0.24	-0.33	-0.07	-0.24
w_p					1	0.34	-0.50	-0.64	0.52	-0.64	0.32	-0.34
awc						1	0.14	0.33	-0.36	0.33	-0.70	0.03
α							1	0.84	-0.72	0.84	-0.47	0.86
n								1	-0.78	1	-0.77	0.64
h_b									1	-0.78	0.63	-0.44
λ										1	-0.77	0.64
b											1	-0.31
K_s												1

Table B-12. Correlation coefficients for Clay

	θ_s	θ_r	p_e	f_c	w_p	awc	α	n	h_b	λ	b	K_s
θ_s	1	0.00	0.93	0.88	0.73	0.76	0.00	-0.01	0.00	-0.01	-0.26	-0.01
θ_r		1	-0.36	-0.38	-0.50	0.13	0.70	0.79	-0.85	0.79	-0.52	0.53
p_e			1	0.96	0.85	0.66	-0.25	-0.29	0.31	-0.29	-0.06	-0.20
f_c				1	0.95	0.55	-0.38	-0.45	0.36	-0.45	0.08	-0.30
w_p					1	0.25	-0.47	-0.63	0.57	-0.63	0.33	-0.32
awc						1	0.09	0.28	-0.38	0.28	-0.63	-0.06
α							1	0.82	-0.61	0.82	-0.46	0.86
n								1	-0.78	1	-0.73	0.64
h_b									1	-0.78	0.67	-0.37
λ										1	-0.73	0.64
b											1	-0.30
K_s												1

B.1 References

Ang, A. H-S. and W. H. Tang, *Probability Concepts in Engineering Planning and Design, Volume 1, Basic Principles*, John Wiley & Sons, New York, 409 pp., 1975.

Carsel, R. F., and R. S. Parrish, "Developing joint probability distributions of soil water retention characteristics," *Water Resources Research*, 24(5):755-770, 1988.

Iman, R. L. and W. J. Conover, "A distribution-free approach to inducing rank correlation among input variables," *Communications in Statistics*, B11(3):311-334, 1982.

Iman, R. L. and M. J. Shortencarier, "A FORTRAN 77 Program and User's Guide for the Generation of Lain Hypercube and Random Samples for Use with Computer Models," *NUREG/CR-3624* (also SAND83-2365), U.S. Nuclear Regulatory Commission, Washington, D.C., 1984.

Meyer, P.D., M.L. Rockhold, and G.W. Gee, "Uncertainty Analyses of Infiltration and Subsurface Flow and Transport for SDMP Sites," *NUREG/CR-6565*, U.S. Nuclear Regulatory Commission, Washington, DC, 1997.

Appendix C: Recommended Soil Bulk Density Distributions

Dry soil bulk density data were obtained from the U.S. Natural Resources Conservation Service Soil Characterization Database, dated May 1994. The data were divided according to USDA soil textural class based on the sand, silt, and clay percentages. The distribution of these data over textural classes can be seen in Figure 5-5 of NUREG/CR-6656 (Meyer and Gee, 1999).

For each textural class, the Kolmogorov-Smirnov D-statistic was calculated using hypothetical normal and lognormal distributions. The parameters for the hypothetical normal and lognormal distributions were based on the data. In all cases the D-statistic from the normal distribution was smaller than that from the lognormal distribution. In addition, plots of the bulk density histogram for each soil texture were examined and appeared to better fit a normal distribution. For these reasons, the normal distribution is recommended for modeling bulk density.

The mean and standard deviation of the bulk density data are given in the table below. These values reflect the elimination of outliers from the dataset for each textural class. Outliers were defined as those points outside the mean plus or minus four times the standard deviation, where the mean and standard deviation were calculated as the sample mean and sample standard deviation with the potential outliers eliminated. The upper and lower limits given in the table are the actual limits of the data extracted from the Soil Characterization Database. Samples with a bulk density less than 0.5 g/cm3 or greater than 2.0 g/cm3 were not included in the analysis.

Bulk density is highly correlated to saturated water content and effective porosity with correlations generally between -0.95 and -0.99.

C.1 References

Meyer, P.D. and G.W. Gee, “Information on Hydrologic Conceptual Models, Parameters, Uncertainty Analysis, and Data Sources for Dose Assessments at Decommissioning Sites,” *NUREG/CR-6656*, U.S. Nuclear Regulatory Commission, Washington, DC, 1999.

Table C-1. Recommended parameters of normal distributions for bulk density

Soil Texture	Number of Samples	Mean	Std. Deviation	Lower Limit	Upper Limit
Sand	811	1.578	0.158	1.0	1.99
Loamy Sand	1889	1.515	0.262	0.5	2.0
Sandy Loam	7195	1.461	0.268	0.5	2.0
Sandy Clay Loam	2189	1.518	0.186	0.76	2.0
Loam	5198	1.418	0.240	0.54	1.99
Silt Loam	6411	1.366	0.227	0.5	1.99
Silt	195	1.330	0.202	0.63	1.74
Clay Loam	3396	1.410	0.197	0.63	2.0
Silty Clay Loam	3139	1.405	0.148	0.8	1.91
Sandy Clay	386	1.491	0.177	0.87	1.94
Silty Clay	2165	1.37	0.154	0.73	1.82
Clay	4539	1.292	0.177	0.58	1.9

Appendix D: Summary of Water Retention and Conductivity Models

This appendix defines the parameters appearing in the tables of Appendices A and B. The information in this appendix was taken from NUREG/CR-6565 (Meyer et al., 1997).

Richards equation (Richards, 1931) forms the basis for most process-based descriptions of water movement in the unsaturated zone. Richards equation can be expressed as

$$\frac{\partial \theta}{\partial t} = \frac{\partial}{\partial z}\left[-K(h)\frac{\partial h}{\partial z} - K(h)\right] + u \qquad \text{(D-1)}$$

where

θ = volumetric water content, or volume of water per unit bulk volume of soil,

h = soil water tension, $h \geq 0$

z = depth, measured positive downward from the soil surface,

t = time,

$K(h)$ = hydraulic conductivity, and

u = a source or sink term used to account for water uptake by plant roots.

To solve Richards equation, constitutive functions relating the unsaturated hydraulic conductivity and the water content to the pressure head are needed. The most commonly used relationships are those of van Genuchten (1980), Brooks and Corey (1964), and Campbell (1974), although other expressions are available (Mualem, 1992; Rossi and Nimmo, 1994; Fayer and Simmons, 1995).

D.1 Van Genuchten Model

The van Genuchten water retention relationship is

$$S_e(h) = [1 + (\alpha h)^n]^{-m} \qquad \text{(D-2)}$$

where

S_e = effective saturation = $\frac{\theta - \theta_r}{\theta_s - \theta_r}$, $0 \leq S_e \leq 1$

α = curve fitting parameter related to air entry pressure

n, m = curve fitting parameters related to pore size distribution; the relationship, m=1-1/n, is often assumed

θ_r = residual water content

θ_s = saturated water content

The van Genuchten hydraulic conductivity relationship, based on the hydraulic conductivity model of Mualem (1976) is

$$K(S_e) = K_s\sqrt{S_e}\left[1 - (1 - S_e^{1/m})^m\right]^2. \qquad \text{(D-3)}$$

or

$$K(h) = K_s\frac{\{1 - (\alpha h)^{n-1}[1 + (\alpha h)^n]^{-m}\}^2}{[1 + (\alpha h)^n]^{0.5m}} \qquad \text{(D-4)}$$

where

K_s = saturated hydraulic conductivity

D.2 Brooks-Corey Model

The Brooks-Corey water retention relationship is

$$S_e(h) = \left(\frac{h_b}{h}\right)^{\lambda} \text{ for } h \geq h_b \qquad \text{(D-5)}$$

$$S_e(h) = 1 \text{ otherwise.} \qquad \text{(D-6)}$$

When combined with the relative permeability model of Burdine (1953), Brooks and Corey derived the following hydraulic conductivity relationship.

$$K(S_e) = K_s(S_e)^{3 + 2/\lambda} \qquad \text{(D-7)}$$

or

$$K(h) = K_s\left(\frac{h_b}{h}\right)^{2 + 3\lambda} \text{ for } h \geq h_b \qquad \text{(D-8)}$$

$$\text{and } K(h) = K_s \text{ otherwise.} \qquad \text{(D-9)}$$

where

h_b = curve fitting parameter related to air entry pressure

λ = curve fitting parameter related to pore size distribution.

Carsel and Parrish (1988) used the following equivalence between the Brooks-Corey and van Genuchten parameters:

$h_b = \alpha^{-1}$ and $\lambda = n - 1$.

D.3 Campbell Model

Campbell (1974) adopted a water retention relationship similar to Brooks and Corey's, but with $\theta_r = 0$.

$$\frac{\theta}{\theta_s} = \left(\frac{h_b}{h}\right)^{1/b} \text{ for } h \geq h_b \qquad \text{(D-10)}$$

$$\frac{\theta}{\theta_s} = 1 \text{ otherwise.} \qquad \text{(D-11)}$$

Note that because $\theta_r = 0$, $b \neq 1/\lambda$. Campbell (1974) derived a corresponding hydraulic conductivity relationship.

$$K(\theta) = K_s\left(\frac{\theta}{\theta_s}\right)^{2b + 3} \qquad \text{(D-12)}$$

or

$$K(h) = K_s\left(\frac{h_b}{h}\right)^{2+3/b} \quad \text{for } h \geq h_b \qquad \text{(D-13)}$$

$$\text{and } K(h) = K_s \text{ otherwise.} \qquad \text{(D-14)}$$

where

b = curve fitting parameter related to pore size distribution.

Note that all of these single-valued relationships (Equations D-2 through D-14) assume that hysteresis is not important.

D.3.1 Calculation of Campbell's b Parameter

An expression for b in terms of θ_s, θ_r, and λ is derived by assuming that the Brooks-Corey model (Equation D-7) and the Campbell model (Equation D-12) predict the same hydraulic conductivity for a given value of water content. In this case, the water content used is that corresponding to an effective saturation of 0.5. Assuming $S_e = 0.5$ and using the definition of effective saturation given above, it follows that

$$\frac{\theta}{\theta_s} = \frac{0.5(\theta_s - \theta_r) + \theta_r}{\theta_s} = 0.5(1 + \theta_r/\theta_s) \qquad \text{(D-15)}$$

Substituting this expression in Equation D-12 and equating this with Equation D-7 leads to

$$(0.5(1 + \theta_r/\theta_s))^{3+2b} = 0.5^{3+2/\lambda} \qquad \text{(D-16)}$$

Equation D-16 can be solved for b,

$$b = 0.5\left\{\frac{\ln(0.5)(3 + 2/\lambda)}{\ln[0.5(1 + \theta_r/\theta_s)]} - 3\right\} \qquad \text{(D-17)}$$

D.4 Additional Parameters

Several additional soil hydraulic parameters may be required by dose assessment codes. These parameters and the methods by which they were calculated are discussed here.

- Effective porosity, $p_e = \theta_s - \theta_r$
- Field capacity, $f_c = \theta(K = 10^{-8}$ cm/s)
  Field capacity is generally interpreted as the water content at which drainage from a field soil becomes negligible (see the discussion by Hillel, 1980). Field capacity is often calculated as the water content at a specified tension, usually taken to be 340 cm (1/3 bar). Hillel (1980) argues, however, that the field capacity should be based on the drainage rate considered negligible (which is a function of the intended application). Field capacity was calculated here as the water content at which the unsaturated hydraulic conductivity equals 10^{-8} cm/s using the van Genuchten model (10^{-8} cm/s ≅ 3 mm/yr).The value of 10^{-8} cm/s was chosen because it represents a water flux at which contaminant transport is likely to be insignificant. This value also results in somewhat larger field capacity values and a more realistic available water capacity for very coarse textured soils than using the water content at 1/3 bar soil pressure. See Meyer and Gee (1999) for a more detailed discussion of field capacity.
- Wilting point, $w_p = \theta(h = 15{,}300$ cm)
  Wilting point is the minimum water content (or maximum tension) at which plants can extract water from the soil. Wilting point was calculated as the water content at a tension of 15,300 cm (15 bars).
- Available water capacity, $awc = f_c - w_p$
  Available water capacity represents the amount of water available for plant uptake.

D.5 References

Brooks, R. H., and A. T. Corey, "Hydraulic Properties of Porous Media," *Hydrology Paper 3*, Colorado State Univ., Ft. Collins, CO, 1964.

Burdine, N. T. "Relative permeability calculations from pore-size distribution data." *Petr. Trans.*, Am. Inst. Mining Metall. Eng., 198:71-77, 1953.

Campbell, G. S., "A simple method for determining unsaturated conductivity from moisture retention data," *Soil Sci.*, 117:311-314, 1974.

Fayer, M. J., and C. S. Simmons, "Modified soil water retention functions for all matric suctions," *Water Resources Research*, 31:1233-1238, 1995.

Meyer, P.D., M.L. Rockhold, and G.W. Gee, "Uncertainty Analyses of Infiltration and Subsurface Flow and Transport for SDMP Sites," *NUREG/CR-6565*, U.S. Nuclear Regulatory Commission, Washington, DC, 1997.

Meyer, P. D. and G. W. Gee, "Flux-based estimation of field capacity," *Journal of Geotechnical and Geoenvironmental Engineering*, 125(7):595-599, 1999.

Mualem, Y., "A new model for predicting the hydraulic conductivity of unsaturated porous media," *Water Resources Research*, 12(3):513-522, 1976.

Mualem, Y., "Modeling the Hydraulic Conductivity of Unsaturated Porous Media," in *Indirect Methods for Estimating the Hydraulic Properties of Unsaturated Soils*, M. Th. van Genuchten, F. J. Leij, and L. J. Lund (eds.), University of California, Riverside, CA, pp. 15-36, 1992.

Richards, L. A., "Capillary conduction of liquids through porous mediums," Physics, 1, 318-333, 1931.

Rossi, C. and J. R. Nimmo, "Modeling of soil water retention from saturation to oven dryness," *Water Resources Research*, 30(3):701-708, 1994.

van Genuchten, M. Th., "A closed-form equation for predicting the hydraulic conductivity of unsaturated soils," *Soil Sci. Soc. Am. J.*, 44:892-898, 1980.